Q:1 *Genetic mechanism of high-quality reservoirs in Permian tight fan delta conglomerates at the northwestern margin of the Junggar basin, Q:2 northwestern China*

Guanghui Yuan, Yingchang Cao, Longwei Qiu, and Zhonghong Chen

ABSTRACT

Fan delta conglomerate reservoirs in the Permian Jiamuhe Formation in the Zhongguai area at the northwestern margin of the Junggar Basin, northwestern China, are reservoirs for large accumulations of natural tight gas. The tight conglomerates and sandstones are mainly litharenites with a large amount of texturally and compositionally immature volcanic clastic materials. Core porosities demonstrate the development of anomalously high porosities at depths of 3200–4200 m (10,500–13,800 ft) and 4500–4900 m (14,800–16,100 ft). The Permian reservoirs experienced initial rapid subsidence, uplift, and further subsidence, and diagenetic reactions occurred in these reservoirs involving compaction; precipitation of chlorite clays, calcites, zeolites, iron oxides, kaolinite, and quartz cements; and dissolution of unstable minerals including analcite, laumontite, feldspars, and rock fragments. Low-porosity reservoirs, with extensive compaction and (or) cementation of calcite and heulandite-Ca, consist of only few visible secondary pores formed by dissolution of feldspars and rock fragments. Reservoirs with anomalously high porosity, however, experienced relatively weak compaction and contain significant amounts of secondary pores formed by dissolution of mainly laumontites, some feldspars, and rock fragments. Comprehensive studies of sedimentary features and diagenesis of the reservoirs indicate that these anomalously high porosities originate from chronological coupling of four important geological processes. (1) Sedimentary facies and detrital compositions controlled

Manuscript received November 1, 2015; provisional acceptance November 1, 2015; revised manuscript received December 7, 2016; final acceptance February 7, 2017.
DOI:10.1306/02071715214

AUTHORS

GUANGHUI YUAN ~ *Geology Department, School of Geosciences, China University of Petroleum, Qingdao 266580, China; yuan.guanghui86@gmail.com* Q:3

Guanghui Yuan is now a postdoctor at China University of Petroleum. His research focuses on sandstone diagenesis, reservoir quality prediction, and hydrocarbon work–rock interactions.

YINGCHANG CAO ~ *Geology Department, School of Geosciences, China University of Petroleum, Qingdao 266580, China; caoych@upc.edu.cn*

Yingchang Cao is a professor at China University of Petroleum. His research interests lie in the fields of sequence stratigraphy, sedimentology, and sandstone reservoir quality prediction.

LONGWEI QIU ~ *Geology Department, School of Geosciences, China University of Petroleum, Qingdao 266580, China; qiulwsd@163.com*

Longwei Qiu is a professor at China University of Petroleum. His research interests lie in the fields of sedimentology, diagenesis, and reservoir geology.

ZHONGHONG CHEN ~ *Resource Department, School of Geosciences, China University of Petroleum, Qingdao 266580, China; hongczh@163.com*

Zhonghong Chen is a professor at China University of Petroleum. His research interests lie in the fields of geochemistry, fluid flow in sedimentary basins, and hydrocarbon accumulation mechanisms.

ACKNOWLEDGMENTS

This study was financially supported by the Natural Science Foundation of China projects U1262203 and 41602138, a National Science and Technology special grant (2016ZX05006-007), the National Basic Research Program of China (973 Program) (E1401004B), China Postdoctoral Science Foundation (2015M580617), and Shandong postdoctoral innovation project 201502028. We also thank Xinjiang Oilfield Company of PetroChina for

providing of all the related core samples and some geological data of Junggar Basin. AAPG Editors Barry J. Katz and Michael L. Sweet, AAPG consulting geologist Frances P. Whitehurst, and two other anonymous reviewers are thanked for their constructive comments and advice.

EDITOR'S NOTE

Color versions of Figures 1–16 can be seen in the online version of this paper.

distribution of various zeolites in reservoirs, with abundant laumonites developed in reservoirs in the fan delta front subfacies. (2) Early precipitation of the laumontites inhibited compaction during deep burial; however, they provided unstable minerals for secondary porosity development. (3) The Permian reservoirs experienced subaerial exposure erosion during the uplift stage, and meteoric freshwater leached laumontite cements and aluminosilicate grains to form secondary pores in reservoirs beneath the unconformity. (4) Hydrocarbon emplacement at relative shallow depth during a second subsidence period preserved the secondary pores in reservoirs by retarding late carbonate cementation.

INTRODUCTION

Hydrocarbon exploration targets in deeply buried tight reservoirs are growing increasingly significant as most shallow petroleum reservoir exploration has been accomplished in the last few decades (Bloch et al., 2002; Higgs et al., 2007; Olson et al., 2009; Dutton and Loucks, 2010b; Cao et al., 2014; Chen et al., 2014). Global basin studies reveal that in specific geological conditions, deeply buried reservoirs may still be effective for accumulation and production of hydrocarbon and in particular that some areas exhibit unexpectedly high porosity and permeability at substantial burial depth (Bloch et al., 2002; Dutton and Loucks, 2010; Cao et al., 2014). Studies of the origin and distribution of high quality reservoirs are of great significance for accurate prediction of sweet spots in deeply buried tight reservoirs with low porosity and permeability (Higgs et al., 2007; Cao et al., 2014; Grant et al., 2014; Lai et al., 2015, 2016; Yuan et al., 2015b; Jia et al., 2016).

Tight gas plays have recently received considerable attention resulting from strength in the gas market and technology improvement; thus, possibilities for previously noncommercial gas accumulations have been explored (Higgs et al., 2007; Olson et al., 2009; Lai et al., 2015). Conglomerate reservoirs in the Permian Jiamuhe Formation are typical tight reservoirs with approximately 90% of the tested core permeability lower than 1 md. The conglomerate reservoirs in the Jiamuhe Formation of the Zhongguai area located in the northwestern margin of Junggar Basin are currently significant exploration targets for tight gas plays with exceptional natural potential (Wan, 2011; Chen et al., 2014, 2016). Volcanic lithic rock fragments (mainly tuff clasts and andesite clasts) dominate the detrital grains, and various zeolites are significant cements in these reservoirs. Core porosity data demonstrate the development of anomalously high porosities at depths of 3200–4200 m (10,500–13,800 ft) and 4500–4900 m (14,800–16,100 ft). Great successes have been achieved in oil–gas

exploration in these Jiamuhe conglomerate reservoirs with relative high porosity in recent years. For example, well C67, well C501, well C502, well XG1, well G3, and well G9 all obtained stable yields after formation fracture (Figure 1C). To date, however, the genetic mechanism of such anomalously high porosity is still unclear.

The purpose of this article is to (1) investigate petrography and disgenesis of the Permian tight conglomerate reservoirs, (2) identify types of pores in reservoirs with anomalously high porosity and low porosity, and (3) analyze genetic mechanisms of the high-quality reservoirs in the tight conglomerates. The results of this study can aid hydrocarbon exploration in the study area and other similar tight reservoirs in global basins.

GEOLOGICAL BACKGROUND

The Junggar Basin is a petroliferous basin in the northwestern China (Figure 1A), covering an area of approximately 13×10^4 km^2 (50,000 mi^2), and is surrounded by mountains including Yilinheibiergen Mountains in the south, Halalate Mountains in the north, Zhayier Mountains in the west, and Kelameili Mountains in the east (Chen et al., 2014) (Figure 1B). The Zhongguai area is located at the northwestern margin of the Junggar Basin (Figure 1B), with Hongche fault to the west, Hong3 well fault to the north, Penyijingxi sag to the east, and Shawan sag to the south (Figure 1C). The Zhongguai area is positionally favorable for gathering hydrocarbons from the Shawan sag and the Penyijingxi sag (Chen et al., 2014, 2016), and reservoirs in the Permian Jiamuhe Formation have a natural gas resource of approximately 148×10^8 m^3 (5226×10^8 ft^3)(Wan, 2011).

Sediments filled in the Zhongguai area comprise the Carboniferous, Permian, Triassic, Jurassic, Cretaceous, Paleogene, Neogene, and Quaternary (Figure 1D) (Ma et al., 2015). The Permian consists of the Jiamuhe (P_1j), Fengcheng (P_1f), Xiazijie (P_2x), and Wuerhe (P_2w and P_3w) Formations from base to top (Figure 1D). Formations in the Shawan sag are currently complete, whereas most of the P_1f, P_2x, and P_2w Formations have been eroded to form a regional unconformity in the Zhongguai area in the upper Permian (Figure 1D). The P_3w with thick mudstones was deposited on top of the unconformity, serving as a regional seal (Chen et al., 2014, 2016). The Jiamuhe Formation is divided into two members, P_1j_1 and P_1j_2 (from base to top), and is a downdip stratum with burial depth ranging from approximately 2.0 km (1.2 mi) at the northwest to 7.0 km (4.3 mi) at the southeast part of the Zhongguai area (Figure 1D). This study focuses on the P_1j_2 member in the Zhongguai area where drilling wells are available and sediments deposited are typically fan deltas composed of fan delta plain, fan delta front, and profan delta subfacies (Wan, 2011). The P_1j_2 member is subdivided into three submembers, P_1j_2-1, P_1j_2-2, and P_1j_2-3, from top to base (Figure 1D).

METHODS AND DATABASE

Data collected from the Geological Scientific Research Institute of PetroChina Xinjiang Oilfield Company included rock composition data of 260 thin section samples, 1030 porosity and permeability core data, well log porosity data of five wells (XG1, XG2, G3, G13, and G201), 116 formation temperature data, and 21 pore water data. The core porosity and permeability were analyzed using CMS^{tm}-300 Core Measurement system with a confining pressure of 6 MPa. The well log porosity data were interpreted with acoustic time logging, bulk density logging, and compensated neutron logging.The pore water chemistry data were tested with a 930 Compact ion chromatograph. The distribution histograms of core porosity over every 200-m (656-ft) depth interval were plotted to identify the normal porosity subpopulation and the anomalously high porosity subpopulation (Bloch et al., 2002). The compaction porosity curve was obtained by connecting the maximum porosity of the normal subpopulation of porosities at different depth intervals.

Samples for this study were selected from the Permian cores of 16 wells (Figure 1C), at positions where porosity and permeability data are available. One hundred and twenty blue epoxy resin-impregnated thin sections were prepared for analysis of rock mineralogy, diagenesis, and porosity. Point counts were performed on thin sections for the content of detrital grains with at least 300 points, which can provide a standard deviation of 6% or less (Van der Plas and Tobi, 1965). For the amount of secondary pores and cements,

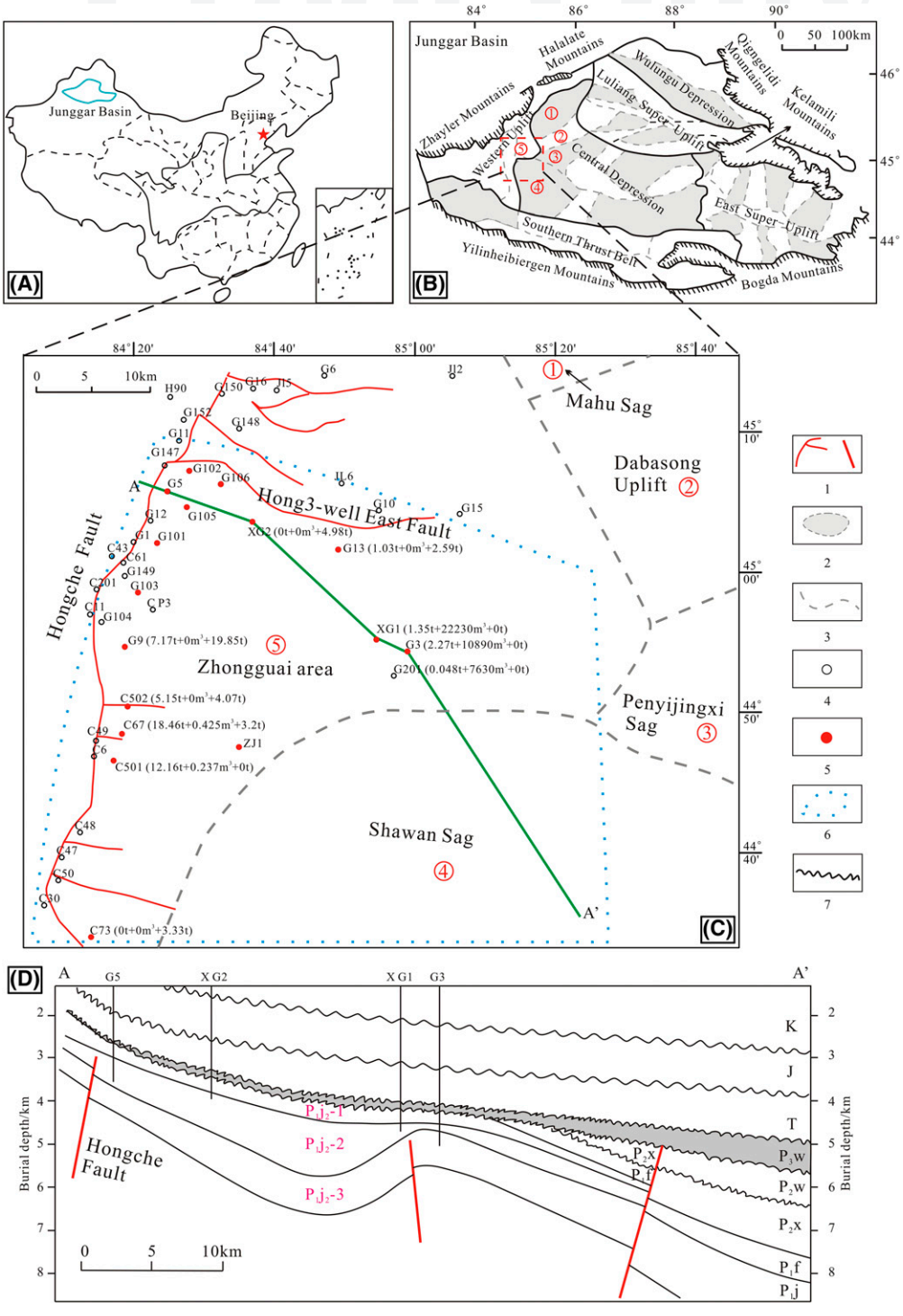

Q:12 Figure 1. (A) Location map showing geographic location of the Junggar Basin in northwestern China. (B) Map showing subtectonic units of the Junggar Basin and location of the Zhongguai area. (C) Permian structural map and well location of the Zhongguai area and testing data (oil + gas + water/each day) of the Jiamuhe conglomerate reservoirs in some wells. (D) Northwest–southeast cross section showing strata profile of the Zhongguai area. (Modified from Chen et al., 2016, and used with permission of Elsevier.). Numbers indicate the following: 1 = fault; 2 = sag; 3 = boundary of tectonic units; 4 = well; 5 = wells with cores and sample analysis; 6 = boundary of the study
Q:13 area; 7 = unconformity. Note: A color version can be seen in the online version.

20 micrographs of each thin section were taken first using the Zeiss microscope. Objectives of 50× for these thin sections were used, and each micrograph has an area of 25.80 mm^2 (0.04 $in.^2$). Then the pores in each micrograph were identified under the microscope and were drawn on a computer screen using CorelDRAW, and the total areas of each target mineral and pore in every micrograph were obtained using Image-Pro Plus software. Finally, the contents of the target minerals and pores in each thin section were obtained by taking an average of all values in its micrographs (Yuan et al., 2015a). Fifteen samples were identified using a Quanta200 scanning electron microscope (SEM) combined with EDAX energy dispersive spectroscopy.

Burial and thermal histories of the Zhongguai area were studied using the BasinMod software (Guo et al., 2012), with knowledge of lithologies for various formations from exploration wells, the evolution of geothermal gradient data of the Junggar Basin from previous studies (Zhou et al., 1989; Qiu et al., 2000), and the eroded strata thickness. Thickness of eroded strata with unconformity was estimated by applying the ratios of reference sequence strata thickness method (Li et al., 2006) with seismic profiles and wells. Absolute ages of depositional and erosional events were defined with the chronostratigraphic framework of the Junggar Basin (Ma et al., 2015).

RESULTS

Lithofacies

Based on 350-m (1148-ft) cores from 16 wells in the Zhongguai area, the fan delta sediments were divided into seven main lithofacies (Table 1): (1) massive medium-grained conglomerates (Figure 2A, B); (2) fine-grained conglomerates with graded bedding or massive bedding (Figure 2C); (3) sandy conglomerates and pebbly sandstones with massive bedding, graded bedding, and parallel bedding (Figure 2D); (4) massive medium- to coarse-grained sandstones (Figure 2E); (5) fine sandstones with parallel bedding or cross-bedding (Figure 2F); (6) massive or laminated siltstones–shaly sandstones (Figure 2G); and (7) massive or laminated mudstones (Figure 2H). Samples for this study were selected mainly from lithofacies 2 and 3 and from lithofacies 4–6.

Petrography

The studied Permian conglomerate reservoirs are fine- to very coarse–grained (Figure 2). Rock samples for this study are texturally immature and typically range from fine-grained sandstones to fine-grained conglomerates, with some medium-grained conglomerates (Figure 2). Grain sorting is commonly poor, and roundness of most detrital grains ranges from subangular to subrounded. Sorting coefficient (σ) of rocks from lithofacies 2 and 3 are generally higher than 2.5, whereas σ of rocks from lithofacies 4–6 ranges mainly from 1.0 to 2.5. The rocks are primarily litharenite (Figure 3A), compositionally immature with an average framework composition of 3% quartz (Q), 4% feldspar (F), and 93% rock fragment (R) ($Q_3F_4R_{93}$). Detrital quartz grains are primarily monocrystalline, and their content ranges mainly from 0% to 10%. The content of detrital feldspars ranges from 0% to 15%, and K-feldspars account for 60%–70% of the feldspars. Volcanic lithic rock fragments, ranging from 83% to 100%, dominate the detrital grains and are composed mainly of tuff clasts and andesite clasts. Though most grains are subangular to subrounded, tuff clasts generally show subrounded to rounded shape, indicating transporting of these clasts from provenance area to deposition area.

Significant differences exist between the mineral compositions of reservoirs in the fan delta plain subfacies (Figure 3B, C) and the fan delta front subfacies (Figure 3D, E). On average, the rocks in the fan delta plain subfacies contain approximately 2% quartz, 5% feldspars, 50% tuff clasts, 30% andesite clasts, and 8% sedimentary rock debris (Figure 3B, C); authigenic cements include 1% calcite, 1% laumonite, 2%–3% heulandite-Ca, less than 0.5% analcite and 2% iron oxides, and matrix including 2% tuff matrix and 1% mud matrix. Rocks in the fan delta front subfacies, however, contain approximately 1%–2% quartz and feldspars, 15% tuff clasts, and 70% andesite clasts on average (Figure 3D, E); authigenic cements include an average of 8% laumonite and less than 1% calcite, and the content of matrix is less than 0.5%.

Table 1. Characterization of Different Lithofacies in the Permian Fan Delta in the Zhongguai Area, Junggar Basin

Lithofacies	Description	Depositional Environment
Lithofacies 1: medium-grained conglomerates	Sand-supported or mud-supported medium-grained conglomerates. This lithofacies comprises beds (1–20 m thick) of mixed gravels, sands, and muds. Sediments are generally angular and poorly sorted, with much matrix.	Fan delta plain subfacies.
Lithofacies 2: fine-grained conglomerates	One important lithofacies. Mainly sand-supported conglomerates, characterized by bed thickness ranges from a half to several meters. Sediments are generally subangular and poorly sorted, with little matrix.	Fan delta plain subfacies and fan delta front subfacies.
Lithofacies 3: sandy conglomerates and pebbly sandstones	Another important lithofacies. These rocks are composed mainly of fine-grained gravels and medium–coarse sand grains. Sediments are generally subangular to subrounded and moderately–poorly sorted, with little detrital clay. Some rocks contain graded bedding and parallel bedding, but most are massive. Amalgamated beds are several meters to tens of meters thick.	Braided channels in the fan delta front subfacies.
Lithofacies 4: medium- to coarse-grained sandstones	These rocks are composed mainly of medium and coarse sand grains and are rare in the sediments. Such sandstones are thin bedded, commonly less than 0.5 m.	Braided channels in the fan delta front subfacies.
Lithofacies 5: fine-grained sandstones	This lithofacies contains manily of fine-grained, subrounded, poorly sorted sediments, with massive matrix.	Marginal setting away from the main axis of sand input.
Lithofacies 6: siltstones–shaly sandstones	This lithofacies has fine-grained sandstones with abundant mudstone laminates; the siltstones generally have more detrital clays.	Marginal setting away from the main axis of sand input.
Lithofacies 7: mudstones	Laminated mudstone with occasional siltstones.	Out of channels with low hydrodynamic force.

The fine-grained conglomerate refers to the conglomerate with the size of gravels ranging mainly from 2 to 10 mm, the medium-grained conglomerate refers to gravel size from 10 to 100 mm, and the coarse-grained conglomerate refers to gravel size from 100 to 1000 mm.

Porosity and Permeability

The Permian conglomerate reservoirs exhibit a wide range of porosity from 2% to 18% and permeability from 0.001 to 25 md (Figures 4, 5). The compaction porosity curve and vertical distribution of all available core porosities demonstrate the development of anomalously porosities at depths of 3200–4200 m (10,500–13,800 ft) and 4500–4900 m (14,800–16,100 ft) (Figure 4A), with anomalously high permeability also existing at such depth intervals (Figure 4B). For porosity data in one individual well, however, there is no depth interal (e.g., well G5 and well G105) or just one depth interval with anomalously high porosity (e.g., well XG1 and well ZJ1) (Figure 4C–H).

The porosity versus permeability plots and distribution histograms of porosity and permeability data indicate that tight reservoirs with low porosity and

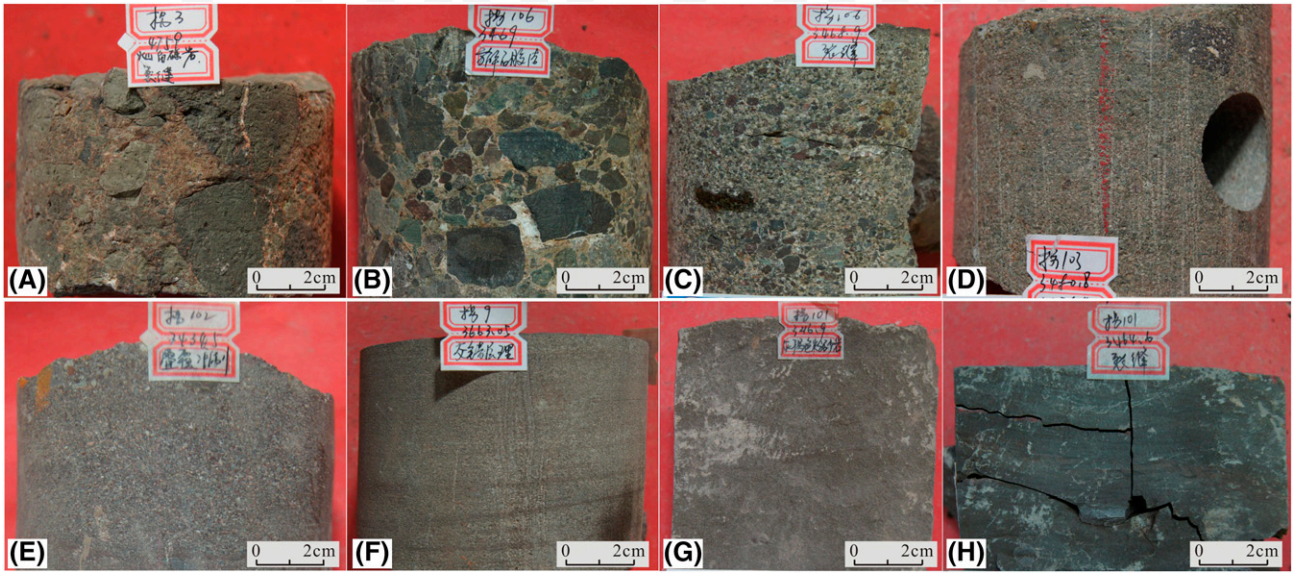

Figure 2. Different lithofacies in the Permian fan deltas in the Zhongguai area, Junggar Basin. (A) Massive medium-grained conglomerate, 4759 m, well G3. (B) Massive medium-grained conglomerate, 3469.0 m, well G106. (C) Amalgamated fine-grained conglomerate with graded bedding, 3468.9 m, G106. (D) Massive pebbly sandstone, 3480.8 m, well G103. (E) Massive medium- to coarse-grained sandstone, 3438.5 m, G102. (F) Fine-grained sandstone with crossing bedding, 3663.05 m, G9. (G) Siltstone, 3216.9 m, G101. (H) Gray mudstone, 3464.6 m, G101. Note: A color version can be seen in the online version.

ultralow permeability account for most of the reservoirs in the Zhuangguai area (Figure 5). Normal porosity subpopulation and anomalously high–porosity subpopulation, at depths of 3200–4200 m (10,500–13,800 ft), account for 72% and 28% of total porosities (Figure 5C), respectively, whereas at depths of 4500–4900 m (14,800–16,100 ft), normal porosity subpopulation and anomalously high–porosity subpopulation account for 15% and 85% of total porosities (Figure 5D), respectively. Generally, reservoirs in fan delta plain subfacies have relatively low porosity and permeability compared with reservoirs in fan delta front subfacies (Figure 5A, B).

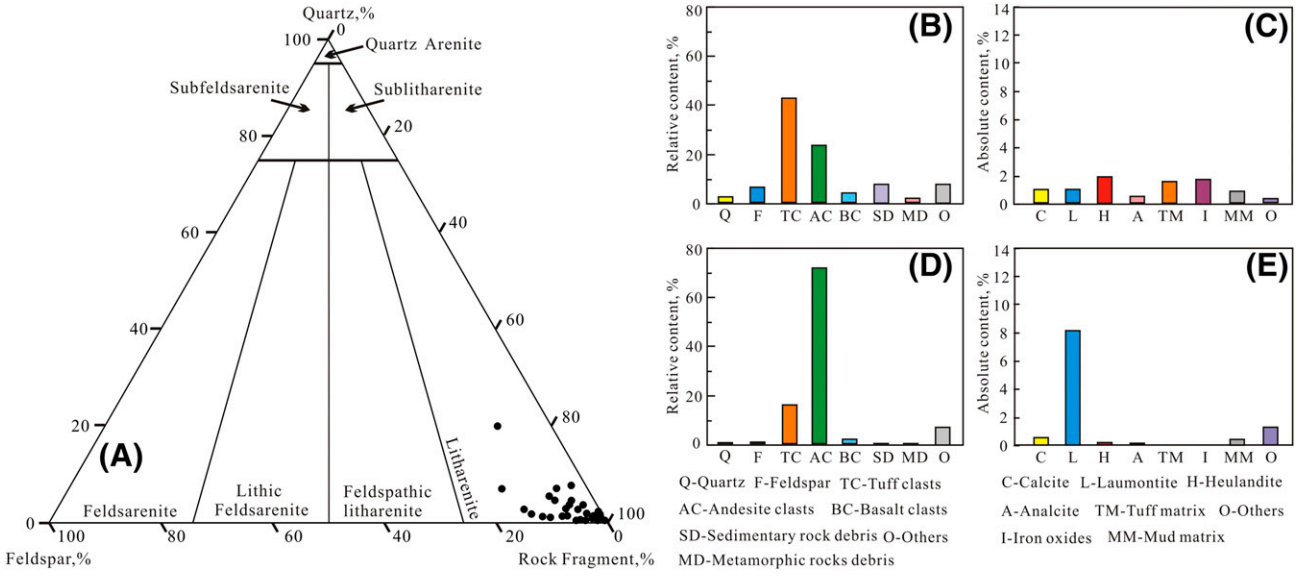

Figure 3. (A) Ternary plot showing rock compositions of the Permian conglomerate reservoirs in the Zhongguai area (refer to sandstone classification standard of Folk et al., 1970). (B–E) Histograms showing the content of various compositions in reservoirs in the delta plain subfacies (B, C) and the fan delta front subfacies (D, E). Note: A color version can be seen in the online version.

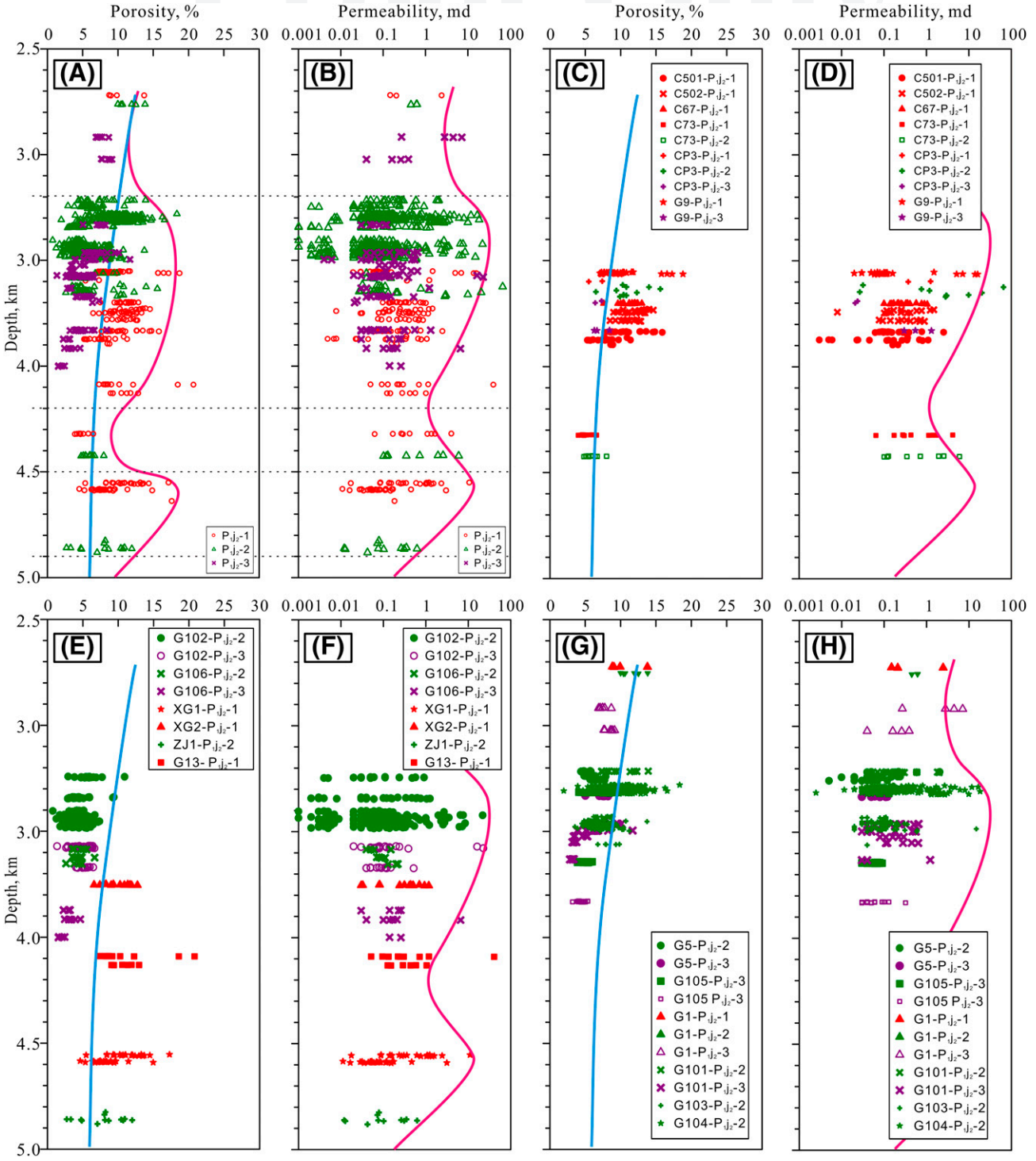

Figure 4. Vertical distribution of core porosity and core permeability of (A, B) all data from 19 wells and (C–H) some individual wells in the Jiamuhe Formation in the Zhongguai area. The blue curve represents the compaction porosity curve. Note: A color version can be seen in the online version.

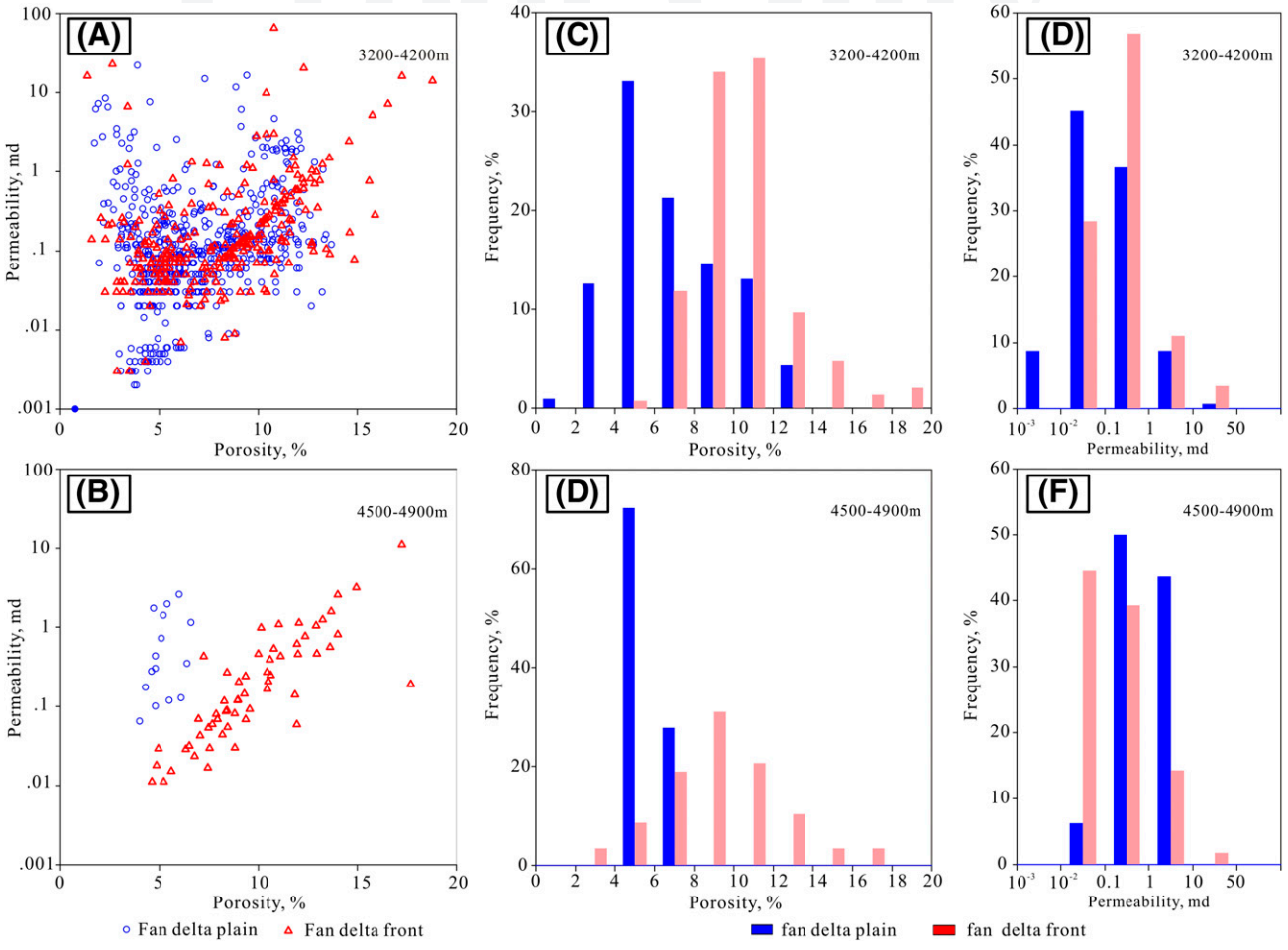

Figure 5. (A, B) Core porosity versus core permeability diagrams and histograms of (C, D) porosity and (E, F) permeability of the reservoirs in different subfacies in the fan deltas at depths of 3200–4200 m (10,499–13,780 ft) and 4500–4900 m (14,764–16,076 ft) in Zhongguai area. Note: A color version can be seen in the online version.

Burial and Thermal History

Accurate evaluation of burial and thermal history requires knowledge of parameters including lithology of various formations; geological ages; porosities, timing, duration, and thickness of erosion; and geothermal gradient data (Guo et al., 2012; Nguyen et al., 2013). Burial history of the Zhongguai area was investigated using one-dimensional (1-D) modeling of 10 wells. Detailed data on lithology, thickness, and start and end time of various formations of well XG1 are listed in Table 2. Porosity exerts significant influence on thermal conductivity and heat capacity of sediments closely related with thermal properties of a basin and maturation level of source rocks. Empirical relationships between porosity and initial porosity and burial depths are widely applied in basin modeling (Guo et al., 2012). The porosity–depth relationship for decompaction correction of Falvey and Middleton (1981) was adopted in this study (Falvey and Middleton, 1981), with initial porosity and compaction factors of a pure lithology adopted from default values in the BasinMod 1-D software and mixed lithologies created by specifying percentages of the pure lithologies for 1-D modeling of individual wells (Table 2).

The modeling results indicate a variable rate of burial from the Permian period to present (Figure 6) at different locations in the Zhongguai area. Burial history of the Zhongguai area in the Permian period overall consists of several stages, including rapid subsidence in the early Permian with sedimentation of P_1j, P_1f, P_2x, and P_2w; rapid uplift in the middle

Table 2. Input Parameters for the One-Dimensional Burial–Thermal History Modeling of Well XG1 in the Zhonguai Area

Start Time (Ma)	End Time (Ma)	Formation	Depth of Bottom Boundary (m [ft])	Depth of Top Boundary (m [ft])	Thickness (m [ft])	Erosion Thickness (m [ft])	Lithology			Temperature Gradient (°C/km [°F/mi])
							Sandstone	Siltstone	Mudstone	
145	0	K–Q	2409 (7903)	0	2409 (7903)	–	8%	20%	72%	19.5 (56.5)
164	145	Erosion	–	–	–	400 (1312)	–	–	–	30 (87)
205	164	J	3483 (11,427)	2409 (7903)	1074 (3523)	–	26%	19%	55%	
242	205	T	4394 (14,416)	3483 (11,427)	910 (2985)	–	14%	26%	60%	35 (101)
248	242	Erosion	–	–	–	350 (1148)	–	–	–	40 (116)
255	248	P_3w	4550 (14,927)	4394 (14,416)	156 (512)	–	19%	26%	65%	
260	255	Erosion	–	–	–	1800 (5905)	–	–	–	
285	266	P_1j	4730 (15,518)	455 (14,927)	180 (590)	–	93%	2%	5%	

Q:21 Temperature gradient data are from Qiu et al. (2000) and Zhou et al. (1989).

Permian with erosion of P_2w, P_2x, P_1f, and upper part of P_1j; rapid burial in the late Permian with sedimentation of P_3w; and following erosion of the upper part of P_3w. Triassic and Early–Middle Jurassic are represented by rapid subsidence with thickness of sediments up to approximately 3000 m (9800 ft). During the Late Jurassic, the high sedimentation rate waned, and a basin-wide unconformity is associated with approximately 400 m (1300 ft) of missing sections in the latest Jurassic. Burial history was characterized by a return to high rates of subsidence and sediment supply from Cretaceous to present, and from the northwestern to the southeastern areas in the Zhongguai area, burial history demonstrates differences caused by development of the downdip slope. Maximum burial depth of the Jiamuhe Formation in the Zhongguai area occurs today.

Goodness of fit between the modeled temperature and tested formation temperature provides the best available comparison of model to reality (Figure 6). Maximum temperatures of Jiamuhe Formation with current shallow depth at the northwestern part of the Zhongguai area were reached before the uplift in the late Permian, when paleogeothermal gradient was approximately 40°C/km (116°F/mi) (Table 2) and burial depth was deeper than 2500 m (8200 ft), whereas maximum temperatures of the deeply buried Jiamuhe Formation in the southeastern part of the Zhongguai area occur today with a geothermal gradient of approximately 19.5°C/km (56.5°F/mi) (Table 2).

Diagenesis

Authigenic Minerals

Authigenic minerals in the reservoirs consist of various zeolites, calcite, quartz, clays (kaolinite and chlorite), and iron oxides.

Zeolites—Zeolite cements are the most abundant cements, and three types, analcite, heulandite-Ca, and laumontite, were identified in the reservoirs (Tang et al., 1997; Zhu et al., 2012). Analcite occurs as euhedral dodecahedron crystal (Figures 7A, 8A) or patchy aggregation (Figure 7E) in some medium- to coarse-grained sandstones, pebbly sandstones, and fine-grained conglomerates. Anhedral heulandite-Ca in shaly sandstones and fine-grained sandstones with much matrix was transformed from volcanic ashes and is characterized by orange patch aggregation with no development of euhedral prismatic crystals (Figure 7L), whereas in medium- to coarse-grained sandstones, pebbly sandstones, and fine-grained conglomerates, heulandite-Ca is characterized by orange euhedral prismatic morphology and their aggregation (Figures 7B, 8B). Laumontite occurs typically as blocky pore-filling cement characterized by well-developed cleavages in medium- to coarse-grained sandstones, pebbly sandstones, and fine-grained conglomerates (Figures 7C, 8D); in addition, some feldspar grains were identified to be replaced by laumontite cements. Heulandite-Ca was identified in the outer part of primary pores in some thin

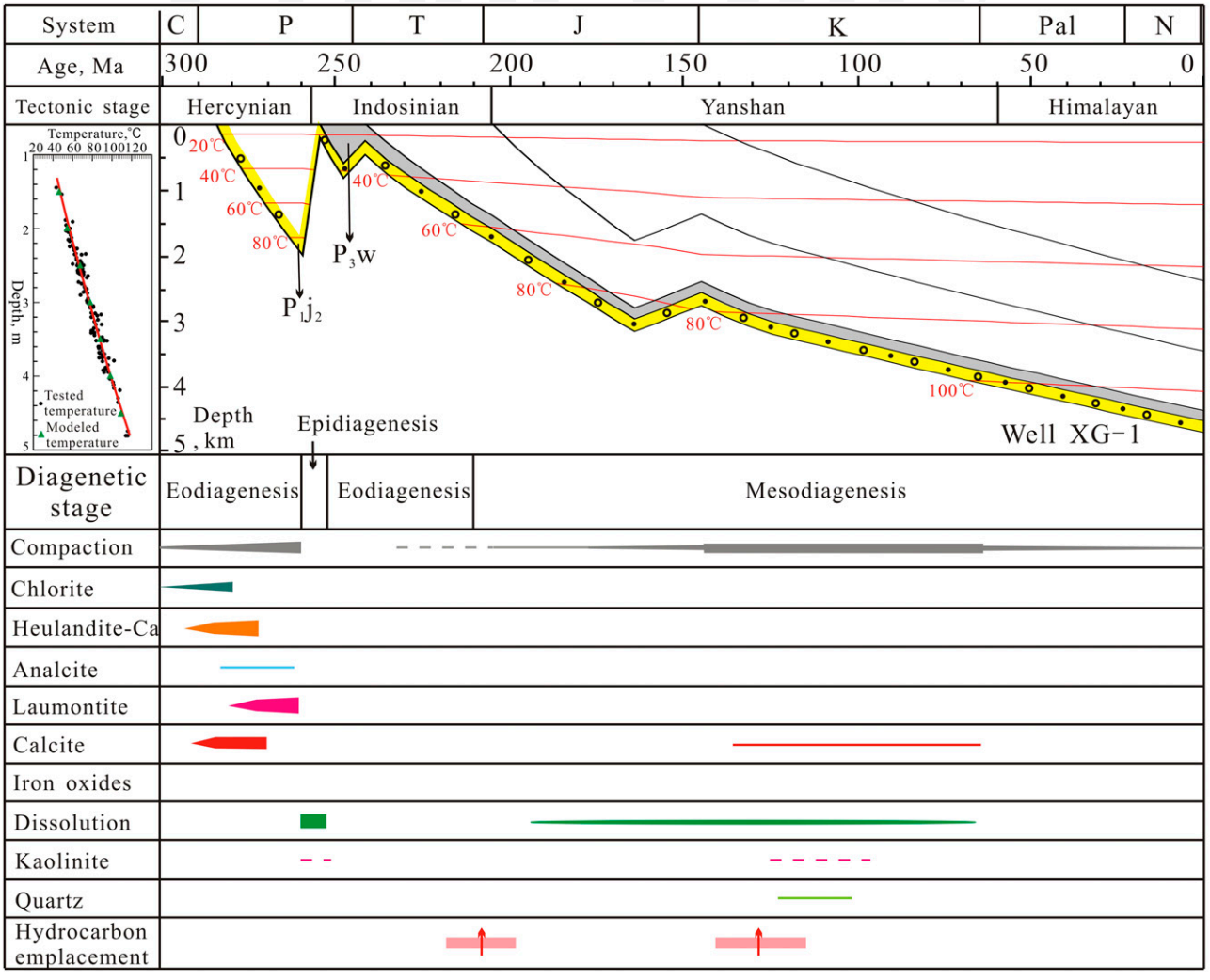

Figure 6. Plots of burial, thermal, diagenetic, and hydrocarbon emplacement history of the Permian reservoirs in the Zhongguai area. The hydrocarbon emplacement stage is after Chen et al. (2016). Note: A color version can be seen in the online version.

sections, whereas analcite or laumontite was identified in the inner parts of the primary pores (Figure 7G–J). This texture relationship suggests that heulandite-Ca was formed relatively earlier than analcite and laumonite. Low–homogenization temperature data (55–60°C [131–140°F]) of aqueous fluid inclusions (Chen et al., 2016) identified in some laumontite also suggest early precipitation of these zeolites.

Calcite—Calcites are important authigenic minerals in some reservoirs, ranging in abundance from trace to 25% in thin sections. Two types of calcite cements were identified in thin sections. Early calcites were precipitated prior to extensive compaction and are characterized by poikilotopic textures and are up to 20%–25% in volume in thin sections (Figure 7D). Low homogenization temperature (50°C [122°F]) of aqueous fluid inclusions in early calcites (Chen et al., 2016) also demonstrates early formation of these cements. Rocks with early calcites are commonly supported by grains with point contacts or floating textures. Late calcite cements, in contrast, typically feature a low content of less than 2%–5% of rock volume. The late calcites replaced early zeolite cements in thin sections and filled secondary pores and fractures in grains and zeolite (Figure 7D), indicating that the late calcites were likely to be precipitated after dissolution of zeolites and feldspars.

Iron Oxides—Iron oxides were identified in thin sections from several wells (e.g., wells G5, G11, G105, G102, and G106) at the northwestern part of the

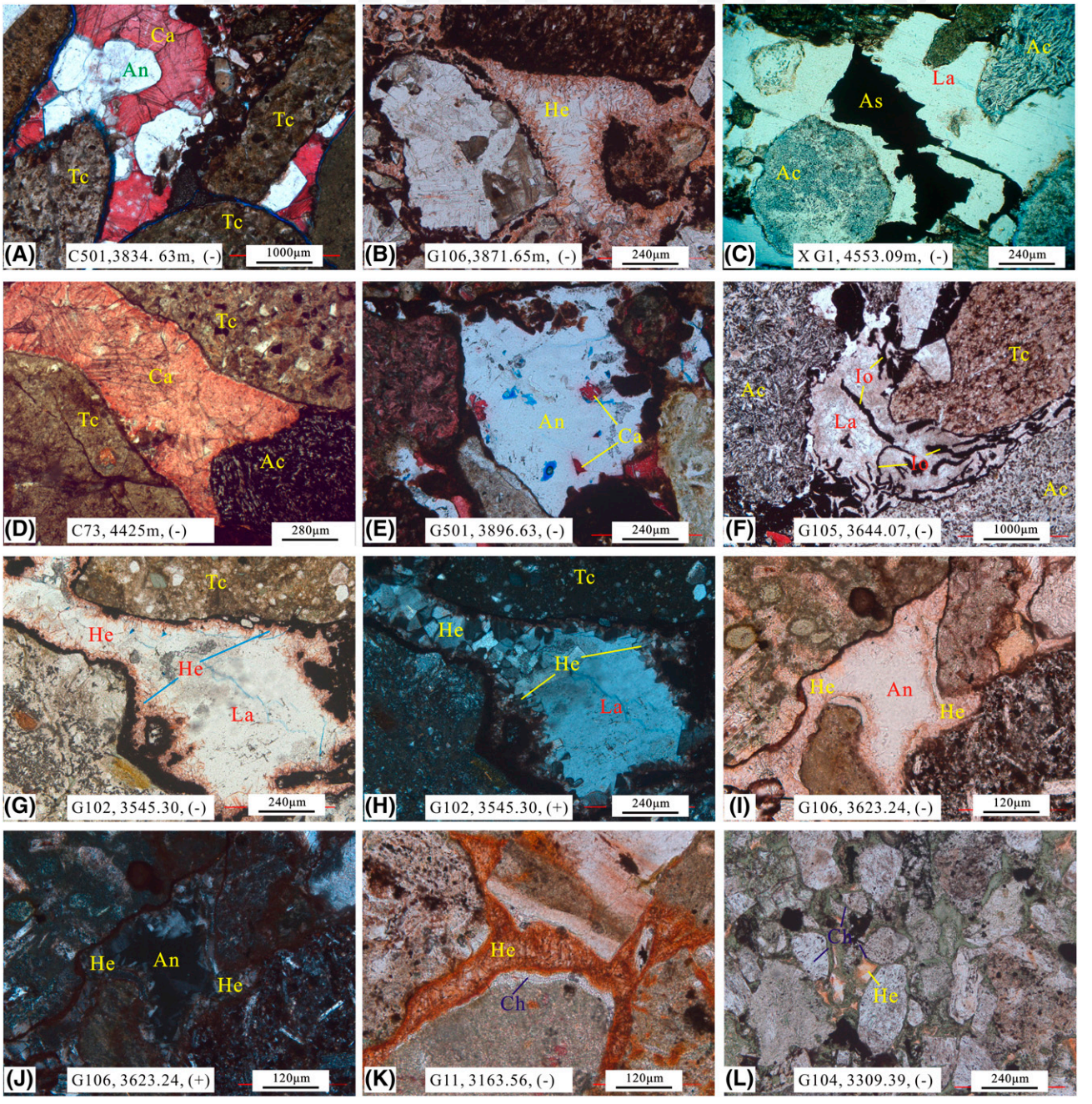

Figure 7. Thin section images of the conglomerate reservoirs in Jiamuhe Formation in the Zhongguai area (pore space is shown in blue). (A) Calcite (Ca) and analcite (An) cement in primary pores. Tuff clasts (Tc) are subrounded or rounded. (B) Heulandite-Ca (He) cement in primary pores. (C) Laumontite (La) cement in primary pores and asphalt (As) in secondary pores formed by dissolution of La. (D) Early-stage Ca in primary pores. Floating texture can be easily identified, and Tc are subrounded or rounded. (E) Secondary pores formed by dissolution of An, partial filling of these secondary pores by late-stage Ca. (F) Replacement of La by iron oxides (Io). (G, H) Heulandite-Ca in outer part of primary pores and La in inner part of pores. (I, J) Heulandite-Ca in outer part of primary pores and An in inner part of pores. (K) Chlorite (Ch) in outer part of primary pores and He in inner part of pores. (L) Green Ch and orange patch He. Dash indicates plane-polarized light view; plus indicates cross-polarized light view. Ac = andesite clasts. Note: A color version can be seen in the online version.

downdip slope constrained by the Hongche fault and the Hong3 well fault (Figure 1C). Iron oxides were identified to replace zeolites (Figure 7F) and calcites and fill fractures or secondary pores in grains, indicating that these iron oxides formed later than the early precipitated cements. The amount of iron oxides generally increases in thin sections as the distance from rock samples to the unconformity decreases, suggesting these iron oxides were potentially products of meteoric freshwater flushing during the uplift period in the late Permian.

Clay Minerals—Kaolinite and chlorite are two types of authigenic clays in the Jiamuhe conglomerate reservoirs. Chlorite occurs predominantly as pore fillings, grain coatings, or rims. In shaly sandstones and fine-grained sandstones with much matrix, considerable amounts of volcanic ashes were transformed to chlorite and were identified as green patchy pore filling minerals in thin sections (Figure 7L). Coating or rim chlorite (Figures 7K, 8E) were, in contrast, formed in medium- to coarse-grained sandstones and pebbly sandstones with low amount of matrix. The coatings are generally of homogeneous thickness and uniform distribution (Figure 7K), whereas the rims commonly exhibit preferred orientation perpendicular to the grain surfaces (Figure 8E). Chlorite crystals are characterized by euhedral foliaceous morphology in SEM samples (Figure 8E). Petrography textures (Figure 7K) demonstrate that chlorite likely formed earlier than other authigenic minerals.

Kaolinite occurs mainly as vermicular aggregates and anhedral–pseudohexagonal plates filling in primary and secondary pores (Figure 8G) with the amount of kaolinite ranging from trace to less than 1%. Texture relationships indicate that kaolinite formed later and is likely a secondary mineral following the dissolution of zeolites and feldspars.

Quartz—Authigenic quartz in the reservoirs occurs as discrete euhedral and subhedral crystals (Figure 8F) that generally postdate chlorite grain-coating; rare quartz overgrowths can be identified in thin sections (Figure 7). The quartz crystals, with size generally less than 10 μm, are evident in SEM samples but cannot be identified easily in thin sections because of the small size. Quartz cements commonly represent less than 0.1% of the whole rock and are likely secondary minerals of dissolution of zeolites and feldspars.

Dissolution

Mineral dissolution occurred in reservoirs and improved reservoir quality through generation of a substantial amount of secondary pores (Zhu et al., 2012) (Figures 9, 10A–E). Thin sections and SEM samples demonstrate that dissolution occurred primarily in laumontite (Figures 8C, D; 10A–D) and analcite (Figure 10E) and some feldspar and andesite fragment grains (Figure 10C), whereas little petrography evidence indicates obvious dissolution of tuff fragment grains (Figure 10G), heulandite-Ca (Figure 10H), and calcite cement (Figure 7D). Extensive dissolution occurred mainly in medium- to coarse-grained sandstones, pebbly sandstones, and fine-grained conglomerates (Figure 10A–F), whereas shaly sandstones and fine-grained sandstones experienced weak dissolution (Figure 10I). Reservoirs closely related to the unconformity commonly contain more secondary pores and higher core porosity (Figure 9), indicating mineral dissolution probably occurred through meteoric water leaching during the uplift period (Emery et al., 1990). Abundant bitumen and heavy oil (Figures 7C, 10D) were identified in secondary pores formed by laumontite dissolution, indicating that hydrocarbon emplacement probably occurred after mineral dissolution.

Diagenetic Sequences

The relative timing of major diagenetic sequences (Figure 6) of the Jiamuhe conglomerate reservoirs in the Zhongguai area at the northwestern margin of Junggar Basin, which has been determined from thin sections and SEM examination, is based on texture relationships (Figures 7–10) (Tang et al., 1997). The dominant eogenetic features in the reservoirs are, in summary, (1) initial compaction immediately following deposition; (2) formation of chlorite clay coatings or rims and chlorite pore fills; and (3) early precipitation of calcite, heulandite-Ca, analcite, and laumontite. Diagenesis occurring at the Permian uplift stage includes (1) dissolution of unstable minerals including analcite, laumontite, and some feldspars and rock fragments; (2) precipitation of kaolinite; and (3) precipitation of iron oxides from

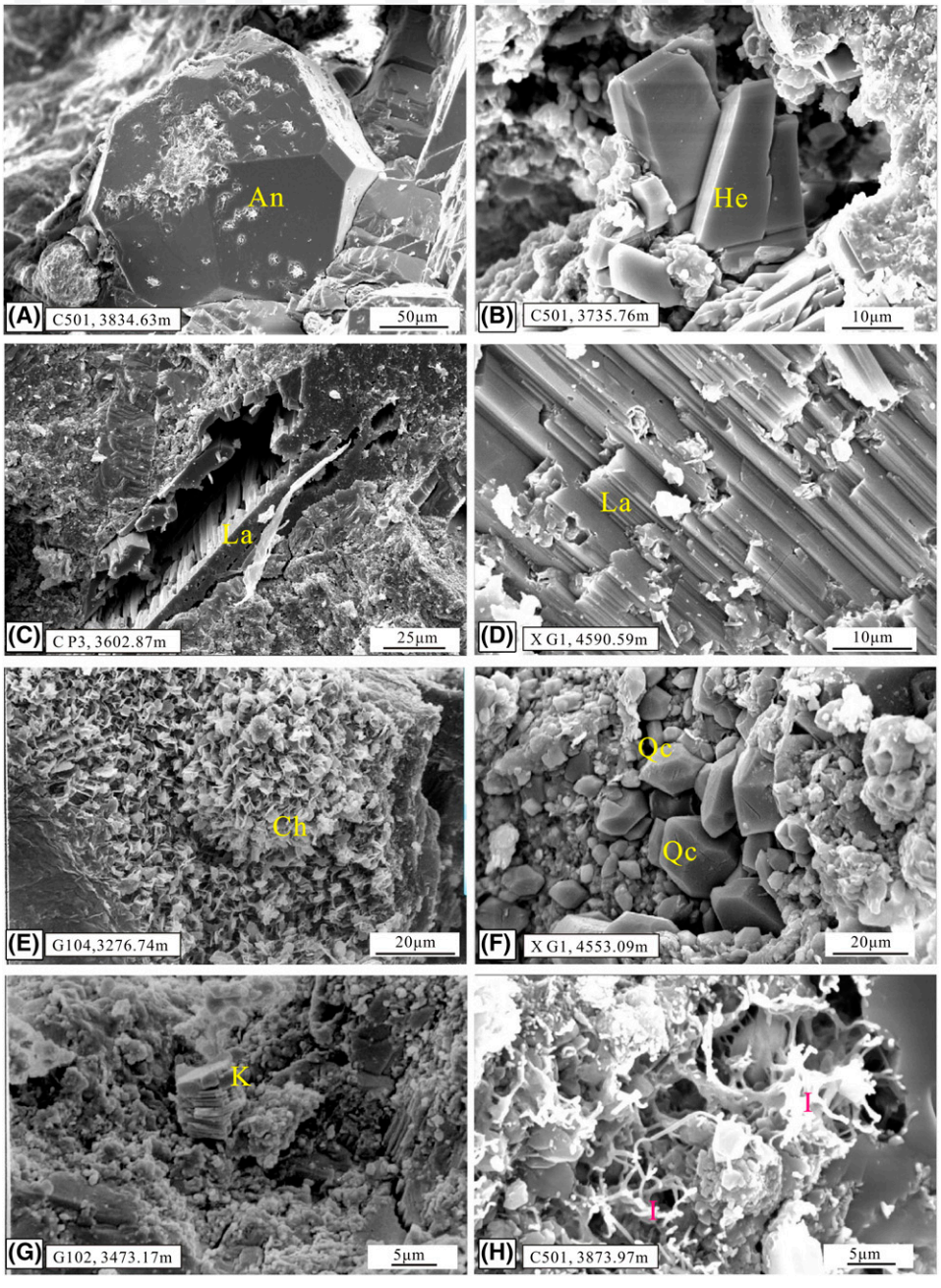

Figure 8. Scanning electron microscope images of the conglomerate reservoirs in Jiamuhe Formation in the Zhongguai area. (A) Single analcite (An) crystal. (B) Single heulandite-Ca (He) crystal. (C) Secondary pores in laumontite (La). (D) Dissolution of La. (E) Chlorite (Ch) rim on grain surface. (F) Authigenic quartz crystal (Qc). (G) Authigenic kaolinite (K). (H) Authigenic illite (I). Note: A color version can be seen in the online version.

interactions with oxidized meteoric water. Subsequent diagenetic processes during the resubsidence stage experienced by these reservoirs include (1) compaction; (2) dissolution of some aluminosilicate minerals; and (3) precipitation of kaolinite, quartz, and late calcite. With constraints of the texture relationships, the homogenization temperature (T_h) of aqueous fluid inclusions in cements, and burial–thermal history of well XG1 in the Zhongguai area, the diagenetic history of the Permian conglomerate reservoirs is summarized in Figure 6.

Pores in Reservoirs

Pores in the Permian reservoirs are currently mainly secondary pores as a result of extensive compaction, cementation, and mineral dissolution (Figures 9, 10), and only a few residual primary pores can be identified in some samples. Thin sections and SEM samples demonstrate distinct differences among pores in various reservoirs. Most primary pores in medium- to coarse-grained sandstones, pebbly sandstones, and fine-grained conglomerates in fan delta

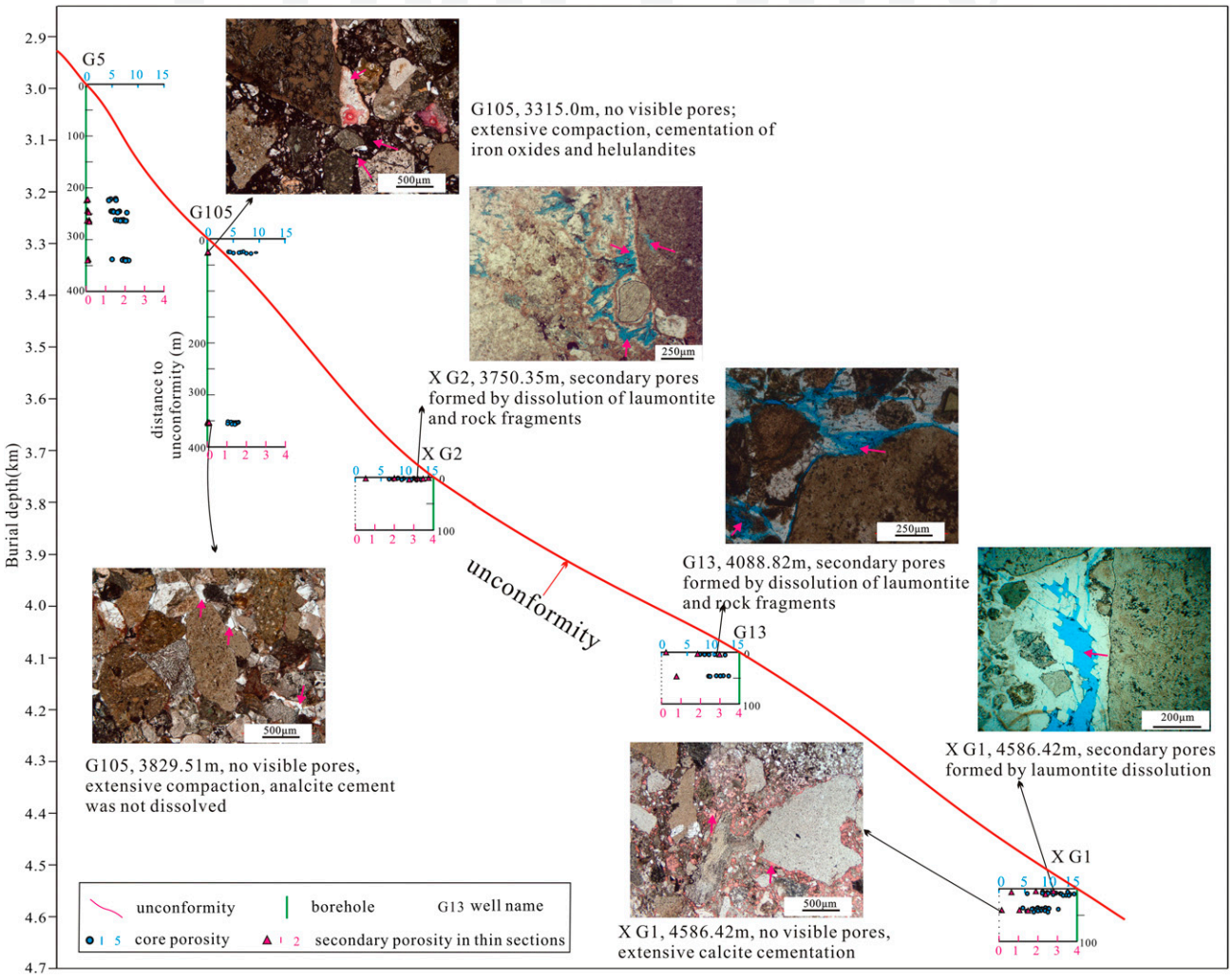

Figure 9. Core porosity and secondary porosity in thin sections in individual wells on a northwest–southeast cross section profile (well G5 to well G105 to well XG2 to well G13 to well XG1) (Figure 1C) and features of the secondary pores in the reservoirs beneath the unconformity and the reservoirs far from the unconformity. Note: A color version can be seen in the online version.

plain subfacies have been reduced by extensive compaction, and some pores are occupied by various cements including calcite, analcite, heulandite-Ca, and iron oxides; few secondary pores can be identified in feldspar grains or analcite (Figure 10G, H). In shaly sandstones and fine sandstones with much matrix, almost all primary pores have been destroyed by extensive compaction and/or authigenic cements including patchy chlorite and heulandite-Ca aggregates (Figure 10I); rare secondary pores can only be identified in few feldspar grains in such rocks. The amount of visible pores in these two types of tight rocks is generally less than 0.1%, and such rocks also exhibit low core porosity.

The medium- to coarse-grained sandstones, pebbly sandstones, and fine-grained conglomerates in fan delta front subfacies, contrastingly, contain abundant secondary pores formed by dissolution of analcite, laumontite, and some detrital grains (Figure 10A–E), although primary pores have been occupied by these zeolite cements at the early diagentic stage. The amount of visible secondary pores in thin sections can generally reach up to 2%–4% (Figure 9), and anomalously high core porosities are typically exhibited in these reservoirs.

Pore Waters

Data of 21 pore water samples in the Jiamuhe Formation reservoirs show that pore waters are characterized by $CaCl_2$ water. The salinity of these pore

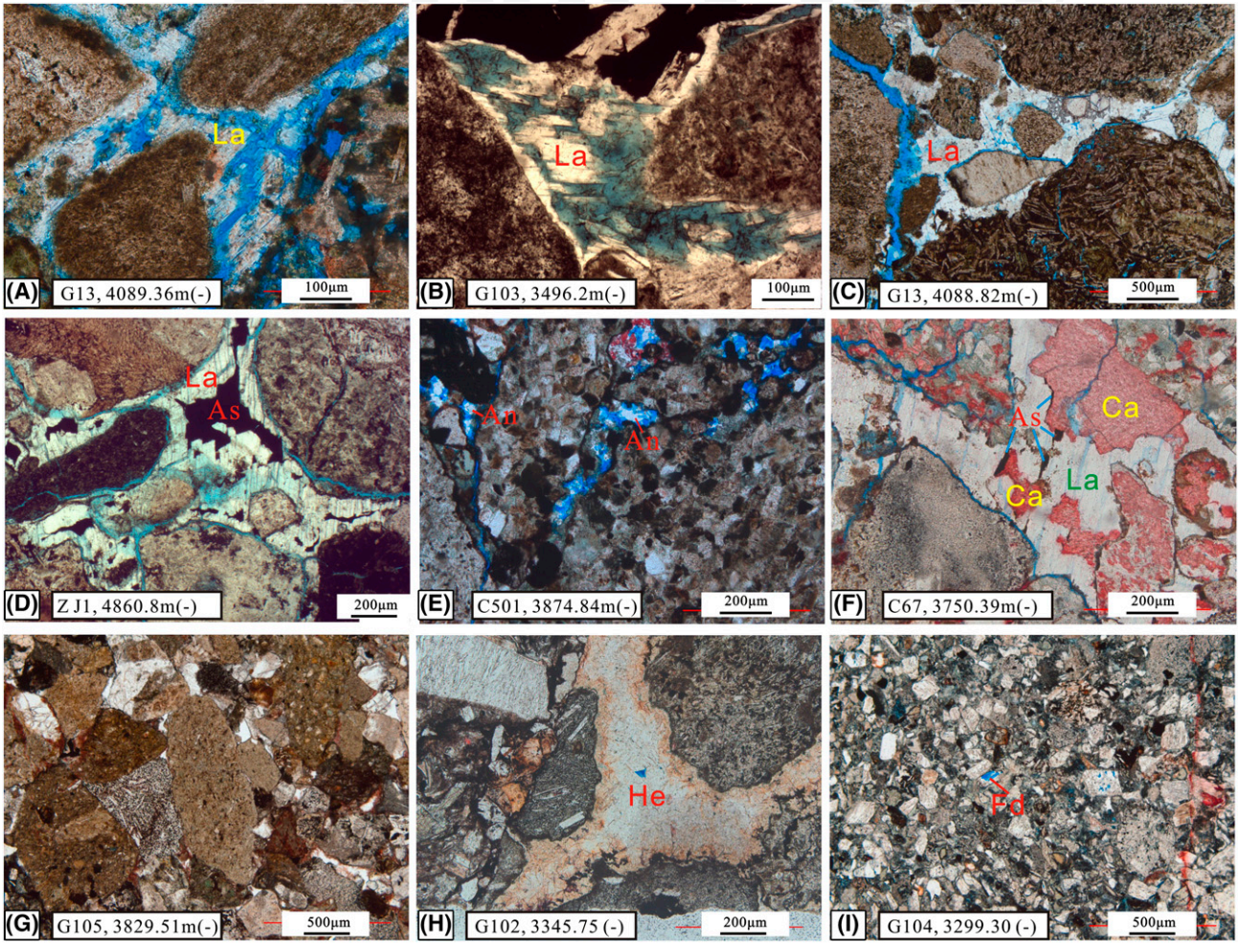

Figure 10. Photomicrographs of various pores in reservoirs with (A–E) anomalously high porosity and (F–I) low porosity. (A, B) Intergranular secondary pores formed by dissolution of laumontite (La). (C) Dissolution of La along cement–grain boundary and dissolution of andesite fragment grain. (D) Filling of secondary pores by asphalt (As). Pores were formed by La dissolution. (E) Secondary pores formed by analcite (An) dissolution. (F) Secondary pores left in La. Most secondary pores were occupied by As and calcite (Ca) cement. (G) No visible pores in reservoirs with strong compaction. (H) Few remnant primary pore was left after cementation of heulandite-Ca (He) cement. (I) Secondary pores formed by dissolution of feldspar grain (Fd). All plane-polarized light. Note: A color version can be seen in the online version.

waters ranges from 8819.0 mg/L to 76,618.0 mg/L (Table 3). The main cations are Na^+, K^+, and Ca^{2+}, and Cl^- dominates the anions. The plots of salinity and ion concentrations versus the distance of these water samples to the unconformity at the top of the Jiamuhe Formation show low salinity and low concentrations of Cl^- and Na^+ in pore waters of reservoirs beneath the reginal unconformity (Figure 11).

DISCUSSION

Reservoir quality evolution may be a function of several controls (Taylor et al., 2010; Tobin et al., 2010; Cao et al., 2014) including the depositional controls of sedimentary facies, lithofacies, grain sizes, sorting, and compositions and the diagenetic controls of cementation, dissolution, and compaction (Dutton and Loucks, 2010; Yuan et al., 2015b). Q:7 Results from the previous sections are integrated and discussed below to decipher genetic mechanism of the anomalously high porosities developed in the Permian conglomerate reservoirs.

Effect of Deposition on Cementation

Sedimentary Facies and Lithofacies

Zeolites are the most prominent cements in the Permian tight reservoirs, and types of zeolites vary

Table 3. Ranges of Salinity and Concentration of Different Ions in the Pore Waters in the Permian Tight Conglomerate Reservoirs in the Zhongguai Area

	Ions (mg/L)						
Concentration	$Na^+ + K^+$	Ca^{2+}	Mg^{2+}	Cl^-	SO_4^{2-}	HCO_3^-	Salinity
Maximum	2140	1046	0	5040	61	37	8819
Minimum	13,955	18,437	638	47,010	1466	1165	76,618
Average	4289	8262	118	21,000	461	382	34,332

in different rocks and different subfacies. Few analcite or laumontite cements were identified in shaly and fine-grained sandstones with much matrix including detrital clays and volcanic ashes, whereas the anhedral heulandite-Ca originating from volcanic ashes dominated the zeolite cements (Figure 12). In pebbly sandstones and fine-grained conglomerates with little matrix, different zeolites were identified in reservoirs from different subfacies. Statistic data indicate that laumontite dominates the reservoir cements in the fan delta front subfacies, with the absolute amount of laumontite ranging from 2% to 20% and relative content (relative to the amount of all zeolite cements) ranging from 80% to 100%, whereas heulandite-Ca dominates the cements in reservoirs in the fan delta plain subfacies, with absolute amount of heulandite-Ca ranging from 1% to 8% and relative content ranging from 60% to 100% (Figure 13). Analcite developed primarily in some sandstones in the fan delta plain subfacies, with the absolute amount ranging from 0.5% to 5% and relative content ranging from 10% to 85%. Thus, sedimentary subfacies and lithofacies significantly affect the distribution of analcite, heulandite-Ca, and laumontite in the Permian reservoirs (Fu et al., 2010; Sun et al., 2014).

Rock Compositions

In the medium- to coarse-grained sandstones, pebbly sandstones, and fine-grained conglomerates, the relative content of tuff clasts and andesite clasts (relative to the amount of rock fragments) controlled the relative content of heulandite-Ca and laumonite cement (relative to the amount of zeolites) (Figure 14). When the relative content of tuff clasts ranges from 0% to 20% and andestite clasts ranges from 100% to 80%, laumontite dominates the zeolites in reservoirs, and few heulandite-Ca can be identified; when when tuff clasts ranges from 100% to 80%, the heulandite-Ca dominates, and few laumontite cements can be identified. The heulandite-Ca dominates in shaly

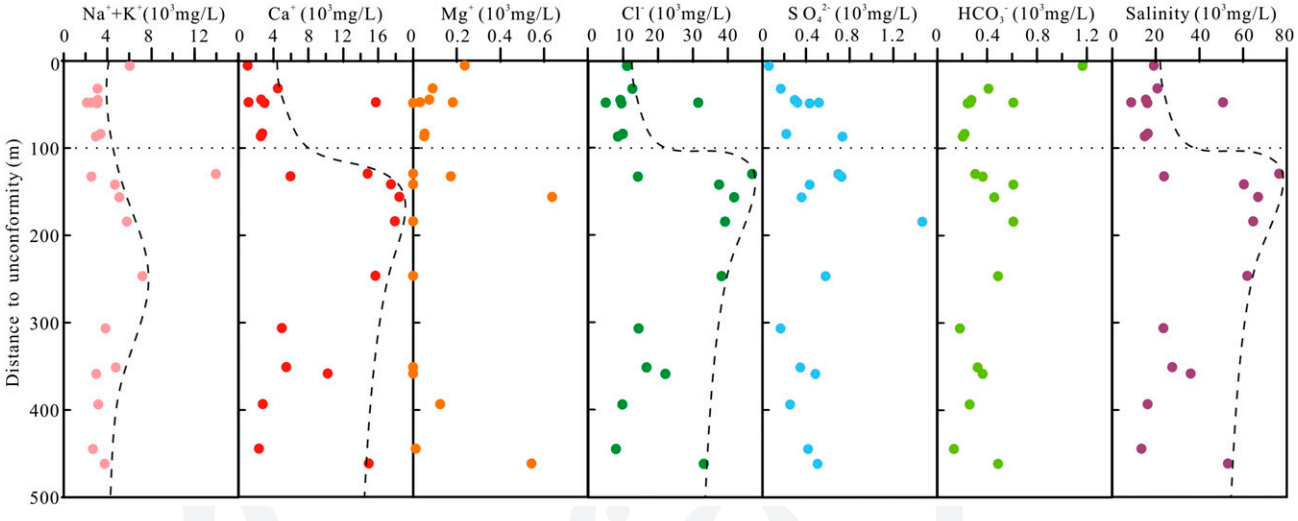

Figure 11. Salinity and concentrations of different ions in the pore waters in the Permian reservoirs in the Zhongguai area. Note: A color version can be seen in the online version.

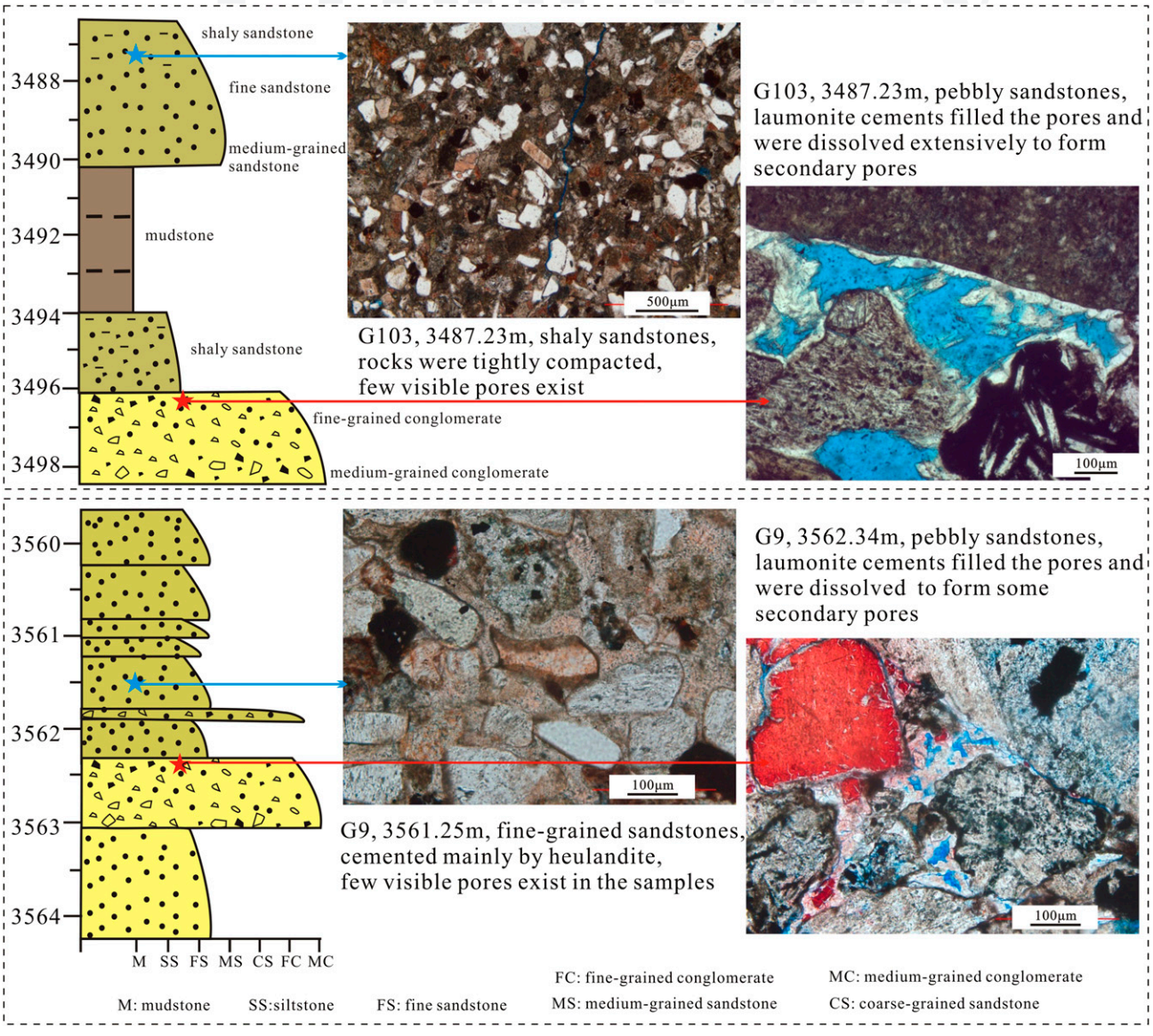

Figure 12. Distribution of heulandite-Ca and laumontite cement in reservoirs with different lithofacies in the Permian Jiamuhe Formation in the Zhongguai area. Note: A color version can be seen in the online version.

sandstones and fine-grained sandstones because of the existence of volcanic ash. Thus, despite the effect of sedimentary facies, rock compositions also affected the distribution of heulandite-Ca and laumontite (Tang et al., 1997; Zhu et al., 2012; Sun et al., 2014).

Early Cementation Retarded Later Compaction

Considerable amounts of volcanic rock fragments in the sandstones, particularly the tuff clasts, are plastic grains that may promote mechanic compaction during burial (Figure 10G) (Pittman and Larese, 1991). In the Permian reservoirs, petrography textures of line contact and concavo–convex contact demonstrate extensive compaction in rocks with few calcite and laumontite cements (Figures 7L, 10G). Point contact pattern and floating textures of detrital grains are common (Figure 10A–D), however, in reservoirs with large amount of calcite and laumontite cements (or secondary pores formed by laumonite dissolution), suggesting that these early precipitated cements have retarded compaction effectively during the later burial (Huang et al., 2007; Zhu et al., 2007).

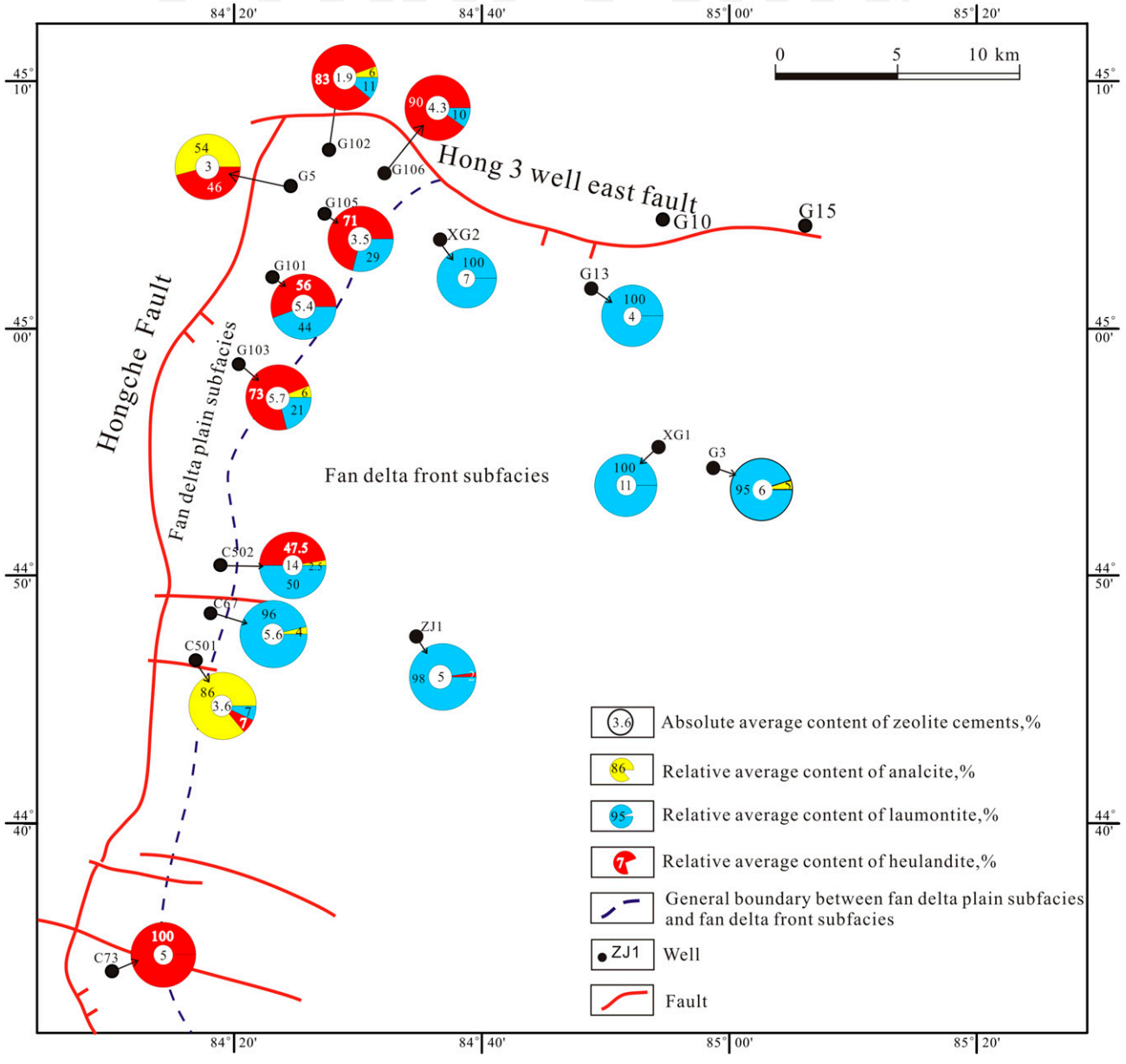

Figure 13. Distribution of analcite, heulandite-Ca, and laumontite in different subfacies in the Permian fan delta reservoirs in the Zhongguai area. Note: A color version can be seen in the online version.

Meteoric Water Leaching Formed Secondary Pores

The regional unconformity on the top of the Jiamuhe Formation suggests long-term subaerial exposure of the studied reservoirs in the late Permian, leading to meteoric water flushing of the reservoirs beneath the unconformity (Emery et al., 1990). Extensive diagenetic reactions (particularly mineral dissolution) tend to increase salinity of pore water (Frape et al., 1984; Egeberg and Aagaard, 1989); however, pore waters in reservoirs with extensive dissolution beneath the unconformity generally exhibit much lower salinity and ion concentrations (Figure 11), indicating that large amounts of meteoric freshwater probably entered into these reservoirs during the uplift period (França et al., 2003).

Dissolution of aluminosilicate minerals is generally accompanied by precipitation of secondary minerals including clays and quartz cements in relatively closed sandstone geochemical systems (Giles and De Boer, 1990; Zhang et al., 2011;

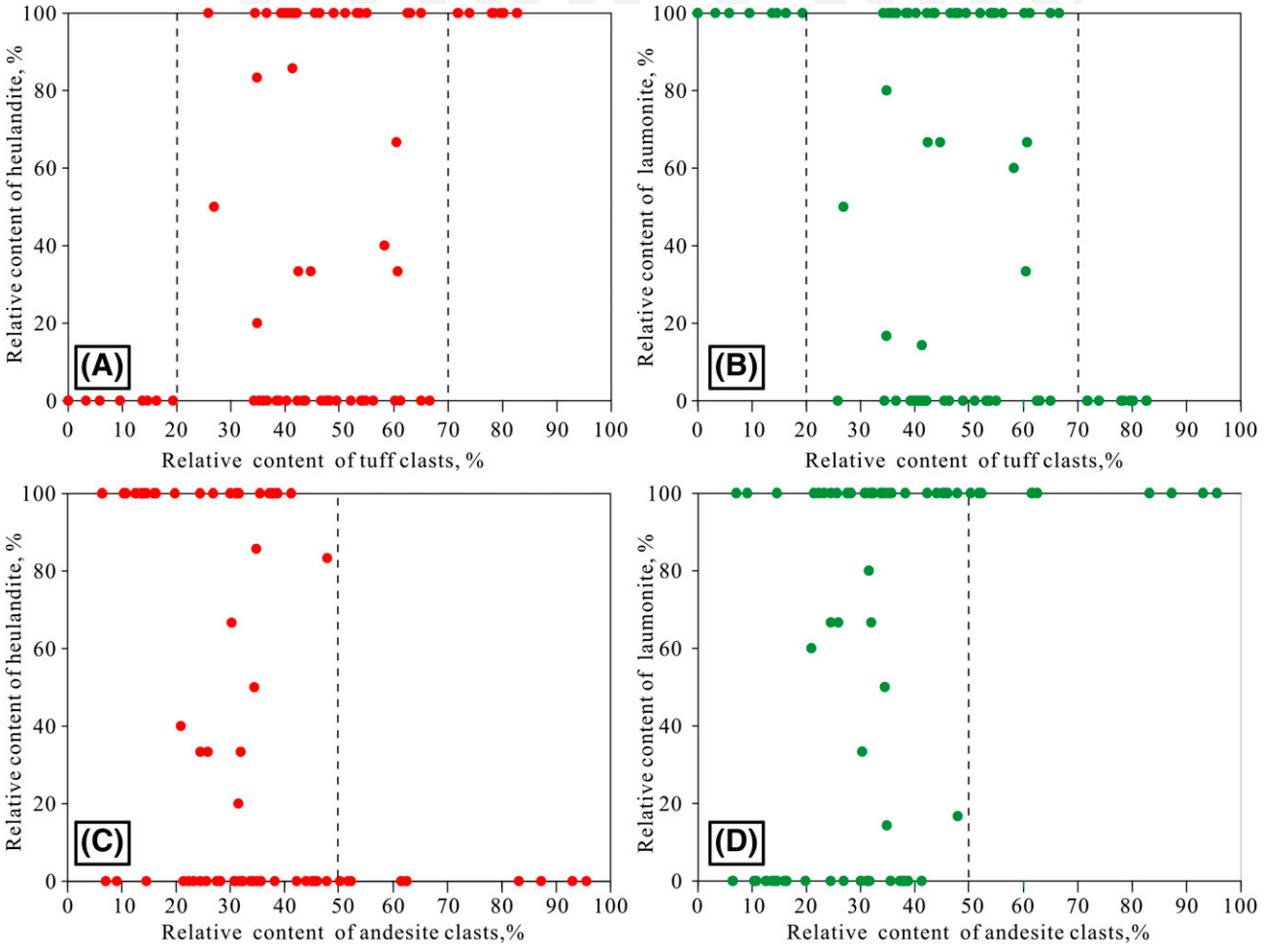

Q:19 **Figure 14.** Relationships between types of zeolite and mineral composition in the Permian reservoirs in the Zhongguai area. Note: A color version can be seen in the online version.

Yuan et al., 2013). However, few kaolinite and quartz cements were identified in the Permian reservoirs with abundant secondary pores, suggesting that solutes released by dissolution of laumonites and feldspars may have been removed from the reservoirs effectively (Giles, 1987; Emery et al., 1990). Thin sections show that reservoirs closer to the unconformity typically exhibit large amount of secondary pores formed by dissolution of mainly laumontite and some feldspars, and tested core porosity and interpreted log porosity confirmed the development of anomalously high porosities beneath the unconformity (Figures 9, 15). Thin sections demonstrate that most secondary pores developed in the central part of the laumonite cements and feldspar grains (Figure 10A, B), and the marginal remnants likely contributed to preservation of the secondary pores by preventing secondary compaction during later burial.

Hydrocarbon Emplacement Retarded Later Cementation

Hydrocarbon emplacement has been suggested in previous studies to preserve porosity by retarding mineral cementation (Marchand et al., 2001, 2002; Wang, 2010), with the concept questioned by some scientists (Aase and Walderhaug, 2005). Previous studies with evidence of fluid inclusions, reconstructed burial history, and thermal history suggested two stages (218–198 Ma and 145–112 Ma) of hydrocarbon emplacement in the Permian reservoirs when burial depth was shallower than 1800 and 3000 m, respectively **Q:8**

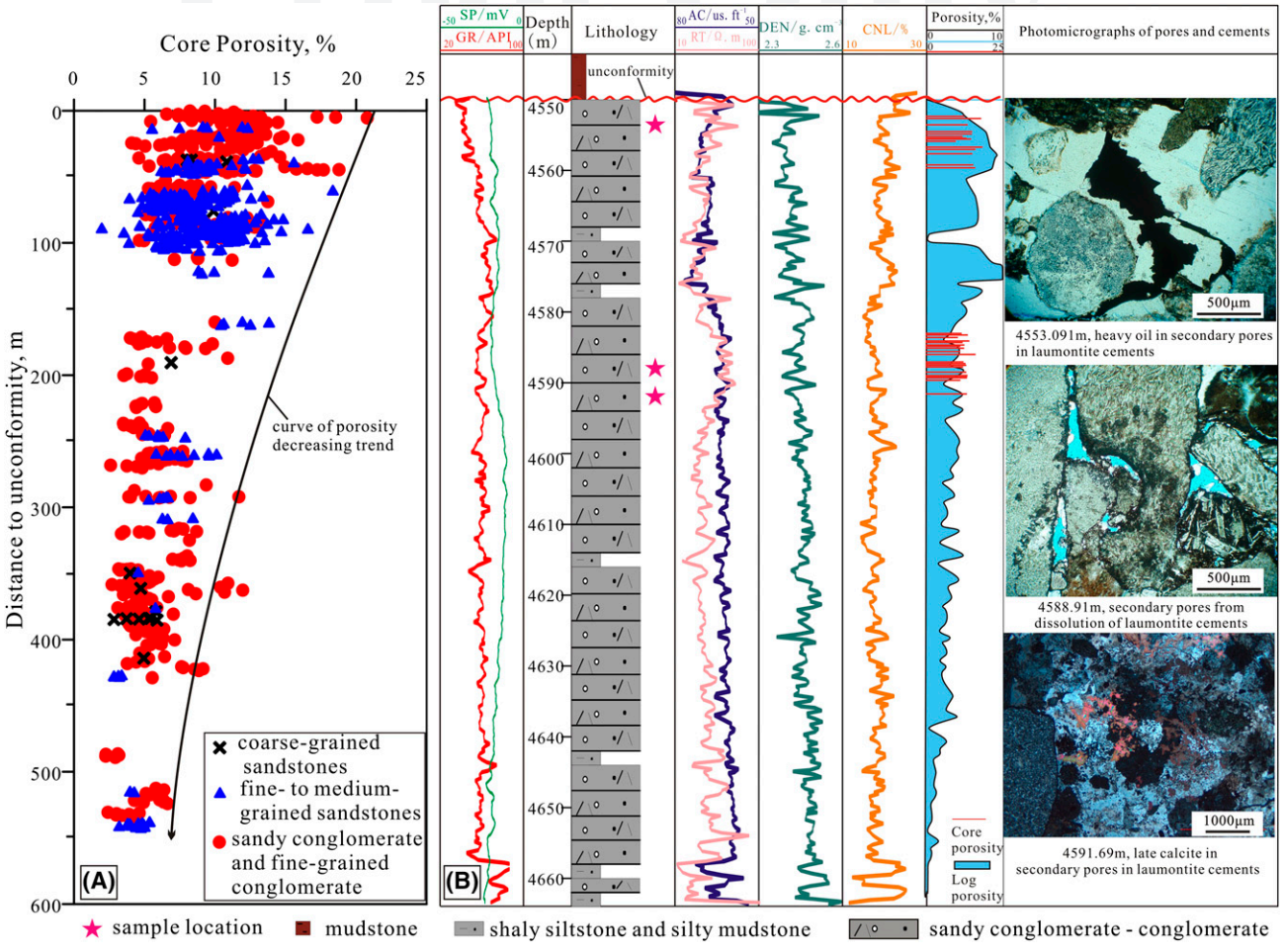

Figure 15. (A) Plot of core porosity versus the distance between the rock samples and the unconformity. (B) The lithology, porosity, and micropetrography of well XG1 beneath the unconformity. AC = acoustic time logging curve; CNL = compensated neutron logging; DEN = bulk density logging curve; GR = natural gamma log curve; RT = resistivity logging curve; SP = spontaneous potential logging curve. Note: A color version can be seen in the online version.

(Figure 5) (Chen et al., 2016). Thin sections demonstrate that few later calcite cements were formed in secondary pores in reservoirs from oil or gas layer (Figures 10A, B; 15), whereas more later calcite can be identified in secondary pores in reservoirs from water layers and dry layers (Figures 10F, 15), suggesting that later calcite cementation reactions were retarded following hydrocarbons emplacement in the Permian Jiamuhe reservoirs.

Genetic Model of the High-Quality Reservoirs

The deeply buried Jiamuhe conglomerate reservoirs experienced various diagenetic reactions including compaction, cementation, and dissolution. Discussion in the previous four sections suggests that the generation of the high-quality reservoirs in the deeply buried Permian fan delta conglomerates are a result of a chronological combination of four important geological processes. A synthetic and succinct genetic model for generation of the high-quality reservoirs was proposed through integration of sedimentary features and diagenetic processes (Figure 16). Sediments in the fan delta plain subfacies were cemented first in the initial subsidence period primarily by some heulandite-Ca and early calcite cements at approximately 50–60°C (122–140°F) (Figure 16B), whereas simultaneously, sediments in the fan delta front subfacies were cemented by large amounts of laumontite, retarding compaction effectively during the subsequent deep burial (Figure 16B). Second, large amounts of laumontite and some feldspars in

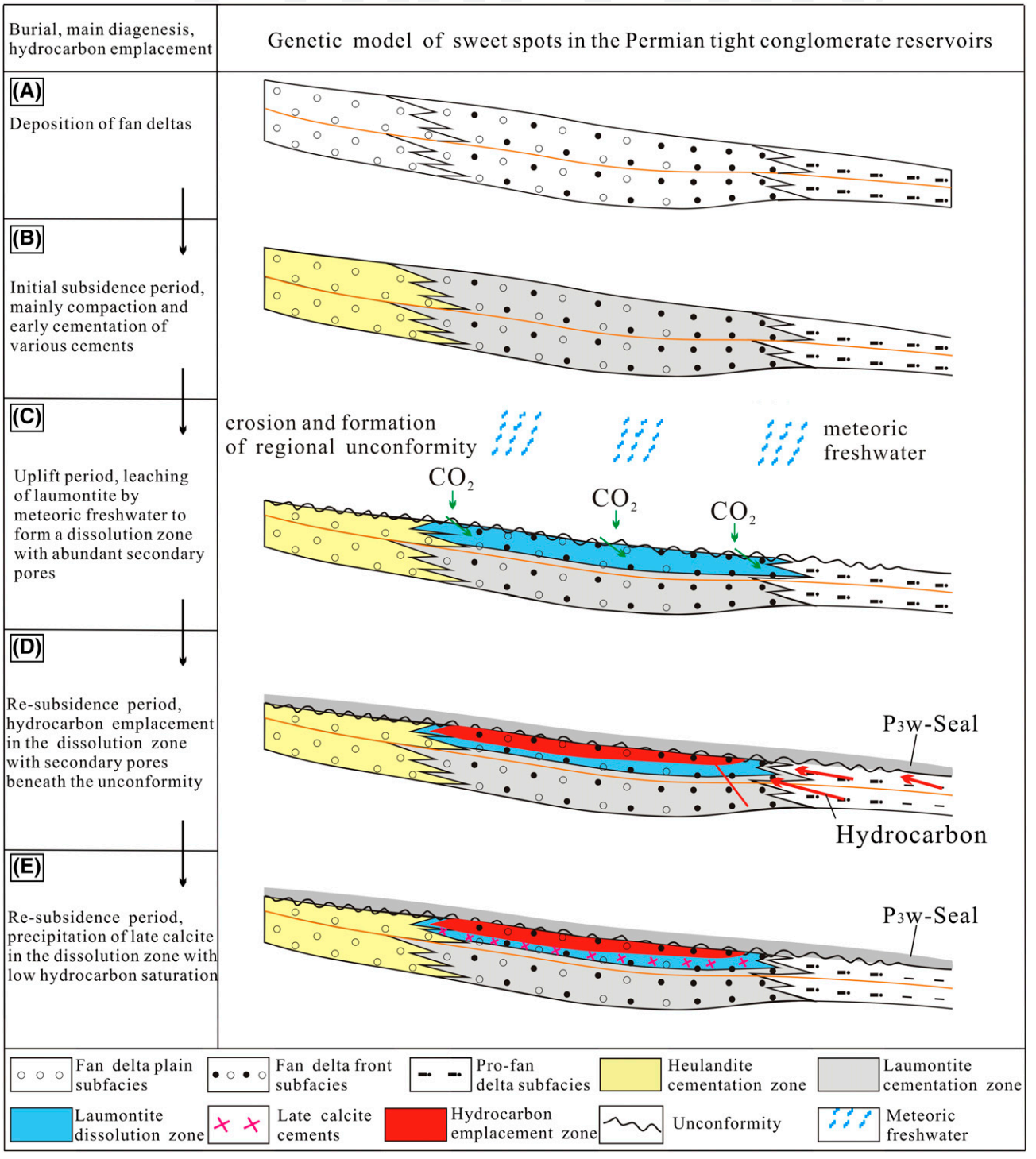

Q:20 Figure 16. Genetic model of the high-quality reservoir in the Permian fan delta tight conglomerates in the Zhongguai area, Junggar Basin. Note: A color version can be seen in the online version.

reservoirs of the fan delta front subfacies were selectively dissolved by meteoric freshwater to form secondary pores (Figures 9; 10A, B; 15) during formation of the regional unconformity in the uplift period. Heulandite-Ca cements in fan delta plain subfacies, however, were not dissolved, evidently (Figure 16C). Third, P_3w mudstones were deposited on top of the unconformity in the resubmission period, serving as a regional seal for reservoir traps (Figure 16D). Hydrocarbon emplacement then occurred, and hydrocarbons were trapped in the reservoirs beneath the unconformity and occupied large amounts of secondary pores (Figure 16D) (Chen et al., 2014). Finally, during the subsequent burial stage, calcite was formed in reservoirs with secondary pores but limited hydrocarbon, whereas the calcite cementation reaction was retarded in the reservoirs with large amount of hydrocarbons (Figure 16E) (Marchand et al., 2001; Wang, 2010), and the secondary pores in these hydrocarbon-saturated reservoirs were effectively preserved to present. Thus, exploration targets should then focus on medium- to coarse-grained sandstones, pebbly sandstones, and fine-grained conglomerates in the fan delta front subfacies and beneath the unconformity based on the comprehensive studies.

The Jiamuhe Formation in the Zhongguai area developed on the southeastern downdip slope with a large strata angle. The vertical distribution of medium- to coarse-grained sandstones, pebbly sandstones, and fine-grained conglomerates in the fan delta front subfacies and beneath the unconformity probably spans thousands of meters (Figures 1D, 11). With less than 30 exploration wells and relatively limited cores, the available tested core porosity data show the development of anomalously high porosity at two separate depth intervals (3200–4200 m [10,500–13,800 ft] and 4500–4900 m [14,800–16,100 ft]) (Figure 4). From 4200 to 4500 m (10,500 to 14,800 ft), however, there are still no core samples beneath the unconformity available, leading to the lack of anomalously high porosity in such a depth interval in Figure 4. As the high-quality reservoirs beneath the regional unconformity developed in the downdip Jiamuhe Formation (Figure 16), such high-quality reservoirs probably exist at the depth interval of 4200–4500 m (13,800–14,800 ft) (Figure 9) and may even expand the anomalously high porosity to much deeper depth in the study area.

CONCLUSION

1. The Permian tight conglomerate reservoirs, texturally and compositionally immature, are primarily litharenites and feldspathic litharenites. The Permian tight reservoirs experienced compaction and precipitation of chlorite clays, calcite, and zeolite in the initial subsidence stage; dissolution of unstable minerals including analcites, laumontites, and some feldspars and rock fragments and precipitation of iron oxides from interactions with oxidized meteoric water in the late Permian uplift stage; and compaction, dissolution of aluminosilicate minerals, and precipitation of kaolinite, quartz, and late calcite in the resubsidence stage.
2. The reservoirs exhibit a wide range of porosity mainly from 2% to 18% and permeability from 0.001 to 25 md. Few visible pores were identified in low-porosity tight sandstones because of extensive compaction and/or cementation, whereas secondary pores formed by dissolution of mainly laumontite, and some grains dominate the reservoir spaces in rocks with anomalously high porosity.
3. Generation of high-quality reservoirs in buried tight conglomerates originated from a chronological combination of four favorable geological processes. The prioritized exploration targets should be the medium- to coarse-grained sandstones, pebbly sandstones, and fine-grained conglomerates in the fan delta front subfacies and beneath the regional Permian unconformity.

REFERENCES CITED

Aase, N. E., and O. Walderhaug, 2005, The effect of hydrocarbons on quartz cementation: Diagenesis in the Upper Jurassic sandstones of the Miller Field, North Sea, revisited: Petroleum Geoscience, v. 11, p. 215–223, doi: 10.1144/1354-079304-648.

Bloch, S., R. H. Lander, and L. Bonnell, 2002, Anomalously high porosity and permeability in deeply buried sandstone reservoirs: Origin and predictability: AAPG Bulletin, v. 86, no. 2, p. 301–328.

Cao, Y., G. Yuan, X. Li, Y. Wang, K. Xi, X. Wang, Z. Jia, and T. Yang, 2014, Characteristics and origin of abnormally high porosity zones in buried Paleogene clastic reservoirs in the Shengtuo area, Dongying Sag, east China: Petroleum Science, v. 11, p. 346–362, doi:10.1007/s12182-014-0349-y.

Chen, Z., Y. Cao, Z. Ma, and Y. Zhen, 2014, Geochemistry and origins of natural gases in the Zhongguai area of Junggar Basin, China: Journal of Petroleum Science Engineering, v. 119, p. 17–27, doi:10.1016/j.petrol.2014.05.007.

Chen, Z., Y. Cao, X. Wang, L. Qiu, Y. Tang, and G. Yuan, 2016, Oil origin and accumulation in the Paleozoic Chepaizi–Xinguang field, Junggar Basin, China: Journal of Asian Earth Sciences, v. 115, p. 1–15, doi:10.1016/j.jseaes.2015.09.019.

Dutton, S. P., and R. G. Loucks, 2010a, Diagenetic controls on evolution of porosity and permeability in lower Tertiary Wilcox sandstones from shallow to ultradeep (200–6700m) burial, Gulf of Mexico Basin, U.S.A.: Marine and Petroleum Geology, v. 27, p. 69–81, doi:10.1016/j.marpetgeo.2009.08.008.

Dutton, S. P., and R. G. Loucks, 2010b, Reprint of: Diagenetic controls on evolution of porosity and permeability in lower Tertiary Wilcox sandstones from shallow to ultradeep (200–6700m) burial, Gulf of Mexico Basin, U.S.A.: Marine and Petroleum Geology, v. 27, p. 1775–1787, doi:10.1016/j.marpetgeo.2009.12.010.

Egeberg, P. K., and P. Aagaard, 1989, Origin and evolution of formation waters from oil fields on the Norwegian shelf: Applied Geochemistry, v. 4, p. 131–142, doi:10.1016/0883-2927(89)90044-9.

Emery, D., K. J. Myers, and R. Young, 1990, Ancient subaerial exposure and freshwater leaching in sandstones: Geology, v. 18, p. 1178–1181, doi:10.1130/0091-7613(1990)018<1178:ASEAFL>2.3.CO;2.

Falvey, D. A., and M. F. Middleton, 1981, Passive continental margins evidence for a prebreakup deep crustal metamorphic subsidence mechanism: Oceanlogica Acta, p. 103–114.

França, A. B., L. M. Araújo, J. B. Maynard, and P. E. Potter, 2003, Secondary porosity formed by deep meteoric leaching: Botucatu eolianite, southern South America: AAPG Bulletin, v. 87, no. 7, p. 1073–1082, doi:10.1306/02260301071.

Frape, S. K., P. Fritz, and R. T. McNutt, 1984, Water-rock interaction and chemistry of groundwaters from the Canadian Shield: Geochimica et Cosmochimica Acta, v. 48, p. 1617–1627, doi:10.1016/0016-7037(84)90331-4.

Fu, G., M. Dong, Z. Zhang, L. Sun, and R. Pan, 2010, Formation process and distribution of laumontite in Yanchang 3 reservoir of Fuxian exploration area in North Shanxi Province and the controls of the high quality reservoirs: Earth Science—Journal of China University of Geosciences, v. 35, p. 107–114.

Giles, M. R., 1987, Mass transfer and problems of secondary porosity creation in deeply buried hydrocarbon reservoirs: Marine and Petroleum Geology, v. 4, p. 188–204, doi:10.1016/0264-8172(87)90044-4.

Giles, M. R., and R. B. De Boer, 1990, Origin and significance of redistributional secondary porosity: Marine and Petroleum Geology, v. 7, p. 378–397, doi:10.1016/0264-8172(90)90016-A.

Grant, N. T., A. J. Middleton, and S. Archer, 2014, Porosity trends in the Skagerrak Formation, Central Graben, United Kingdom Continental Shelf: The role of compaction and pore pressure history: AAPG Bulletin, v. 98, no. 6, p. 1111–1143, doi:10.1306/10211313002.

Guo, X., K. Liu, S. He, G. Song, Y. Wang, X. Hao, and B. Wang, 2012, Petroleum generation and charge history of the northern Dongying Depression, Bohai Bay Basin, China: Insight from integrated fluid inclusion analysis and basin modelling: Marine and Petroleum Geology, v. 32, p. 21–35, doi:10.1016/j.marpetgeo.2011.12.007.

Higgs, K. E., H. Zwingmann, A. G. Reyes, and R. H. Funnell, 2007, Diagenesis, porosity evolution, and petroleum emplacement in tight gas reservoirs, Taranaki Basin, New Zealand: Journal of Sedimentary Research, v. 77, p. 1003–1025, doi:10.2110/jsr.2007.095.

Huang, S., P. Huang, Q. Wang, Y. Liu, M. Wu, and M. Zou, 2007, The significance of cementation in porosity preservation in deep-buried sandstone: Lithologic Reservoirs, v. 19, p. 7–13.

Jia, Z. Z., C. Y. Lin, L. H. Ren, and C. M. Dong, 2016, Selective dissolution of eodiagenesis cements and its impact on the quality evolution of reservoirs in the Xing'anling Group, Suderte Oil Field, Hailar Basin, China: Petroleum Science, v. 13, p. 402–417, doi:10.1007/s12182-016-0110-9.

Lai, J., G. Wang, Y. Ran, and Z. Zhou, 2015, Predictive distribution of high-quality reservoirs of tight gas sandstones by linking diagenesis to depositional facies: Evidence from Xu-2 sandstones in the Penglai area of the central Sichuan basin, China: Journal of Natural Gas Science and Engineering, v. 23, p. 97–111, doi:10.1016/j.jngse.2015.01.026.

Lai, J., G. Wang, Y. Ran, Z. Zhou, and Y. Cui, 2016, Impact of diagenesis on the reservoir quality of tight oil sandstones: The case of Upper Triassic Yanchang Formation Chang 7 oil layers in Ordos Basin, China: Journal of Petroleum Science Engineering, v. 145, p. 54–65, doi:10.1016/j.petrol.2016.03.009.

Li, P., Y. Zhou, F. Hao, J. Tian, and D. Tong, 2006, Restoration of eroded strata thickness in Cretaceous/Jurassic unconformity in hinterland of Junggar Basin (in Chinese with English abstract): Acta Petrolei Sinica, v. 27, p. 34–38.

Ma, D., D. He, D. Li, J. Tang, and Z. Liu, 2015, Kinematics of syn-tectonic unconformities and implications for the tectonic evolution of the Hala'alat Mountains at the northwestern margin of the Junggar Basin, Central Asian Orogenic Belt: Geoscience Frontiers, v. 6, p. 247–264, doi:10.1016/j.gsf.2014.07.004.

Marchand, A. M. E., R. S. Haszeldine, P. C. Smalley, C. I. Macaulay, and A. E. Fallick, 2001, Evidence for reduced quartz-cementation rates in oil-filled sandstones: Geology, v. 29, p. 915–918, doi:10.1130/0091-7613(2001)029<0915:EFRQCR>2.0.CO;2.

Marchand, A. M. E., P. C. Smalley, R. S. Haszeldine, and A. E. Fallik, 2002, Note on the importance of hydrocarbon fill for reservoir quality prediction in sandstones: AAPG Bulletin, v. 86, no. 9, p. 1561–1571.

Nguyen, B. T. T., S. J. Jones, N. R. Goulty, A. J. Middleton, N. Grant, A. Ferguson, and L. Bowen, 2013, The role of fluid pressure and diagenetic cements for porosity preservation in Triassic fluvial reservoirs of the Central Graben, North Sea: AAPG Bulletin, v. 97, no. 8, p. 1273–1302, doi:10.1306/01151311163.

Olson, J. E., S. E. Laubach, and R. H. Lander, 2009, Natural fracture characterization in tight gas sandstones: Integrating mechanics and diagenesis: AAPG Bulletin, v. 93, no. 11, p. 1535–1549, doi:10.1306/08110909100.

Pittman, E. D., and R. E. Larese, 1991, Compaction of lithic sands: Experimental results and applications: AAPG Bulletin, v. 75, no. 8, p. 1279–1299.

Qiu, N., M. Zha, and X. Wang, 2000, Simulation of geothermal evolution history in Junggar Basin: Xinjiang: Petroleum Geology, v. 21, p. 38–41.

Sun, Y., X. Liu, Y. Zhang, W. Dong, Y. Xu, G. Shi, Y. Lin, and A. Li, 2014, Analcite cementation facies and forming mechanism of high-quality secondary clastic rock reservoirs in western China: Journal of Palaeogeography, v. 16, p. 517–526.

Tang, Z., P. John, and F. J. Longstaffe, 1997, Diagenesis and reservoir potential of Permian–Triassic fluvial/lacustrine sandstones in the southern Junggar Basin, northwestern China 1: AAPG Bulletin, v. 81, no. 11, p. 1843–1865.

Taylor, T. R., M. R. Giles, L. A. Hathon, T. N. Diggs, N. R. Braunsdorf, G. V. Birbiglia, M. G. Kittridge, C. I. Macaulay, and I. S. Espejo, 2010, Sandstone diagenesis and reservoir quality prediction: Models, myths, and reality: AAPG Bulletin, v. 94, no. 8, p. 1093–1132, doi:10.1306/04211009123.

Tobin, R. C., T. McClain, R. B. Lieber, A. Ozkan, L. A. Banfield, A. M. E. Marchand, and L. E. McRae, 2010, Reservoir quality modeling of tight-gas sands in Wamsutter field: Integration of diagenesis, petroleum systems, and production data: AAPG Bulletin, v. 94, no. 8, p. 1229–1266, doi:10.1306/04211009140.

Van der Plas, L., and A. C. Tobi, 1965, A chart for judging the reliability of point counting results: American Journal of Science, v. 263, p. 87–90, doi:10.2475/ajs.263.1.87.

Wan, M., 2011, Causes of Permian dense conglomerate reservoir and favorable block prediction in Zhongguai Bulge (in Chinese): Xinjiang Oil and Gas, v. 7, p. 17–20.

Wang, Y. Z., 2010, Genetic mechanism and evolution model of secondary pore development zone of Paleogene in the North Zone in Dongying Depression (in Chinese with English abstract), Ph.D. thesis, China University of Petroleum (Huadong), Qingdao, China, 141 p.

Yuan, G., Y. Cao, Z. Jia, J. Gluyas, T. Yang, Y. Wang, and K. Xi, 2015a, Selective dissolution of feldspars in the presence of carbonates: The way to generate secondary pores in buried sandstones by organic CO_2: Marine and Petroleum Geology, v. 60, p. 105–119, doi:10.1016/j.marpetgeo.2014.11.001.

Yuan, G. H., Y. C. Cao, K. L. Xi, Y. Z. Wang, X. Y. Li, and T. Yang, 2013, Feldspar dissolution and its impact on physical properties of Paleogene clastic reservoirs in the northern slope zone of the Dongying sag (in Chinese with English abstract): Acta Petrolei Sinica, v. 34, p. 853–866.

Yuan, G. H., J. Gluyas, Y. C. Cao, N. H. Oxtoby, Z. Z. Jia, Y. Z. Wang, K. L. Xi, and X. Y. Li, 2015b, Diagensis and reservoir quality evolution of the Eocene sandstones in teh northern Dongying Sag, Bohai Bay Basin, east China.: Marine and Petroleum Geology, v. 62, p. 77–89, doi:10.1016/j.marpetgeo.2015.01.006.

Zhang, X., S. Huang, Y. Lan, K. Huang, and R. Liang, 2011, Thermaldynamic calculation of laumontite dissolution and its geologic significance: Lithologic Reservoirs, v. 23, p. 64–69.

Zhou, Z., C. Pan, S. Fan, and L. Han, 1989, Geothermal characteristics of the Junggar Basin and its significance to oil searching: Xinjiang Petroleum Geology, v. 10, p. 67–74.

Zhu, S., X. Zhu, X. Wang, and Z. Liu, 2012, Zeolite diagenesis and its control on petroleum reservoir quality of Permian in northwestern margin of Junggar Basin, China: Science China. Earth Sciences, v. 55, p. 386–396, doi:10.1007/s11430-011-4314-y.

Zhu, X. M., Y. G. Wang, D. K. Zhong, Q. Zhang, Z. H. Zhang, S. W. Zhang, and X. X. Lv, 2007, Pore types and secondary pore evolution of Paleogene reservoir in the Jiyang Sag (in Chinese with English abstract): Acta Geologica Sinica, v. 81, p. 197–204.

Proof Only

AUTHOR QUERIES

AUTHOR PLEASE ANSWER ALL QUERIES 1

Q:1 Please confirm or amend short title "Sweet Spots in Tight Reservoirs" at the bottom of page 2.

Q:2 If you have chosen to publish figures in color online, please review the print version of the proof on the following pages for accuracy and clarity of BW figures. If changes are needed, please upload revised BW versions of the figures or annotate for minor text corrections. There is no need to reannotate your other corrections on this second version of the proof.

Q:3 Please provide street address for all author affiliations.

Q:4 In the sentence "Global basin studies reveal that in specific geological conditions…," please specify whether Dutton and Loucks (2010a) or (2010b) is meant.

Q:5 In the sentence "Fifteen samples were identified using a Quanta200 scanning…," please spell out "EDAX."

Q:6 In the sentence "Accurate evaluation of burial and thermal history requires knowledge of parameters including…," semicolons have been added to distinguish between the subgroups within the list of parameters. Please check.

Q:7 In the sentence "Reservoir quality evolution may be a function of several controls…," please specify whether Dutton and Loucks (2010a) or (2010b) is meant.

Q:8 Where not already done, please include English unit equivalents in parentheses after all metric measurements in the text, figures, and tables.

Q:9 In the sentence "The Jiamuhe Formation in the Zhongguai area developed on the southeastern downdip…," "strara angle" was changed to "strata angle." Please confirm.

Q:10 Reference "Dutton, Loucks, 2010a" is not cited in the text. Please check the reference and the citations.

Q:11 Please provide volume number for Falvey and Middleton (1981).

Q:12 For the latitude and longitude in the maps in Figure 1, please specify north, south, east, or west.

Q:13 In the caption of Figure 1, please define all of the stratigraphic abbreviations (K, P_3w, etc.).

Q:14 In the caption of Figure 3, please provide complete reference information for Folk et al. (1970).

Q:15 In the caption of Figure 4, please define "P_1j_2-1," "P_1j_2-2," and "P_1j_2-3."

Q:16 In the caption of Figure 6, please define C, P, T, J, K, Pal, N, P_1j_2, and P_3w.

AUTHOR QUERIES

AUTHOR PLEASE ANSWER ALL QUERIES 2

Q:17 In the caption of Figure 8, "SEM" has been spelled out as "scanning electron microscope." Please confirm.

Q:18 In the caption of Figure 8, "K" has been defined as "kaolinite." Please confirm.

Q:19 Please provide caption descriptions for parts A–D in Figure 14.

Q:20 In the caption of Figure 16, please define "P_3w."

Q:21 In the legend of Table 2, please define "P_1j," "P_3w," "K," "Q," "J," and "T."

Genetic mechanism of high-quality reservoirs in Permian tight fan delta conglomerates at the northwestern margin of the Junggar basin, northwestern China

Guanghui Yuan, Yingchang Cao, Longwei Qiu, and Zhonghong Chen

ABSTRACT

Fan delta conglomerate reservoirs in the Permian Jiamuhe Formation in the Zhongguai area at the northwestern margin of the Junggar Basin, northwestern China, are reservoirs for large accumulations of natural tight gas. The tight conglomerates and sandstones are mainly litharenites with a large amount of texturally and compositionally immature volcanic clastic materials. Core porosities demonstrate the development of anomalously high porosities at depths of 3200–4200 m (10,500–13,800 ft) and 4500–4900 m (14,800–16,100 ft). The Permian reservoirs experienced initial rapid subsidence, uplift, and further subsidence, and diagenetic reactions occurred in these reservoirs involving compaction; precipitation of chlorite clays, calcites, zeolites, iron oxides, kaolinite, and quartz cements; and dissolution of unstable minerals including analcite, laumontite, feldspars, and rock fragments. Low-porosity reservoirs, with extensive compaction and (or) cementation of calcite and heulandite-Ca, consist of only few visible secondary pores formed by dissolution of feldspars and rock fragments. Reservoirs with anomalously high porosity, however, experienced relatively weak compaction and contain significant amounts of secondary pores formed by dissolution of mainly laumontites, some feldspars, and rock fragments. Comprehensive studies of sedimentary features and diagenesis of the reservoirs indicate that these anomalously high porosities originate from chronological coupling of four important geological processes. (1) Sedimentary facies and detrital compositions controlled

Manuscript received November 1, 2015; provisional acceptance November 1, 2015; revised manuscript received December 7, 2016; final acceptance February 7, 2017.
DOI:10.1306/02071715214

AUTHORS

GUANGHUI YUAN ~ *Geology Department, School of Geosciences, China University of Petroleum, Qingdao 266580, China; yuan.guanghui86@gmail.com*

Guanghui Yuan is now a postdoctor at China University of Petroleum. His research focuses on sandstone diagenesis, reservoir quality prediction, and hydrocarbon work–rock interactions.

YINGCHANG CAO ~ *Geology Department, School of Geosciences, China University of Petroleum, Qingdao 266580, China; caoych@upc.edu.cn*

Yingchang Cao is a professor at China University of Petroleum. His research interests lie in the fields of sequence stratigraphy, sedimentology, and sandstone reservoir quality prediction.

LONGWEI QIU ~ *Geology Department, School of Geosciences, China University of Petroleum, Qingdao 266580, China; qiulwsd@163.com*

Longwei Qiu is a professor at China University of Petroleum. His research interests lie in the fields of sedimentology, diagenesis, and reservoir geology.

ZHONGHONG CHEN ~ *Resource Department, School of Geosciences, China University of Petroleum, Qingdao 266580, China; hongczh@163.com*

Zhonghong Chen is a professor at China University of Petroleum. His research interests lie in the fields of geochemistry, fluid flow in sedimentary basins, and hydrocarbon accumulation mechanisms.

ACKNOWLEDGMENTS

This study was financially supported by the Natural Science Foundation of China projects U1262203 and 41602138, a National Science and Technology special grant (2016ZX05006-007), the National Basic Research Program of China (973 Program) (E1401004B), China Postdoctoral Science Foundation (2015M580617), and Shandong postdoctoral innovation project 201502028. We also thank Xinjiang Oilfield Company of PetroChina for

providing of all the related core samples and some geological data of Junggar Basin. AAPG Editors Barry J. Katz and Michael L. Sweet, AAPG consulting geologist Frances P. Whitehurst, and two other anonymous reviewers are thanked for their constructive comments and advice.

EDITOR'S NOTE

Color versions of Figures 1–16 can be seen in the online version of this paper.

distribution of various zeolites in reservoirs, with abundant laumonites developed in reservoirs in the fan delta front subfacies. (2) Early precipitation of the laumontites inhibited compaction during deep burial; however, they provided unstable minerals for secondary porosity development. (3) The Permian reservoirs experienced subaerial exposure erosion during the uplift stage, and meteoric freshwater leached laumontite cements and aluminosilicate grains to form secondary pores in reservoirs beneath the unconformity. (4) Hydrocarbon emplacement at relative shallow depth during a second subsidence period preserved the secondary pores in reservoirs by retarding late carbonate cementation.

INTRODUCTION

Hydrocarbon exploration targets in deeply buried tight reservoirs are growing increasingly significant as most shallow petroleum reservoir exploration has been accomplished in the last few decades (Bloch et al., 2002; Higgs et al., 2007; Olson et al., 2009; Dutton and Loucks, 2010b; Cao et al., 2014; Chen et al., 2014). Global basin studies reveal that in specific geological conditions, deeply buried reservoirs may still be effective for accumulation and production of hydrocarbon and in particular that some areas exhibit unexpectedly high porosity and permeability at substantial burial depth (Bloch et al., 2002; Dutton and Loucks, 2010; Cao et al., 2014). Studies of the origin and distribution of high quality reservoirs are of great significance for accurate prediction of sweet spots in deeply buried tight reservoirs with low porosity and permeability (Higgs et al., 2007; Cao et al., 2014; Grant et al., 2014; Lai et al., 2015, 2016; Yuan et al., 2015b; Jia et al., 2016).

Tight gas plays have recently received considerable attention resulting from strength in the gas market and technology improvement; thus, possibilities for previously noncommercial gas accumulations have been explored (Higgs et al., 2007; Olson et al., 2009; Lai et al., 2015). Conglomerate reservoirs in the Permian Jiamuhe Formation are typical tight reservoirs with approximately 90% of the tested core permeability lower than 1 md. The conglomerate reservoirs in the Jiamuhe Formation of the Zhongguai area located in the northwestern margin of Junggar Basin are currently significant exploration targets for tight gas plays with exceptional natural potential (Wan, 2011; Chen et al., 2014, 2016). Volcanic lithic rock fragments (mainly tuff clasts and andesite clasts) dominate the detrital grains, and various zeolites are significant cements in these reservoirs. Core porosity data demonstrate the development of anomalously high porosities at depths of 3200–4200 m (10,500–13,800 ft) and 4500–4900 m (14,800–16,100 ft). Great successes have been achieved in oil–gas

exploration in these Jiamuhe conglomerate reservoirs with relative high porosity in recent years. For example, well C67, well C501, well C502, well XG1, well G3, and well G9 all obtained stable yields after formation fracture (Figure 1C). To date, however, the genetic mechanism of such anomalously high porosity is still unclear.

The purpose of this article is to (1) investigate petrography and disgenesis of the Permian tight conglomerate reservoirs, (2) identify types of pores in reservoirs with anomalously high porosity and low porosity, and (3) analyze genetic mechanisms of the high-quality reservoirs in the tight conglomerates. The results of this study can aid hydrocarbon exploration in the study area and other similar tight reservoirs in global basins.

GEOLOGICAL BACKGROUND

The Junggar Basin is a petroliferous basin in the northwestern China (Figure 1A), covering an area of approximately 13×10^4 km^2 (50,000 mi^2), and is surrounded by mountains including Yilinheibiergen Mountains in the south, Halalate Mountains in the north, Zhayier Mountains in the west, and Kelameili Mountains in the east (Chen et al., 2014) (Figure 1B). The Zhongguai area is located at the northwestern margin of the Junggar Basin (Figure 1B), with Hongche fault to the west, Hong3 well fault to the north, Penyijingxi sag to the east, and Shawan sag to the south (Figure 1C). The Zhongguai area is positionally favorable for gathering hydrocarbons from the Shawan sag and the Penyijingxi sag (Chen et al., 2014, 2016), and reservoirs in the Permian Jiamuhe Formation have a natural gas resource of approximately 148×10^8 m^3 (5226×10^8 ft^3)(Wan, 2011).

Sediments filled in the Zhongguai area comprise the Carboniferous, Permian, Triassic, Jurassic, Cretaceous, Paleogene, Neogene, and Quaternary (Figure 1D) (Ma et al., 2015). The Permian consists of the Jiamuhe (P_1j), Fengcheng (P_1f), Xiazijie (P_2x), and Wuerhe (P_2w and P_3w) Formations from base to top (Figure 1D). Formations in the Shawan sag are currently complete, whereas most of the P_1f, P_2x, and P_2w Formations have been eroded to form a regional unconformity in the Zhongguai area in the upper Permian (Figure 1D). The P_3w with thick mudstones was deposited on top of the unconformity, serving as a regional seal (Chen et al., 2014, 2016). The Jiamuhe Formation is divided into two members, P_1j_1 and P_1j_2 (from base to top), and is a downdip stratum with burial depth ranging from approximately 2.0 km (1.2 mi) at the northwest to 7.0 km (4.3 mi) at the southeast part of the Zhongguai area (Figure 1D). This study focuses on the P_1j_2 member in the Zhongguai area where drilling wells are available and sediments deposited are typically fan deltas composed of fan delta plain, fan delta front, and profan delta subfacies (Wan, 2011). The P_1j_2 member is subdivided into three submembers, P_1j_2-1, P_1j_2-2, and P_1j_2-3, from top to base (Figure 1D).

METHODS AND DATABASE

Data collected from the Geological Scientific Research Institute of PetroChina Xinjiang Oilfield Company included rock composition data of 260 thin section samples, 1030 porosity and permeability core data, well log porosity data of five wells (XG1, XG2, G3, G13, and G201), 116 formation temperature data, and 21 pore water data. The core porosity and permeability were analyzed using CMS^{tm}-300 Core Measurement system with a confining pressure of 6 MPa. The well log porosity data were interpreted with acoustic time logging, bulk density logging, and compensated neutron logging.The pore water chemistry data were tested with a 930 Compact ion chromatograph. The distribution histograms of core porosity over every 200-m (656-ft) depth interval were plotted to identify the normal porosity subpopulation and the anomalously high porosity subpopulation (Bloch et al., 2002). The compaction porosity curve was obtained by connecting the maximum porosity of the normal subpopulation of porosities at different depth intervals.

Samples for this study were selected from the Permian cores of 16 wells (Figure 1C), at positions where porosity and permeability data are available. One hundred and twenty blue epoxy resin-impregnated thin sections were prepared for analysis of rock mineralogy, diagenesis, and porosity. Point counts were performed on thin sections for the content of detrital grains with at least 300 points, which can provide a standard deviation of 6% or less (Van der Plas and Tobi, 1965). For the amount of secondary pores and cements,

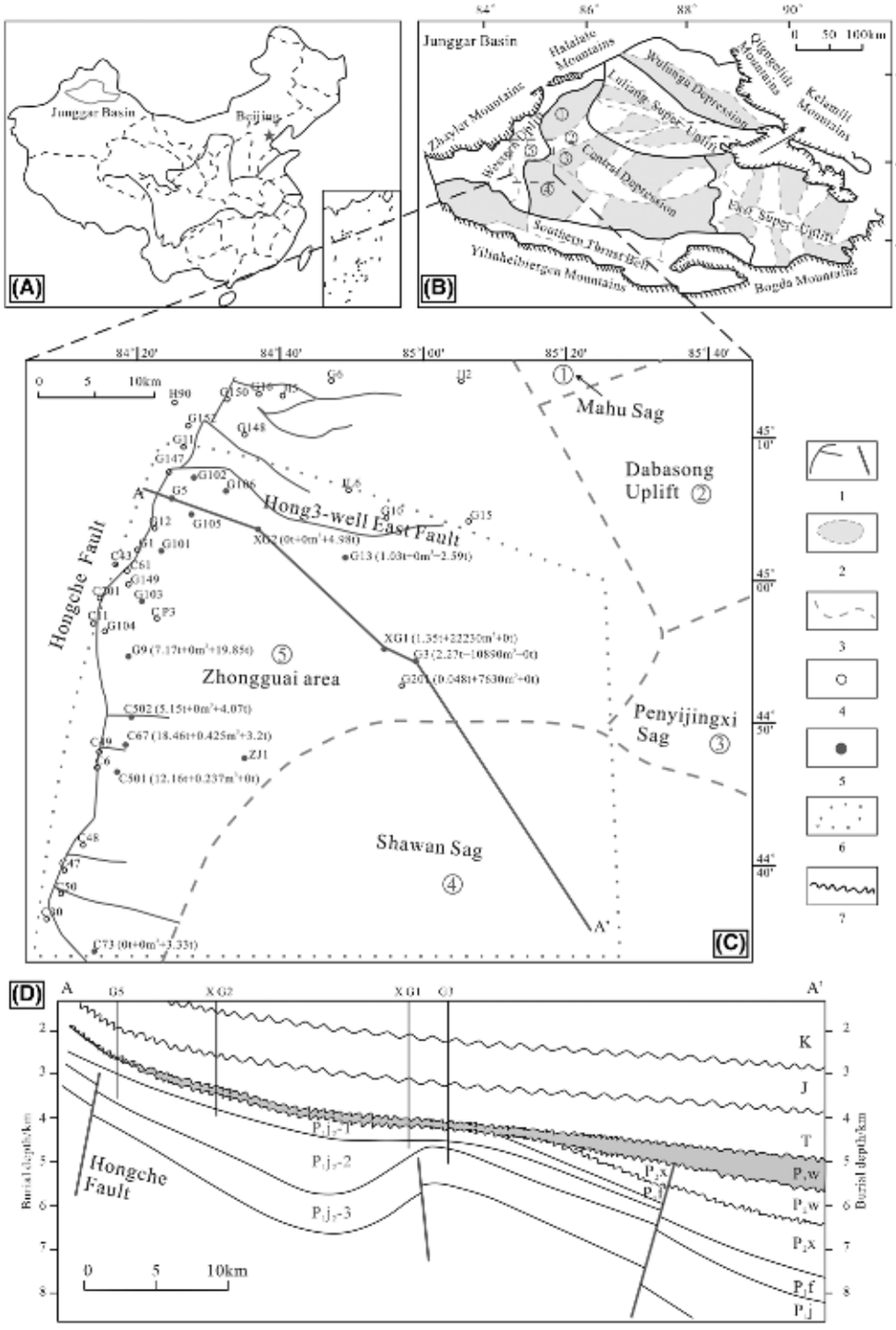

Figure 1. (A) Location map showing geographic location of the Junggar Basin in northwestern China. (B) Map showing subtectonic units of the Junggar Basin and location of the Zhongguai area. (C) Permian structural map and well location of the Zhongguai area and testing data (oil + gas + water/each day) of the Jiamuhe conglomerate reservoirs in some wells. (D) Northwest–southeast cross section showing strata profile of the Zhongguai area. (Modified from Chen et al., 2016, and used with permission of Elsevier.). Numbers indicate the following: 1 = fault; 2 = sag; 3 = boundary of tectonic units; 4 = well; 5 = wells with cores and sample analysis; 6 = boundary of the study area; 7 = unconformity. Note: A color version can be seen in the online version.

20 micrographs of each thin section were taken first using the Zeiss microscope. Objectives of 50× for these thin sections were used, and each micrograph has an area of 25.80 mm^2 (0.04 $in.^2$). Then the pores in each micrograph were identified under the microscope and were drawn on a computer screen using CorelDRAW, and the total areas of each target mineral and pore in every micrograph were obtained using Image-Pro Plus software. Finally, the contents of the target minerals and pores in each thin section were obtained by taking an average of all values in its micrographs (Yuan et al., 2015a). Fifteen samples were identified using a Quanta200 scanning electron microscope (SEM) combined with EDAX energy dispersive spectroscopy.

Burial and thermal histories of the Zhongguai area were studied using the BasinMod software (Guo et al., 2012), with knowledge of lithologies for various formations from exploration wells, the evolution of geothermal gradient data of the Junggar Basin from previous studies (Zhou et al., 1989; Qiu et al., 2000), and the eroded strata thickness. Thickness of eroded strata with unconformity was estimated by applying the ratios of reference sequence strata thickness method (Li et al., 2006) with seismic profiles and wells. Absolute ages of depositional and erosional events were defined with the chronostratigraphic framework of the Junggar Basin (Ma et al., 2015).

RESULTS

Lithofacies

Based on 350-m (1148-ft) cores from 16 wells in the Zhongguai area, the fan delta sediments were divided into seven main lithofacies (Table 1): (1) massive medium-grained conglomerates (Figure 2A, B); (2) fine-grained conglomerates with graded bedding or massive bedding (Figure 2C); (3) sandy conglomerates and pebbly sandstones with massive bedding, graded bedding, and parallel bedding (Figure 2D); (4) massive medium- to coarse-grained sandstones (Figure 2E); (5) fine sandstones with parallel bedding or cross-bedding (Figure 2F); (6) massive or laminated siltstones–shaly sandstones (Figure 2G); and (7) massive or laminated mudstones (Figure 2H). Samples for this study were selected mainly from lithofacies 2 and 3 and from lithofacies 4–6.

Petrography

The studied Permian conglomerate reservoirs are fine- to very coarse–grained (Figure 2). Rock samples for this study are texturally immature and typically range from fine-grained sandstones to fine-grained conglomerates, with some medium-grained conglomerates (Figure 2). Grain sorting is commonly poor, and roundness of most detrital grains ranges from subangular to subrounded. Sorting coefficient (σ) of rocks from lithofacies 2 and 3 are generally higher than 2.5, whereas σ of rocks from lithofacies 4–6 ranges mainly from 1.0 to 2.5. The rocks are primarily litharenite (Figure 3A), compositionally immature with an average framework composition of 3% quartz (Q), 4% feldspar (F), and 93% rock fragment (R) ($Q_3F_4R_{93}$). Detrital quartz grains are primarily monocrystalline, and their content ranges mainly from 0% to 10%. The content of detrital feldspars ranges from 0% to 15%, and K-feldspars account for 60%–70% of the feldspars. Volcanic lithic rock fragments, ranging from 83% to 100%, dominate the detrital grains and are composed mainly of tuff clasts and andesite clasts. Though most grains are subangular to subrounded, tuff clasts generally show subrounded to rounded shape, indicating transporting of these clasts from provenance area to deposition area.

Significant differences exist between the mineral compositions of reservoirs in the fan delta plain subfacies (Figure 3B, C) and the fan delta front subfacies (Figure 3D, E). On average, the rocks in the fan delta plain subfacies contain approximately 2% quartz, 5% feldspars, 50% tuff clasts, 30% andesite clasts, and 8% sedimentary rock debris (Figure 3B, C); authigenic cements include 1% calcite, 1% laumonite, 2%–3% heulandite-Ca, less than 0.5% analcite and 2% iron oxides, and matrix including 2% tuff matrix and 1% mud matrix. Rocks in the fan delta front subfacies, however, contain approximately 1%–2% quartz and feldspars, 15% tuff clasts, and 70% andesite clasts on average (Figure 3D, E); authigenic cements include an average of 8% laumonite and less than 1% calcite, and the content of matrix is less than 0.5%.

Table 1. Characterization of Different Lithofacies in the Permian Fan Delta in the Zhongguai Area, Junggar Basin

Lithofacies	Description	Depositional Environment
Lithofacies 1: medium-grained conglomerates	Sand-supported or mud-supported medium-grained conglomerates. This lithofacies comprises beds (1–20 m thick) of mixed gravels, sands, and muds. Sediments are generally angular and poorly sorted, with much matrix.	Fan delta plain subfacies.
Lithofacies 2: fine-grained conglomerates	One important lithofacies. Mainly sand-supported conglomerates, characterized by bed thickness ranges from a half to several meters. Sediments are generally subangular and poorly sorted, with little matrix.	Fan delta plain subfacies and fan delta front subfacies.
Lithofacies 3: sandy conglomerates and pebbly sandstones	Another important lithofacies. These rocks are composed mainly of fine-grained gravels and medium–coarse sand grains. Sediments are generally subangular to subrounded and moderately–poorly sorted, with little detrital clay. Some rocks contain graded bedding and parallel bedding, but most are massive. Amalgamated beds are several meters to tens of meters thick.	Braided channels in the fan delta front subfacies.
Lithofacies 4: medium- to coarse-grained sandstones	These rocks are composed mainly of medium and coarse sand grains and are rare in the sediments. Such sandstones are thin bedded, commonly less than 0.5 m.	Braided channels in the fan delta front subfacies.
Lithofacies 5: fine-grained sandstones	This lithofacies contains manily of fine-grained, subrounded, poorly sorted sediments, with massive matrix.	Marginal setting away from the main axis of sand input.
Lithofacies 6: siltstones–shaly sandstones	This lithofacies has fine-grained sandstones with abundant mudstone laminates; the siltstones generally have more detrital clays.	Marginal setting away from the main axis of sand input.
Lithofacies 7: mudstones	Laminated mudstone with occasional siltstones.	Out of channels with low hydrodynamic force.

The fine-grained conglomerate refers to the conglomerate with the size of gravels ranging mainly from 2 to 10 mm, the medium-grained conglomerate refers to gravel size from 10 to 100 mm, and the coarse-grained conglomerate refers to gravel size from 100 to 1000 mm.

Porosity and Permeability

The Permian conglomerate reservoirs exhibit a wide range of porosity from 2% to 18% and permeability from 0.001 to 25 md (Figures 4, 5). The compaction porosity curve and vertical distribution of all available core porosities demonstrate the development of anomalously porosities at depths of 3200–4200 m (10,500–13,800 ft) and 4500–4900 m (14,800–16,100 ft) (Figure 4A), with anomalously high permeability also existing at such depth intervals (Figure 4B). For porosity data in one individual well, however, there is no depth interal (e.g., well G5 and well G105) or just one depth interval with anomalously high porosity (e.g., well XG1 and well ZJ1) (Figure 4C–H).

The porosity versus permeability plots and distribution histograms of porosity and permeability data indicate that tight reservoirs with low porosity and

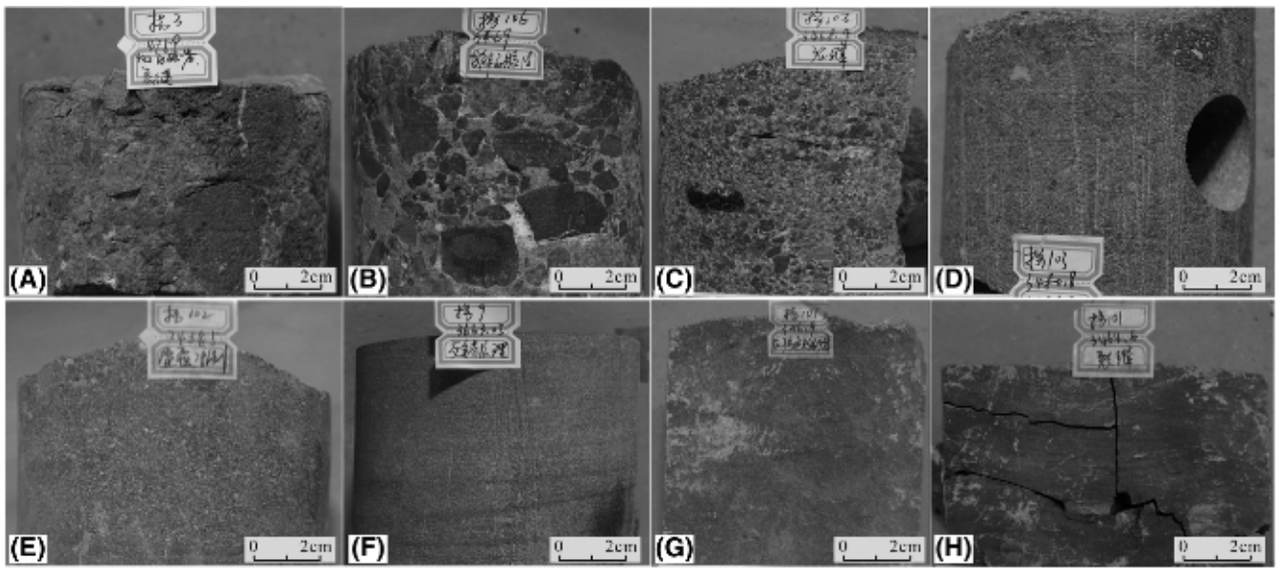

Figure 2. Different lithofacies in the Permian fan deltas in the Zhongguai area, Junggar Basin. (A) Massive medium-grained conglomerate, 4759 m, well G3. (B) Massive medium-grained conglomerate, 3469.0 m, well G106. (C) Amalgamated fine-grained conglomerate with graded bedding, 3468.9 m, G106. (D) Massive pebbly sandstone, 3480.8 m, well G103. (E) Massive medium- to coarse-grained sandstone, 3438.5 m, G102. (F) Fine-grained sandstone with crossing bedding, 3663.05 m, G9. (G) Siltstone, 3216.9 m, G101. (H) Gray mudstone, 3464.6 m, G101. Note: A color version can be seen in the online version.

ultralow permeability account for most of the reservoirs in the Zhuangguai area (Figure 5). Normal porosity subpopulation and anomalously high–porosity subpopulation, at depths of 3200–4200 m (10,500–13,800 ft), account for 72% and 28% of total porosities (Figure 5C), respectively, whereas at depths of 4500–4900 m (14,800–16,100 ft), normal porosity subpopulation and anomalously high–porosity subpopulation account for 15% and 85% of total porosities (Figure 5D), respectively. Generally, reservoirs in fan delta plain subfacies have relatively low porosity and permeability compared with reservoirs in fan delta front subfacies (Figure 5A, B).

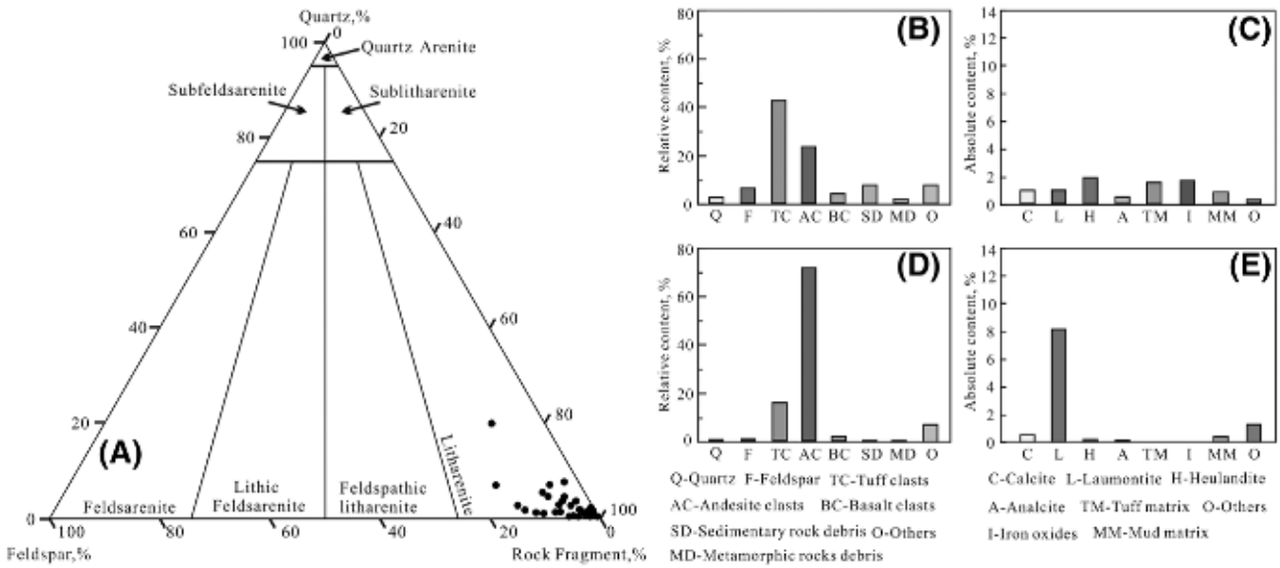

Figure 3. (A) Ternary plot showing rock compositions of the Permian conglomerate reservoirs in the Zhongguai area (refer to sandstone classification standard of Folk et al., 1970). (B–E) Histograms showing the content of various compositions in reservoirs in the delta plain subfacies (B, C) and the fan delta front subfacies (D, E). Note: A color version can be seen in the online version.

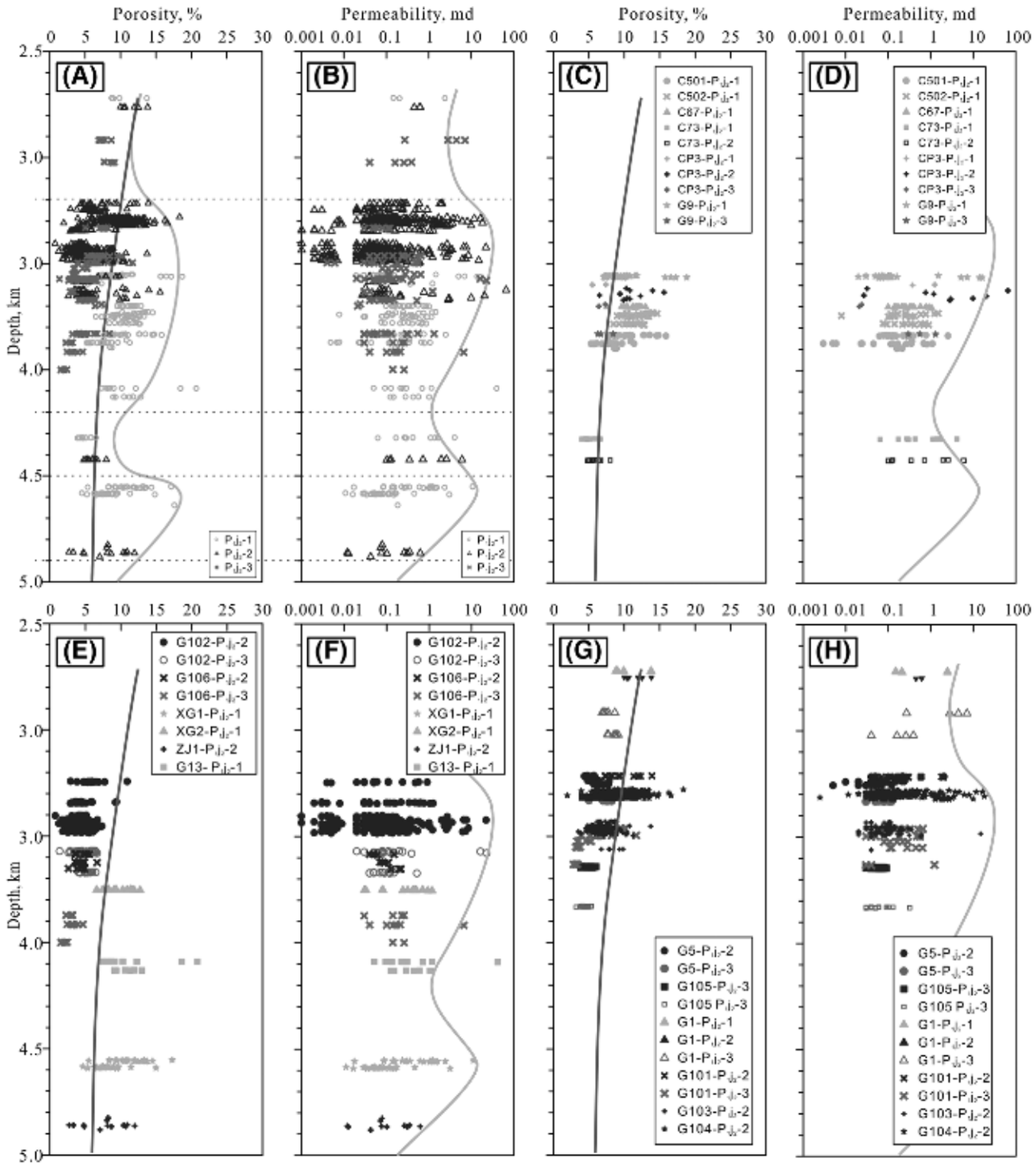

Figure 4. Vertical distribution of core porosity and core permeability of (A, B) all data from 19 wells and (C–H) some individual wells in the Jiamuhe Formation in the Zhongguai area. The blue curve represents the compaction porosity curve. Note: A color version can be seen in the online version.

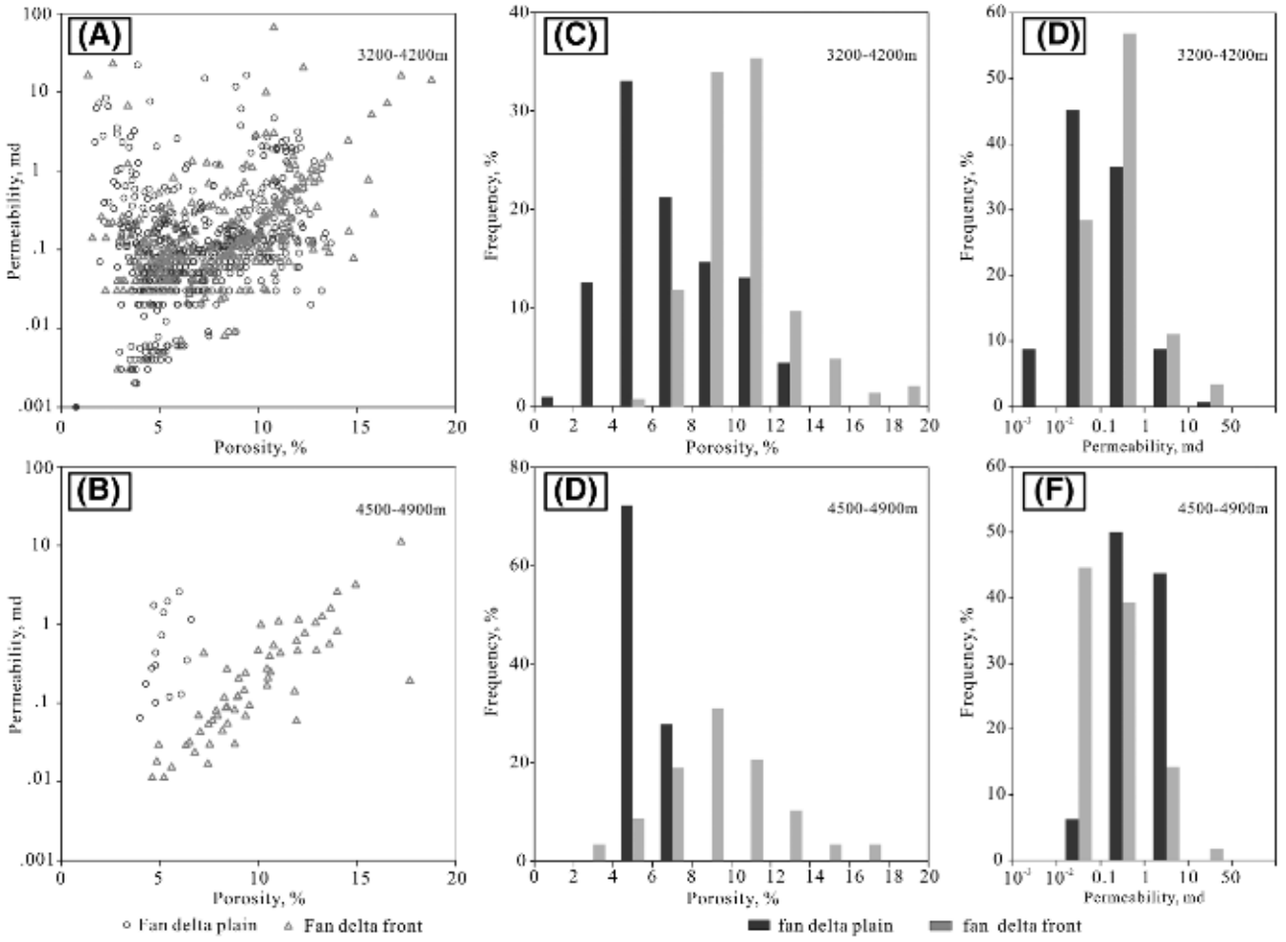

Figure 5. (A, B) Core porosity versus core permeability diagrams and histograms of (C, D) porosity and (E, F) permeability of the reservoirs in different subfacies in the fan deltas at depths of 3200–4200 m (10,499–13,780 ft) and 4500–4900 m (14,764–16,076 ft) in Zhongguai area. Note: A color version can be seen in the online version.

Burial and Thermal History

Accurate evaluation of burial and thermal history requires knowledge of parameters including lithology of various formations; geological ages; porosities, timing, duration, and thickness of erosion; and geothermal gradient data (Guo et al., 2012; Nguyen et al., 2013). Burial history of the Zhongguai area was investigated using one-dimensional (1-D) modeling of 10 wells. Detailed data on lithology, thickness, and start and end time of various formations of well XG1 are listed in Table 2. Porosity exerts significant influence on thermal conductivity and heat capacity of sediments closely related with thermal properties of a basin and maturation level of source rocks. Empirical relationships between porosity and initial porosity and burial depths are widely applied in basin modeling (Guo et al., 2012). The porosity–depth relationship for decompaction correction of Falvey and Middleton (1981) was adopted in this study (Falvey and Middleton, 1981), with initial porosity and compaction factors of a pure lithology adopted from default values in the BasinMod 1-D software and mixed lithologies created by specifying percentages of the pure lithologies for 1-D modeling of individual wells (Table 2).

The modeling results indicate a variable rate of burial from the Permian period to present (Figure 6) at different locations in the Zhongguai area. Burial history of the Zhongguai area in the Permian period overall consists of several stages, including rapid subsidence in the early Permian with sedimentation of P_1j, P_1f, P_2x, and P_2w; rapid uplift in the middle

Table 2. Input Parameters for the One-Dimensional Burial–Thermal History Modeling of Well XG1 in the Zhonguai Area

Start Time (Ma)	End Time (Ma)	Formation	Depth of Bottom Boundary (m [ft])	Depth of Top Boundary (m [ft])	Thickness (m [ft])	Erosion Thickness (m [ft])	Lithology			Temperature Gradient (°C/km [°F/mi])
							Sandstone	Siltstone	Mudstone	
145	0	K–Q	2409 (7903)	0	2409 (7903)	–	8%	20%	72%	19.5 (56.5)
164	145	Erosion	–	–	–	400 (1312)	–	–	–	30 (87)
205	164	J	3483 (11,427)	2409 (7903)	1074 (3523)	–	26%	19%	55%	
242	205	T	4394 (14,416)	3483 (11,427)	910 (2985)	–	14%	26%	60%	35 (101)
248	242	Erosion	–	–	–	350 (1148)	–	–	–	40 (116)
255	248	P_3w	4550 (14,927)	4394 (14,416)	156 (512)	–	19%	26%	65%	
260	255	Erosion	–	–	–	1800 (5905)	–	–	–	
285	266	P_1j	4730 (15,518)	455 (14,927)	180 (590)	–	93%	2%	5%	

Temperature gradient data are from Qiu et al. (2000) and Zhou et al. (1989).

Permian with erosion of P_2w, P_2x, P_1f, and upper part of P_1j; rapid burial in the late Permian with sedimentation of P_3w; and following erosion of the upper part of P_3w. Triassic and Early–Middle Jurassic are represented by rapid subsidence with thickness of sediments up to approximately 3000 m (9800 ft). During the Late Jurassic, the high sedimentation rate waned, and a basin-wide unconformity is associated with approximately 400 m (1300 ft) of missing sections in the latest Jurassic. Burial history was characterized by a return to high rates of subsidence and sediment supply from Cretaceous to present, and from the northwestern to the southeastern areas in the Zhongguai area, burial history demonstrates differences caused by development of the downdip slope. Maximum burial depth of the Jiamuhe Formation in the Zhongguai area occurs today.

Goodness of fit between the modeled temperature and tested formation temperature provides the best available comparison of model to reality (Figure 6). Maximum temperatures of Jiamuhe Formation with current shallow depth at the northwestern part of the Zhongguai area were reached before the uplift in the late Permian, when paleogeothermal gradient was approximately 40°C/km (116°F/mi) (Table 2) and burial depth was deeper than 2500 m (8200 ft), whereas maximum temperatures of the deeply buried Jiamuhe Formation in the southeastern part of the Zhongguai area occur today with a geothermal gradient of approximately 19.5°C/km (56.5°F/mi) (Table 2).

Diagenesis

Authigenic Minerals

Authigenic minerals in the reservoirs consist of various zeolites, calcite, quartz, clays (kaolinite and chlorite), and iron oxides.

Zeolites—Zeolite cements are the most abundant cements, and three types, analcite, heulandite-Ca, and laumontite, were identified in the reservoirs (Tang et al., 1997; Zhu et al., 2012). Analcite occurs as euhedral dodecahedron crystal (Figures 7A, 8A) or patchy aggregation (Figure 7E) in some medium- to coarse-grained sandstones, pebbly sandstones, and fine-grained conglomerates. Anhedral heulandite-Ca in shaly sandstones and fine-grained sandstones with much matrix was transformed from volcanic ashes and is characterized by orange patch aggregation with no development of euhedral prismatic crystals (Figure 7L), whereas in medium- to coarse-grained sandstones, pebbly sandstones, and fine-grained conglomerates, heulandite-Ca is characterized by orange euhedral prismatic morphology and their aggregation (Figures 7B, 8B). Laumontite occurs typically as blocky pore-filling cement characterized by well-developed cleavages in medium- to coarse-grained sandstones, pebbly sandstones, and fine-grained conglomerates (Figures 7C, 8D); in addition, some feldspar grains were identified to be replaced by laumontite cements. Heulandite-Ca was identified in the outer part of primary pores in some thin

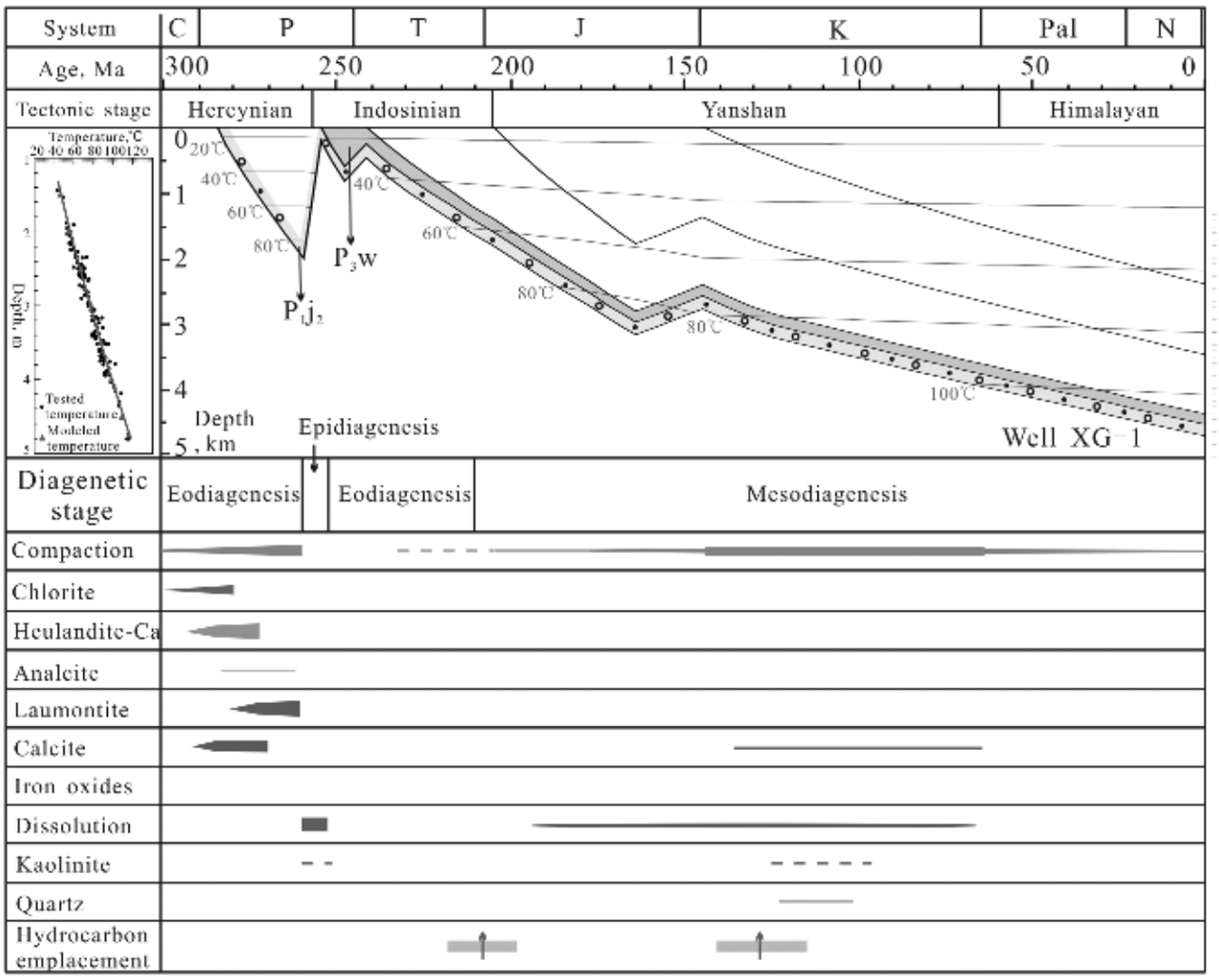

Figure 6. Plots of burial, thermal, diagenetic, and hydrocarbon emplacement history of the Permian reservoirs in the Zhongguai area. The hydrocarbon emplacement stage is after Chen et al. (2016). Note: A color version can be seen in the online version.

sections, whereas analcite or laumontite was identified in the inner parts of the primary pores (Figure 7G–J). This texture relationship suggests that heulandite-Ca was formed relatively earlier than analcite and laumonite. Low–homogenization temperature data (55–60°C [131–140°F]) of aqueous fluid inclusions (Chen et al., 2016) identified in some laumontite also suggest early precipitation of these zeolites.

Calcite—Calcites are important authigenic minerals in some reservoirs, ranging in abundance from trace to 25% in thin sections. Two types of calcite cements were identified in thin sections. Early calcites were precipitated prior to extensive compaction and are characterized by poikilotopic textures and are up to 20%–25% in volume in thin sections (Figure 7D). Low homogenization temperature (50°C [122°F]) of aqueous fluid inclusions in early calcites (Chen et al., 2016) also demonstrates early formation of these cements. Rocks with early calcites are commonly supported by grains with point contacts or floating textures. Late calcite cements, in contrast, typically feature a low content of less than 2%–5% of rock volume. The late calcites replaced early zeolite cements in thin sections and filled secondary pores and fractures in grains and zeolite (Figure 7D), indicating that the late calcites were likely to be precipitated after dissolution of zeolites and feldspars.

Iron Oxides—Iron oxides were identified in thin sections from several wells (e.g., wells G5, G11, G105, G102, and G106) at the northwestern part of the

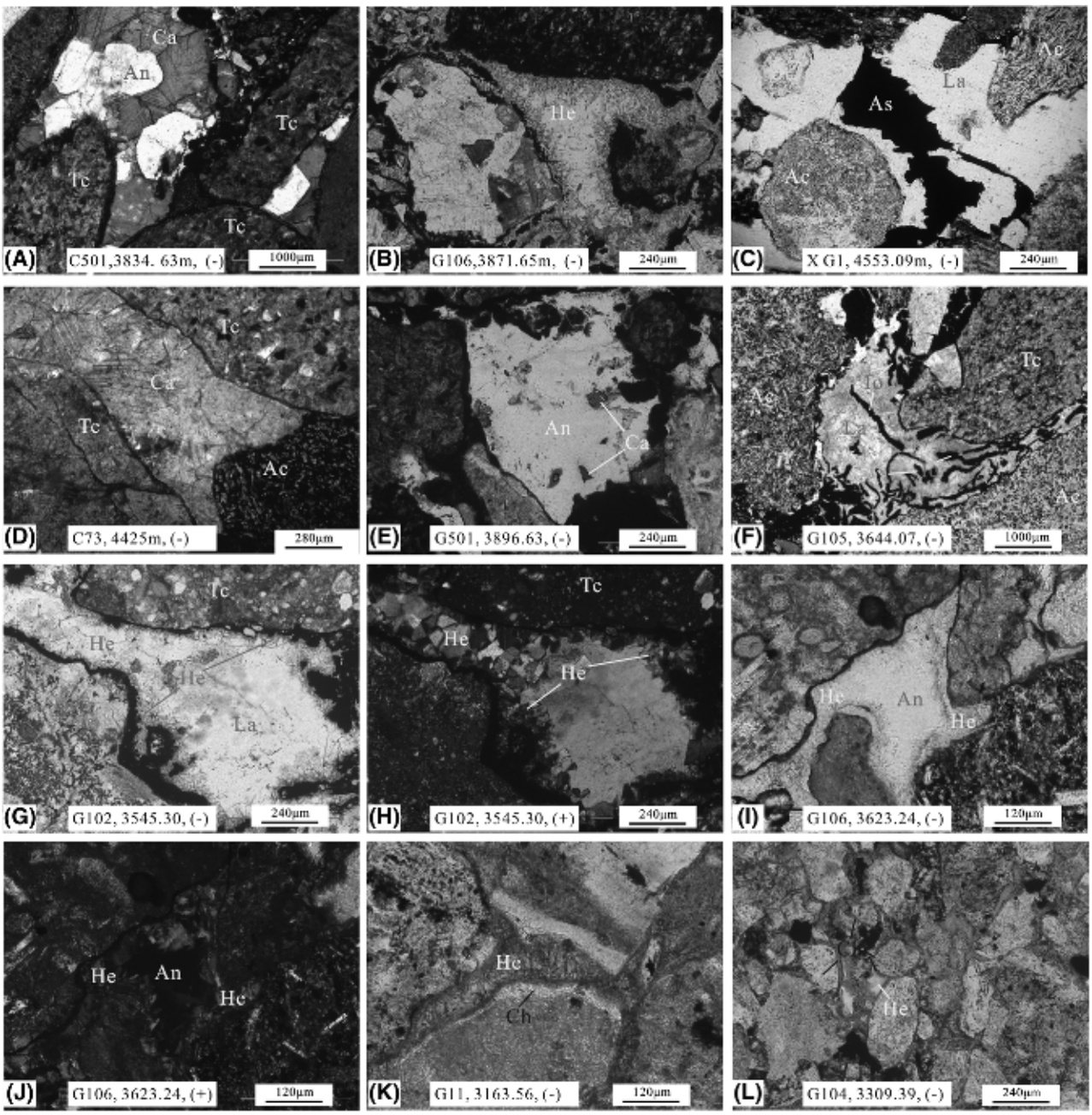

Figure 7. Thin section images of the conglomerate reservoirs in Jiamuhe Formation in the Zhongguai area (pore space is shown in blue). (A) Calcite (Ca) and analcite (An) cement in primary pores. Tuff clasts (Tc) are subrounded or rounded. (B) Heulandite-Ca (He) cement in primary pores. (C) Laumontite (La) cement in primary pores and asphalt (As) in secondary pores formed by dissolution of La. (D) Early-stage Ca in primary pores. Floating texture can be easily identified, and Tc are subrounded or rounded. (E) Secondary pores formed by dissolution of An, partial filling of these secondary pores by late-stage Ca. (F) Replacement of La by iron oxides (Io). (G, H) Heulandite-Ca in outer part of primary pores and La in inner part of pores. (I, J) Heulandite-Ca in outer part of primary pores and An in inner part of pores. (K) Chlorite (Ch) in outer part of primary pores and He in inner part of pores. (L) Green Ch and orange patch He. Dash indicates plane-polarized light view; plus indicates cross-polarized light view. Ac = andesite clasts. Note: A color version can be seen in the online version.

downdip slope constrained by the Hongche fault and the Hong3 well fault (Figure 1C). Iron oxides were identified to replace zeolites (Figure 7F) and calcites and fill fractures or secondary pores in grains, indicating that these iron oxides formed later than the early precipitated cements. The amount of iron oxides generally increases in thin sections as the distance from rock samples to the unconformity decreases, suggesting these iron oxides were potentially products of meteoric freshwater flushing during the uplift period in the late Permian.

Clay Minerals—Kaolinite and chlorite are two types of authigenic clays in the Jiamuhe conglomerate reservoirs. Chlorite occurs predominantly as pore fillings, grain coatings, or rims. In shaly sandstones and fine-grained sandstones with much matrix, considerable amounts of volcanic ashes were transformed to chlorite and were identified as green patchy pore filling minerals in thin sections (Figure 7L). Coating or rim chlorite (Figures 7K, 8E) were, in contrast, formed in medium- to coarse-grained sandstones and pebbly sandstones with low amount of matrix. The coatings are generally of homogeneous thickness and uniform distribution (Figure 7K), whereas the rims commonly exhibit preferred orientation perpendicular to the grain surfaces (Figure 8E). Chlorite crystals are characterized by euhedral foliaceous morphology in SEM samples (Figure 8E). Petrography textures (Figure 7K) demonstrate that chlorite likely formed earlier than other authigenic minerals.

Kaolinite occurs mainly as vermicular aggregates and anhedral–pseudohexagonal plates filling in primary and secondary pores (Figure 8G) with the amount of kaolinite ranging from trace to less than 1%. Texture relationships indicate that kaolinite formed later and is likely a secondary mineral following the dissolution of zeolites and feldspars.

Quartz—Authigenic quartz in the reservoirs occurs as discrete euhedral and subhedral crystals (Figure 8F) that generally postdate chlorite grain-coating; rare quartz overgrowths can be identified in thin sections (Figure 7). The quartz crystals, with size generally less than 10 μm, are evident in SEM samples but cannot be identified easily in thin sections because of the small size. Quartz cements commonly represent less than 0.1% of the whole rock and are likely secondary minerals of dissolution of zeolites and feldspars.

Dissolution

Mineral dissolution occurred in reservoirs and improved reservoir quality through generation of a substantial amount of secondary pores (Zhu et al., 2012) (Figures 9, 10A–E). Thin sections and SEM samples demonstrate that dissolution occurred primarily in laumontite (Figures 8C, D; 10A–D) and analcite (Figure 10E) and some feldspar and andesite fragment grains (Figure 10C), whereas little petrography evidence indicates obvious dissolution of tuff fragment grains (Figure 10G), heulandite-Ca (Figure 10H), and calcite cement (Figure 7D). Extensive dissolution occurred mainly in medium- to coarse-grained sandstones, pebbly sandstones, and fine-grained conglomerates (Figure 10A–F), whereas shaly sandstones and fine-grained sandstones experienced weak dissolution (Figure 10I). Reservoirs closely related to the unconformity commonly contain more secondary pores and higher core porosity (Figure 9), indicating mineral dissolution probably occurred through meteoric water leaching during the uplift period (Emery et al., 1990). Abundant bitumen and heavy oil (Figures 7C, 10D) were identified in secondary pores formed by laumontite dissolution, indicating that hydrocarbon emplacement probably occurred after mineral dissolution.

Diagenetic Sequences

The relative timing of major diagenetic sequences (Figure 6) of the Jiamuhe conglomerate reservoirs in the Zhongguai area at the northwestern margin of Junggar Basin, which has been determined from thin sections and SEM examination, is based on texture relationships (Figures 7–10) (Tang et al., 1997). The dominant eogenetic features in the reservoirs are, in summary, (1) initial compaction immediately following deposition; (2) formation of chlorite clay coatings or rims and chlorite pore fills; and (3) early precipitation of calcite, heulandite-Ca, analcite, and laumontite. Diagenesis occurring at the Permian uplift stage includes (1) dissolution of unstable minerals including analcite, laumontite, and some feldspars and rock fragments; (2) precipitation of kaolinite; and (3) precipitation of iron oxides from

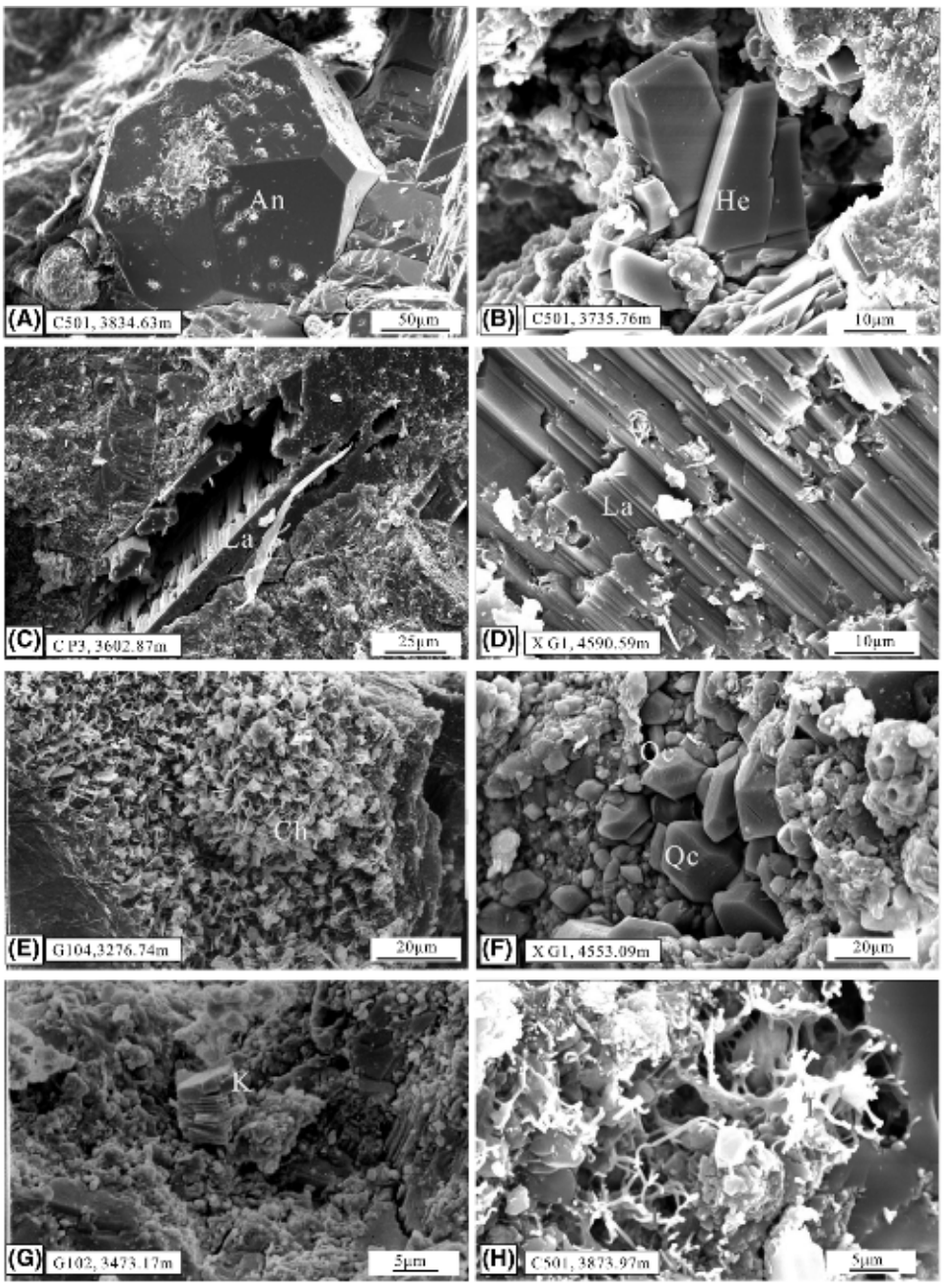

Figure 8. Scanning electron microscope images of the conglomerate reservoirs in Jiamuhe Formation in the Zhongguai area. (A) Single analcite (An) crystal. (B) Single heulandite-Ca (He) crystal. (C) Secondary pores in laumontite (La). (D) Dissolution of La. (E) Chlorite (Ch) rim on grain surface. (F) Authigenic quartz crystal (Qc). (G) Authigenic kaolinite (K). (H) Authigenic illite (I). Note: A color version can be seen in the online version.

interactions with oxidized meteoric water. Subsequent diagenetic processes during the resubsidence stage experienced by these reservoirs include (1) compaction; (2) dissolution of some aluminosilicate minerals; and (3) precipitation of kaolinite, quartz, and late calcite. With constraints of the texture relationships, the homogenization temperature (T_h) of aqueous fluid inclusions in cements, and burial–thermal history of well XG1 in the Zhongguai area, the diagenetic history of the Permian conglomerate reservoirs is summarized in Figure 6.

Pores in Reservoirs

Pores in the Permian reservoirs are currently mainly secondary pores as a result of extensive compaction, cementation, and mineral dissolution (Figures 9, 10), and only a few residual primary pores can be identified in some samples. Thin sections and SEM samples demonstrate distinct differences among pores in various reservoirs. Most primary pores in medium- to coarse-grained sandstones, pebbly sandstones, and fine-grained conglomerates in fan delta

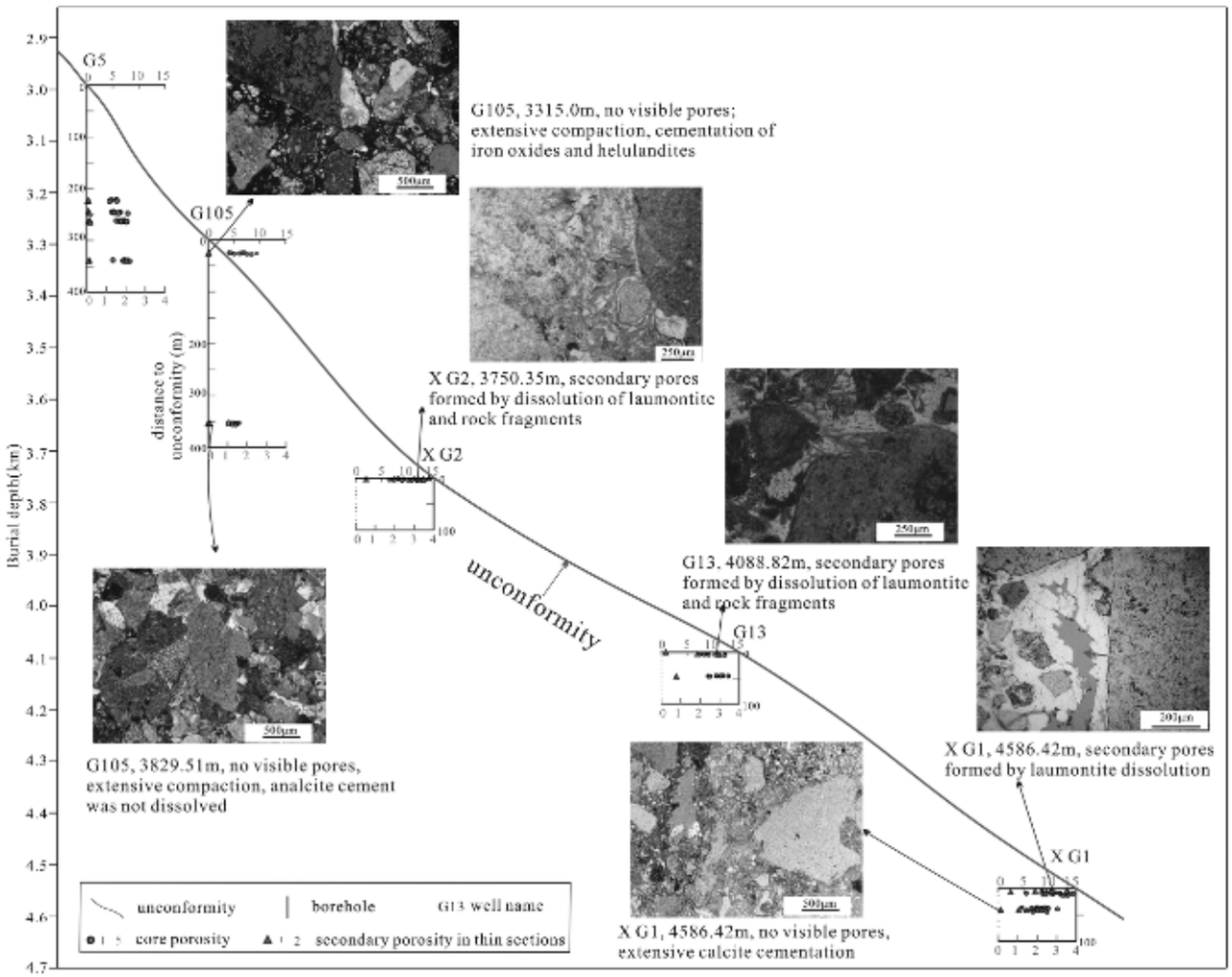

Figure 9. Core porosity and secondary porosity in thin sections in individual wells on a northwest–southeast cross section profile (well G5 to well G105 to well XG2 to well G13 to well XG1) (Figure 1C) and features of the secondary pores in the reservoirs beneath the unconformity and the reservoirs far from the unconformity. Note: A color version can be seen in the online version.

plain subfacies have been reduced by extensive compaction, and some pores are occupied by various cements including calcite, analcite, heulandite-Ca, and iron oxides; few secondary pores can be identified in feldspar grains or analcite (Figure 10G, H). In shaly sandstones and fine sandstones with much matrix, almost all primary pores have been destroyed by extensive compaction and/or authigenic cements including patchy chlorite and heulandite-Ca aggregates (Figure 10I); rare secondary pores can only be identified in few feldspar grains in such rocks. The amount of visible pores in these two types of tight rocks is generally less than 0.1%, and such rocks also exhibit low core porosity.

The medium- to coarse-grained sandstones, pebbly sandstones, and fine-grained conglomerates in fan delta front subfacies, contrastingly, contain abundant secondary pores formed by dissolution of analcite, laumontite, and some detrital grains (Figure 10A–E), although primary pores have been occupied by these zeolite cements at the early diagentic stage. The amount of visible secondary pores in thin sections can generally reach up to 2%–4% (Figure 9), and anomalously high core porosities are typically exhibited in these reservoirs.

Pore Waters

Data of 21 pore water samples in the Jiamuhe Formation reservoirs show that pore waters are characterized by $CaCl_2$ water. The salinity of these pore

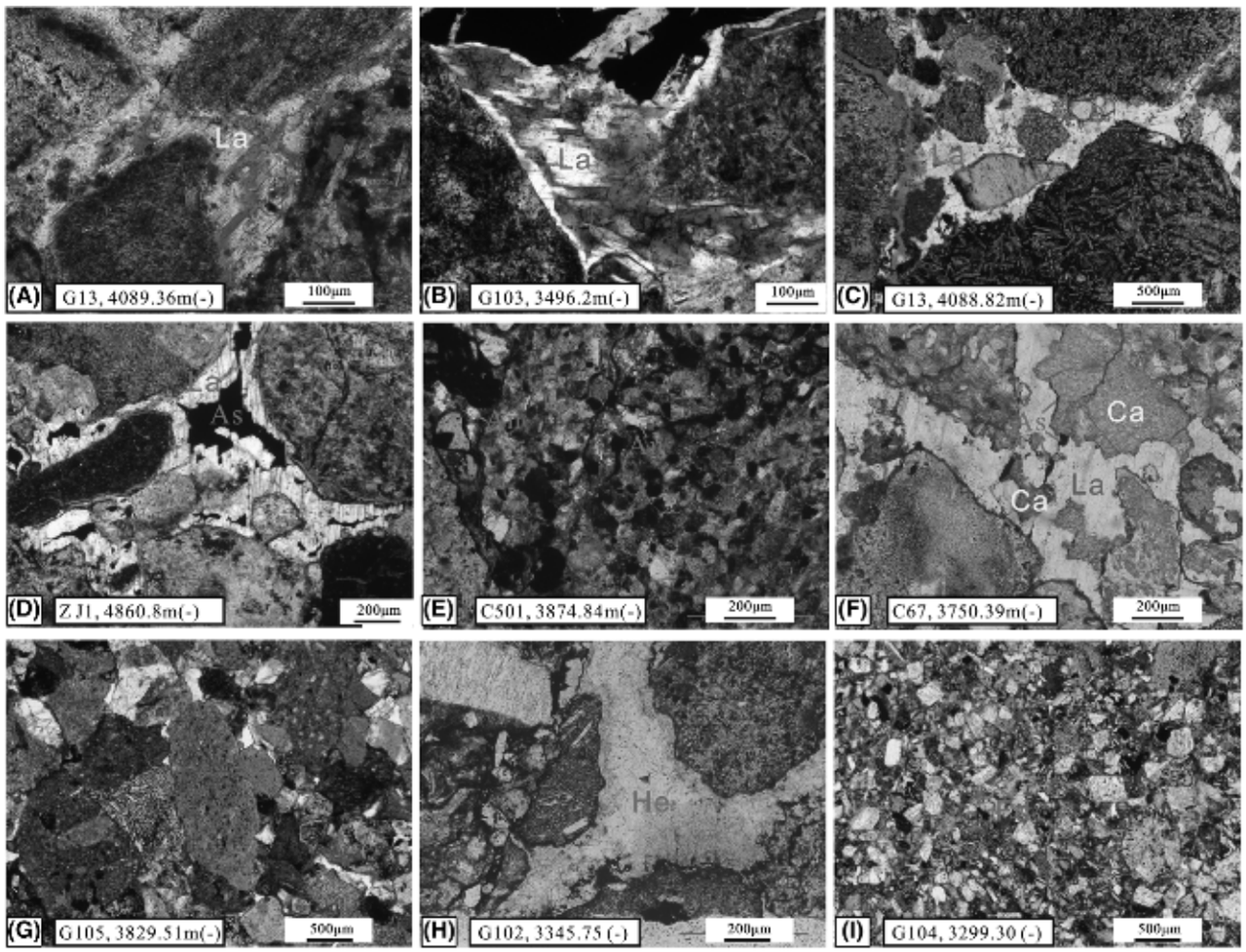

Figure 10. Photomicrographs of various pores in reservoirs with (A–E) anomalously high porosity and (F–I) low porosity. (A, B) Intergranular secondary pores formed by dissolution of laumontite (La). (C) Dissolution of La along cement–grain boundary and dissolution of andesite fragment grain. (D) Filling of secondary pores by asphalt (As). Pores were formed by La dissolution. (E) Secondary pores formed by analcite (An) dissolution. (F) Secondary pores left in La. Most secondary pores were occupied by As and calcite (Ca) cement. (G) No visible pores in reservoirs with strong compaction. (H) Few remnant primary pore was left after cementation of heulandite-Ca (He) cement. (I) Secondary pores formed by dissolution of feldspar grain (Fd). All plane-polarized light. Note: A color version can be seen in the online version.

waters ranges from 8819.0 mg/L to 76,618.0 mg/L (Table 3). The main cations are Na^+, K^+, and Ca^{2+}, and Cl^- dominates the anions. The plots of salinity and ion concentrations versus the distance of these water samples to the unconformity at the top of the Jiamuhe Formation show low salinity and low concentrations of Cl^- and Na^+ in pore waters of reservoirs beneath the reginal unconformity (Figure 11).

DISCUSSION

Reservoir quality evolution may be a function of several controls (Taylor et al., 2010; Tobin et al., 2010; Cao et al., 2014) including the depositional controls of sedimentary facies, lithofacies, grain sizes, sorting, and compositions and the diagenetic controls of cementation, dissolution, and compaction (Dutton and Loucks, 2010; Yuan et al., 2015b). Results from the previous sections are integrated and discussed below to decipher genetic mechanism of the anomalously high porosities developed in the Permian conglomerate reservoirs.

Effect of Deposition on Cementation

Sedimentary Facies and Lithofacies

Zeolites are the most prominent cements in the Permian tight reservoirs, and types of zeolites vary

Table 3. Ranges of Salinity and Concentration of Different Ions in the Pore Waters in the Permian Tight Conglomerate Reservoirs in the Zhongguai Area

	Ions (mg/L)						
Concentration	$Na^+ + K^+$	Ca^{2+}	Mg^{2+}	Cl^-	SO_4^{2-}	HCO_3^-	Salinity
Maximum	2140	1046	0	5040	61	37	8819
Minimum	13,955	18,437	638	47,010	1466	1165	76,618
Average	4289	8262	118	21,000	461	382	34,332

in different rocks and different subfacies. Few analcite or laumontite cements were identified in shaly and fine-grained sandstones with much matrix including detrital clays and volcanic ashes, whereas the anhedral heulandite-Ca originating from volcanic ashes dominated the zeolite cements (Figure 12). In pebbly sandstones and fine-grained conglomerates with little matrix, different zeolites were identified in reservoirs from different subfacies. Statistic data indicate that laumontite dominates the reservoir cements in the fan delta front subfacies, with the absolute amount of laumontite ranging from 2% to 20% and relative content (relative to the amount of all zeolite cements) ranging from 80% to 100%, whereas heulandite-Ca dominates the cements in reservoirs in the fan delta plain subfacies, with absolute amount of heulandite-Ca ranging from 1% to 8% and relative content ranging from 60% to 100% (Figure 13). Analcite developed primarily in some sandstones in the fan delta plain subfacies, with the absolute amount ranging from 0.5% to 5% and relative content ranging from 10% to 85%. Thus, sedimentary subfacies and lithofacies significantly affect the distribution of analcite, heulandite-Ca, and laumontite in the Permian reservoirs (Fu et al., 2010; Sun et al., 2014).

Rock Compositions

In the medium- to coarse-grained sandstones, pebbly sandstones, and fine-grained conglomerates, the relative content of tuff clasts and andesite clasts (relative to the amount of rock fragments) controlled the relative content of heulandite-Ca and laumonite cement (relative to the amount of zeolites) (Figure 14). When the relative content of tuff clasts ranges from 0% to 20% and andestite clasts ranges from 100% to 80%, laumontite dominates the zeolites in reservoirs, and few heulandite-Ca can be identified; when when tuff clasts ranges from 100% to 80%, the heulandite-Ca dominates, and few laumontite cements can be identified. The heulandite-Ca dominates in shaly

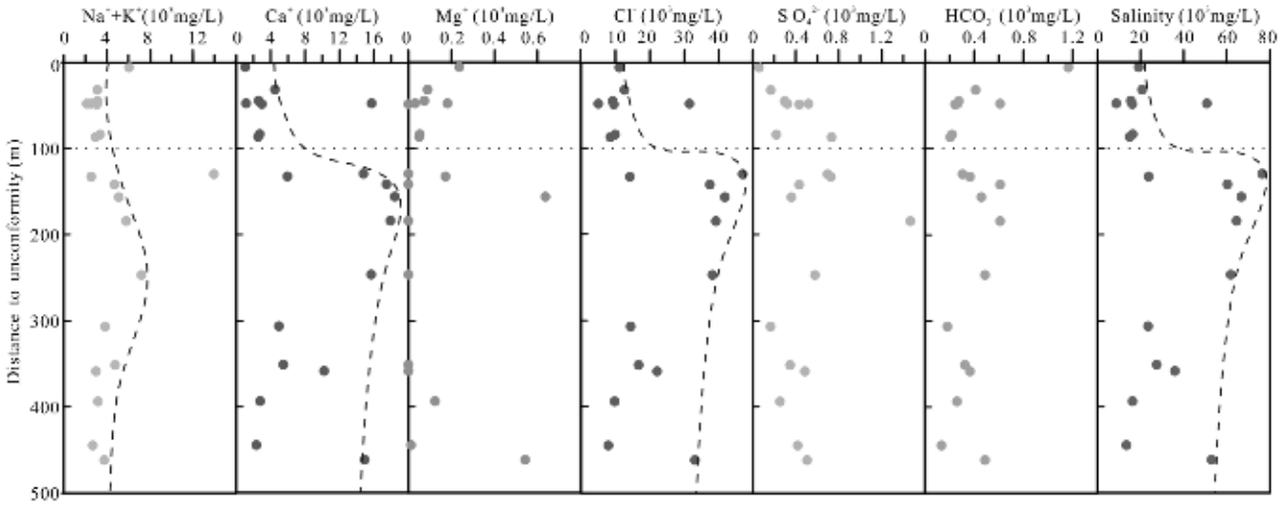

Figure 11. Salinity and concentrations of different ions in the pore waters in the Permian reservoirs in the Zhongguai area. Note: A color version can be seen in the online version.

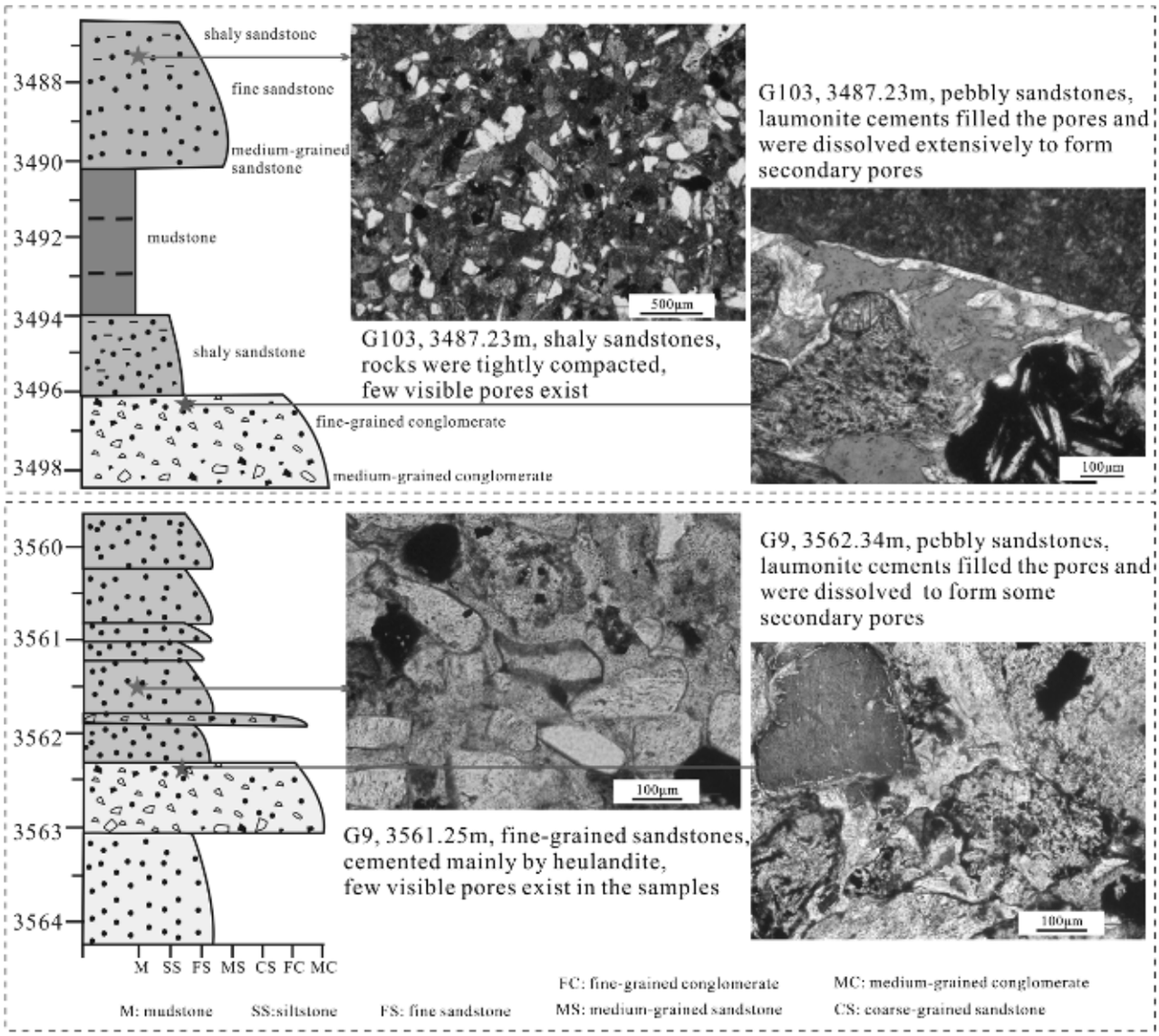

Figure 12. Distribution of heulandite-Ca and laumontite cement in reservoirs with different lithofacies in the Permian Jiamuhe Formation in the Zhongguai area. Note: A color version can be seen in the online version.

sandstones and fine-grained sandstones because of the existence of volcanic ash. Thus, despite the effect of sedimentary facies, rock compositions also affected the distribution of heulandite-Ca and laumontite (Tang et al., 1997; Zhu et al., 2012; Sun et al., 2014).

Early Cementation Retarded Later Compaction

Considerable amounts of volcanic rock fragments in the sandstones, particularly the tuff clasts, are plastic grains that may promote mechanic compaction during burial (Figure 10G) (Pittman and Larese, 1991). In the Permian reservoirs, petrography textures of line contact and concavo–convex contact demonstrate extensive compaction in rocks with few calcite and laumontite cements (Figures 7L, 10G). Point contact pattern and floating textures of detrital grains are common (Figure 10A–D), however, in reservoirs with large amount of calcite and laumontite cements (or secondary pores formed by laumonite dissolution), suggesting that these early precipitated cements have retarded compaction effectively during the later burial (Huang et al., 2007; Zhu et al., 2007).

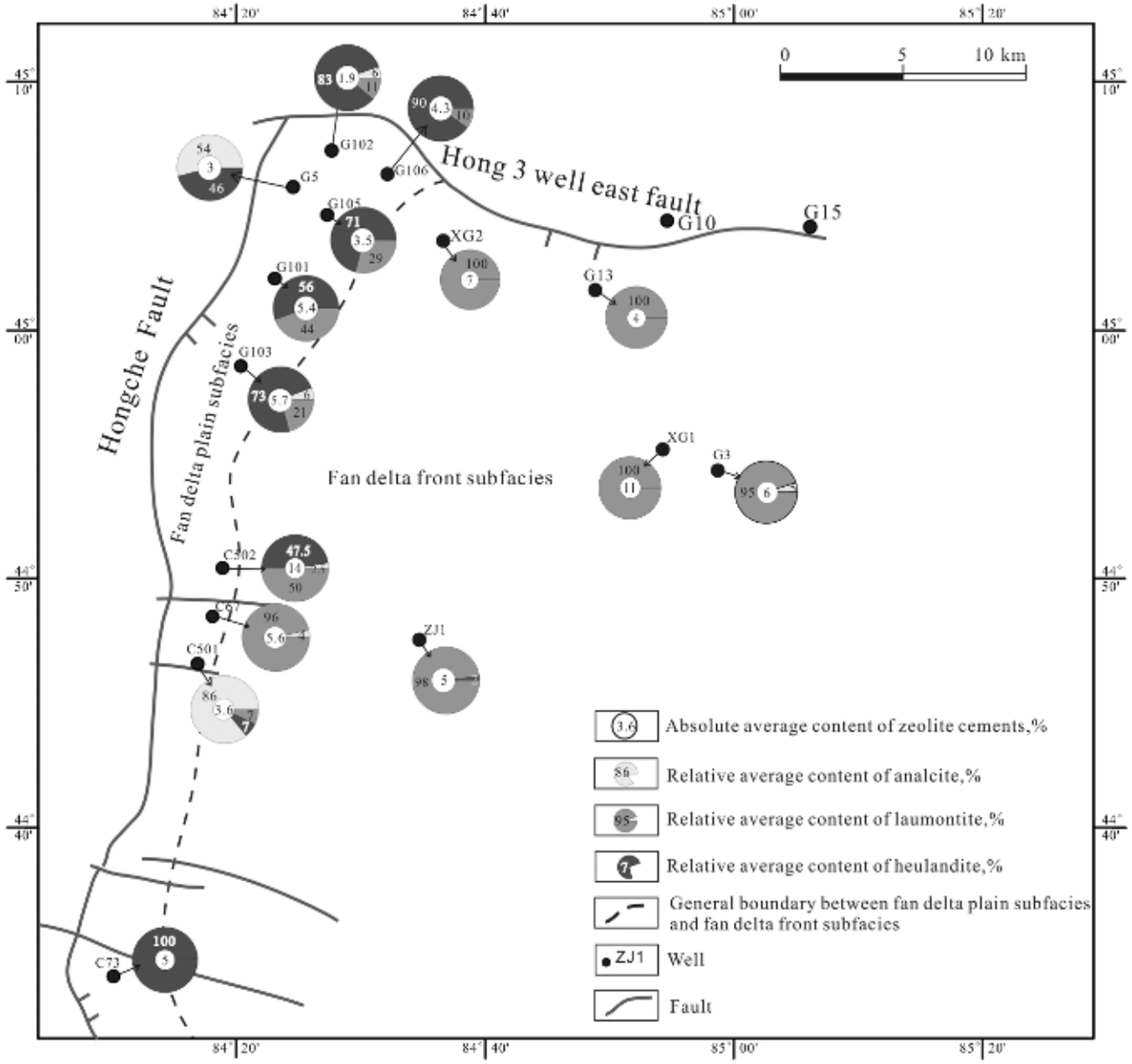

Figure 13. Distribution of analcite, heulandite-Ca, and laumontite in different subfacies in the Permian fan delta reservoirs in the Zhongguai area. Note: A color version can be seen in the online version.

Meteoric Water Leaching Formed Secondary Pores

The regional unconformity on the top of the Jiamuhe Formation suggests long-term subaerial exposure of the studied reservoirs in the late Permian, leading to meteoric water flushing of the reservoirs beneath the unconformity (Emery et al., 1990). Extensive diagenetic reactions (particularly mineral dissolution) tend to increase salinity of pore water (Frape et al., 1984; Egeberg and Aagaard, 1989); however, pore waters in reservoirs with extensive dissolution beneath the unconformity generally exhibit much lower salinity and ion concentrations (Figure 11), indicating that large amounts of meteoric freshwater probably entered into these reservoirs during the uplift period (França et al., 2003).

Dissolution of aluminosilicate minerals is generally accompanied by precipitation of secondary minerals including clays and quartz cements in relatively closed sandstone geochemical systems (Giles and De Boer, 1990; Zhang et al., 2011;

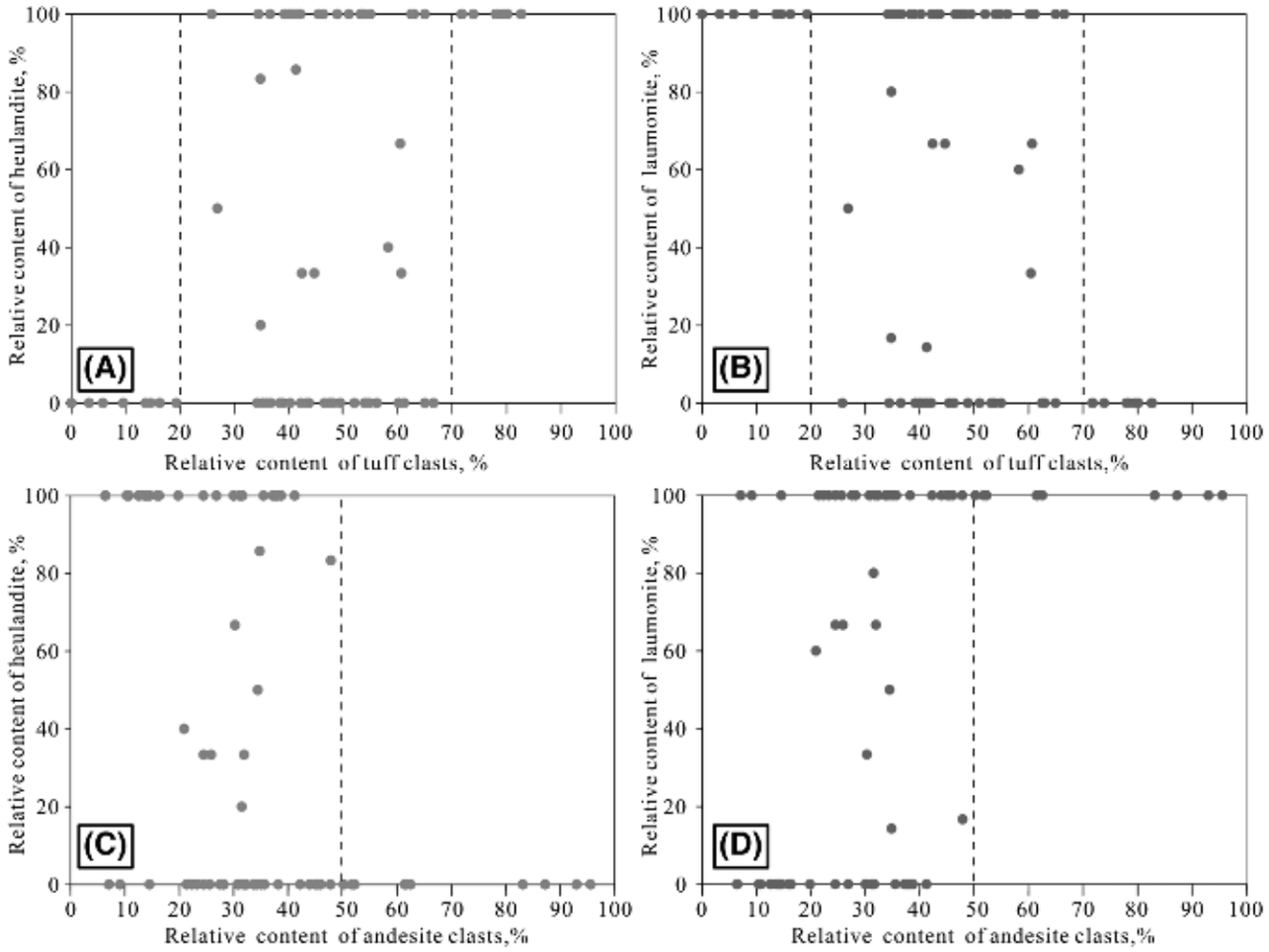

Figure 14. Relationships between types of zeolite and mineral composition in the Permian reservoirs in the Zhongguai area. Note: A color version can be seen in the online version.

Yuan et al., 2013). However, few kaolinite and quartz cements were identified in the Permian reservoirs with abundant secondary pores, suggesting that solutes released by dissolution of laumonites and feldspars may have been removed from the reservoirs effectively (Giles, 1987; Emery et al., 1990). Thin sections show that reservoirs closer to the unconformity typically exhibit large amount of secondary pores formed by dissolution of mainly laumontite and some feldspars, and tested core porosity and interpreted log porosity confirmed the development of anomalously high porosities beneath the unconformity (Figures 9, 15). Thin sections demonstrate that most secondary pores developed in the central part of the laumonite cements and feldspar grains (Figure 10A, B), and the marginal remnants likely contributed to preservation of the secondary pores by preventing secondary compaction during later burial.

Hydrocarbon Emplacement Retarded Later Cementation

Hydrocarbon emplacement has been suggested in previous studies to preserve porosity by retarding mineral cementation (Marchand et al., 2001, 2002; Wang, 2010), with the concept questioned by some scientists (Aase and Walderhaug, 2005). Previous studies with evidence of fluid inclusions, reconstructed burial history, and thermal history suggested two stages (218–198 Ma and 145–112 Ma) of hydrocarbon emplacement in the Permian reservoirs when burial depth was shallower than 1800 and 3000 m, respectively

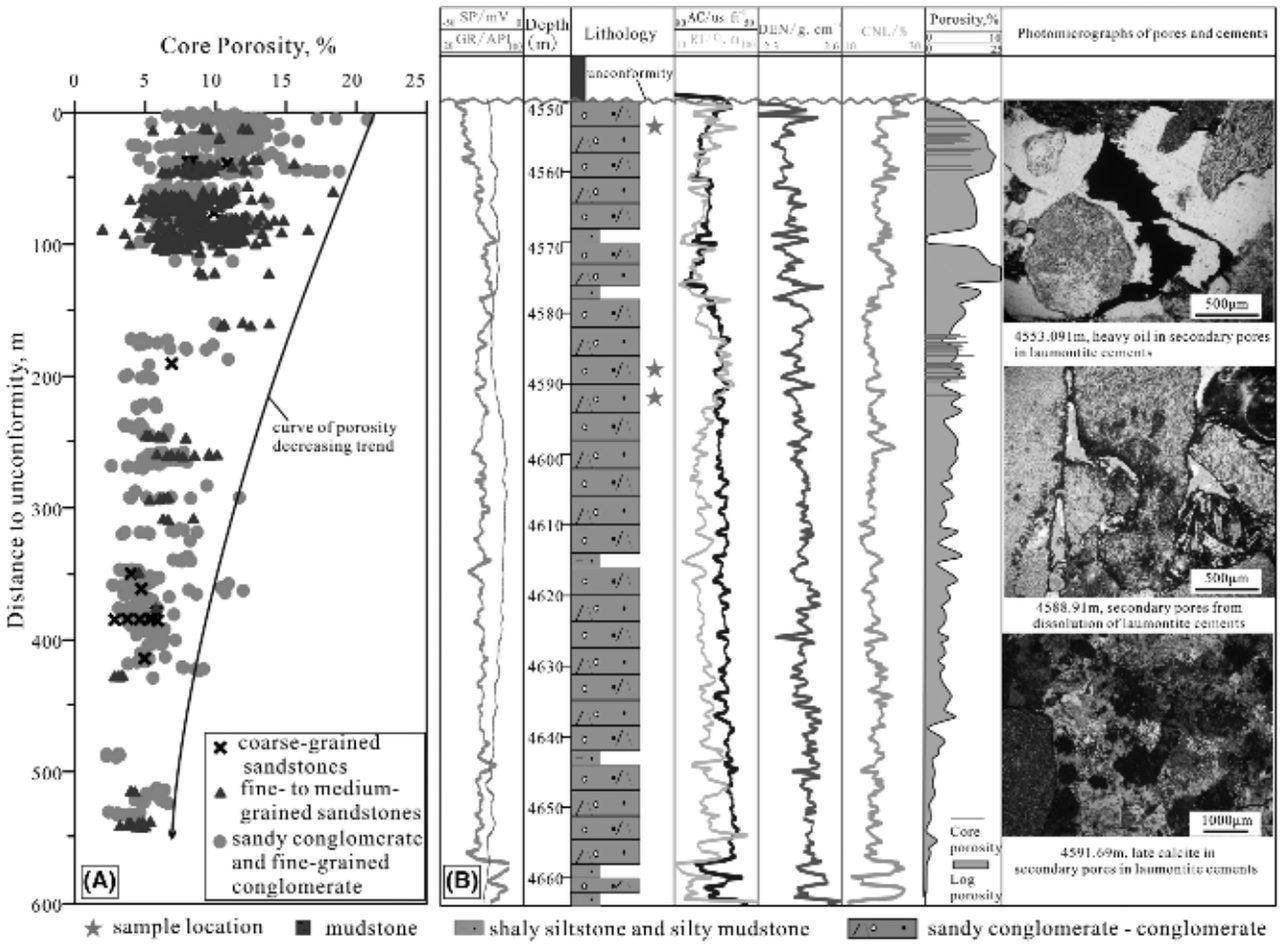

Figure 15. (A) Plot of core porosity versus the distance between the rock samples and the unconformity. (B) The lithology, porosity, and micropetrography of well XG1 beneath the unconformity. AC = acoustic time logging curve; CNL = compensated neutron logging; DEN = bulk density logging curve; GR = natural gamma log curve; RT = resistivity logging curve; SP = spontaneous potential logging curve. Note: A color version can be seen in the online version.

(Figure 5) (Chen et al., 2016). Thin sections demonstrate that few later calcite cements were formed in secondary pores in reservoirs from oil or gas layer (Figures 10A, B; 15), whereas more later calcite can be identified in secondary pores in reservoirs from water layers and dry layers (Figures 10F, 15), suggesting that later calcite cementation reactions were retarded following hydrocarbons emplacement in the Permian Jiamuhe reservoirs.

Genetic Model of the High-Quality Reservoirs

The deeply buried Jiamuhe conglomerate reservoirs experienced various diagenetic reactions including compaction, cementation, and dissolution. Discussion in the previous four sections suggests that the generation of the high-quality reservoirs in the deeply buried Permian fan delta conglomerates are a result of a chronological combination of four important geological processes. A synthetic and succinct genetic model for generation of the high-quality reservoirs was proposed through integration of sedimentary features and diagenetic processes (Figure 16). Sediments in the fan delta plain subfacies were cemented first in the initial subsidence period primarily by some heulandite-Ca and early calcite cements at approximately 50–60°C (122–140°F) (Figure 16B), whereas simultaneously, sediments in the fan delta front subfacies were cemented by large amounts of laumontite, retarding compaction effectively during the subsequent deep burial (Figure 16B). Second, large amounts of laumontite and some feldspars in

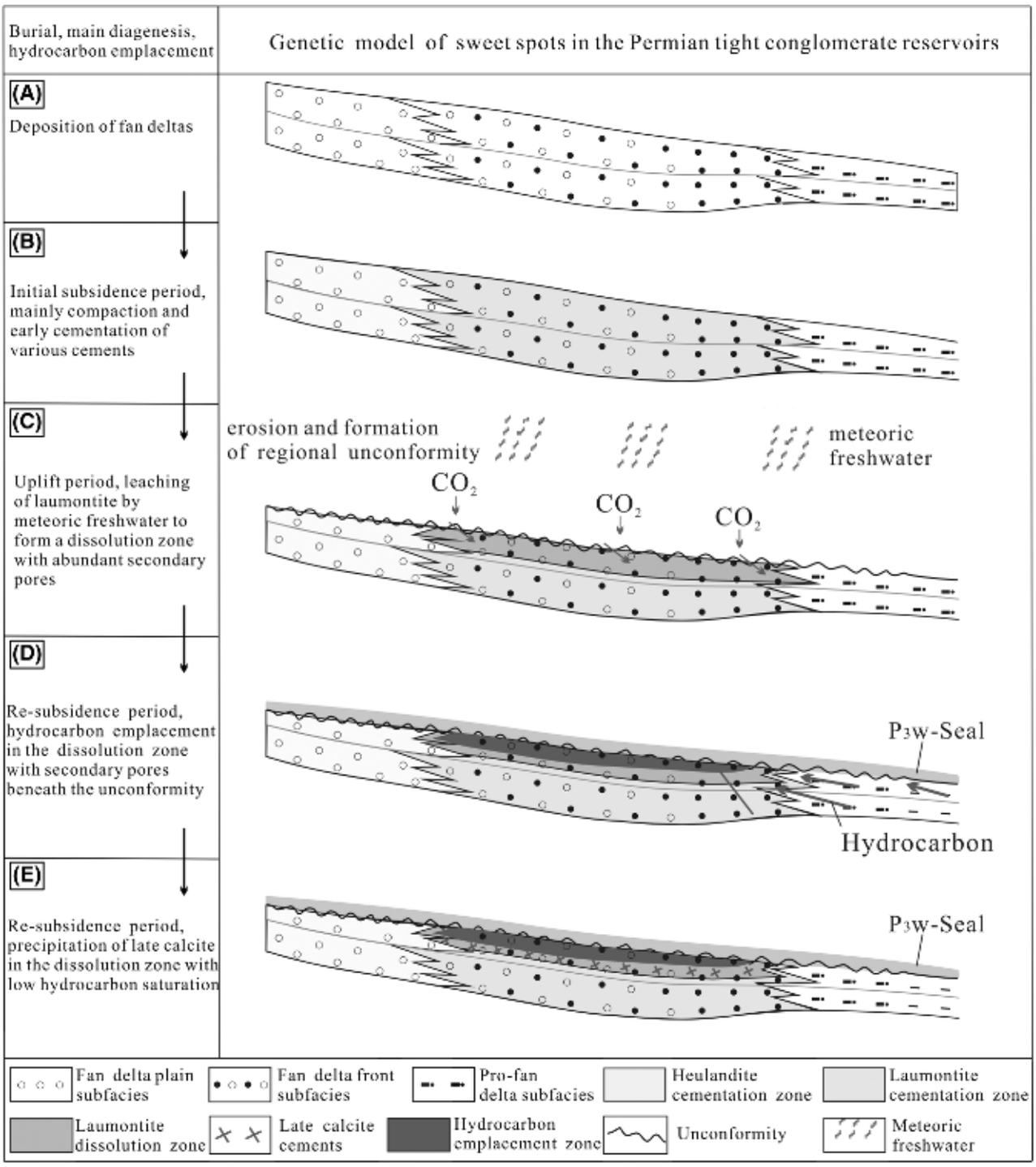

Figure 16. Genetic model of the high-quality reservoir in the Permian fan delta tight conglomerates in the Zhongguai area, Junggar Basin. Note: A color version can be seen in the online version.

reservoirs of the fan delta front subfacies were selectively dissolved by meteoric freshwater to form secondary pores (Figures 9; 10A, B; 15) during formation of the regional unconformity in the uplift period. Heulandite-Ca cements in fan delta plain subfacies, however, were not dissolved, evidently (Figure 16C). Third, P_3w mudstones were deposited on top of the unconformity in the resubmission period, serving as a regional seal for reservoir traps (Figure 16D). Hydrocarbon emplacement then occurred, and hydrocarbons were trapped in the reservoirs beneath the unconformity and occupied large amounts of secondary pores (Figure 16D) (Chen et al., 2014). Finally, during the subsequent burial stage, calcite was formed in reservoirs with secondary pores but limited hydrocarbon, whereas the calcite cementation reaction was retarded in the reservoirs with large amount of hydrocarbons (Figure 16E) (Marchand et al., 2001; Wang, 2010), and the secondary pores in these hydrocarbon-saturated reservoirs were effectively preserved to present. Thus, exploration targets should then focus on medium- to coarse-grained sandstones, pebbly sandstones, and fine-grained conglomerates in the fan delta front subfacies and beneath the unconformity based on the comprehensive studies.

The Jiamuhe Formation in the Zhongguai area developed on the southeastern downdip slope with a large strata angle. The vertical distribution of medium- to coarse-grained sandstones, pebbly sandstones, and fine-grained conglomerates in the fan delta front subfacies and beneath the unconformity probably spans thousands of meters (Figures 1D, 11). With less than 30 exploration wells and relatively limited cores, the available tested core porosity data show the development of anomalously high porosity at two separate depth intervals (3200–4200 m [10,500–13,800 ft] and 4500–4900 m [14,800–16,100 ft]) (Figure 4). From 4200 to 4500 m (10,500 to 14,800 ft), however, there are still no core samples beneath the unconformity available, leading to the lack of anomalously high porosity in such a depth interval in Figure 4. As the high-quality reservoirs beneath the regional unconformity developed in the downdip Jiamuhe Formation (Figure 16), such high-quality reservoirs probably exist at the depth interval of 4200–4500 m (13,800–14,800 ft) (Figure 9) and may even expand the anomalously high porosity to much deeper depth in the study area.

CONCLUSION

1. The Permian tight conglomerate reservoirs, texturally and compositionally immature, are primarily litharenites and feldspathic litharenites. The Permian tight reservoirs experienced compaction and precipitation of chlorite clays, calcite, and zeolite in the initial subsidence stage; dissolution of unstable minerals including analcites, laumontites, and some feldspars and rock fragments and precipitation of iron oxides from interactions with oxidized meteoric water in the late Permian uplift stage; and compaction, dissolution of aluminosilicate minerals, and precipitation of kaolinite, quartz, and late calcite in the resubsidence stage.
2. The reservoirs exhibit a wide range of porosity mainly from 2% to 18% and permeability from 0.001 to 25 md. Few visible pores were identified in low-porosity tight sandstones because of extensive compaction and/or cementation, whereas secondary pores formed by dissolution of mainly laumontite, and some grains dominate the reservoir spaces in rocks with anomalously high porosity.
3. Generation of high-quality reservoirs in buried tight conglomerates originated from a chronological combination of four favorable geological processes. The prioritized exploration targets should be the medium- to coarse-grained sandstones, pebbly sandstones, and fine-grained conglomerates in the fan delta front subfacies and beneath the regional Permian unconformity.

REFERENCES CITED

Aase, N. E., and O. Walderhaug, 2005, The effect of hydrocarbons on quartz cementation: Diagenesis in the Upper Jurassic sandstones of the Miller Field, North Sea, revisited: Petroleum Geoscience, v. 11, p. 215–223, doi: 10.1144/1354-079304-648.

Bloch, S., R. H. Lander, and L. Bonnell, 2002, Anomalously high porosity and permeability in deeply buried sandstone reservoirs: Origin and predictability: AAPG Bulletin, v. 86, no. 2, p. 301–328.

Cao, Y., G. Yuan, X. Li, Y. Wang, K. Xi, X. Wang, Z. Jia, and T. Yang, 2014, Characteristics and origin of abnormally high porosity zones in buried Paleogene clastic reservoirs in the Shengtuo area, Dongying Sag, east China: Petroleum Science, v. 11, p. 346–362, doi:10.1007/s12182-014-0349-y.

Chen, Z., Y. Cao, Z. Ma, and Y. Zhen, 2014, Geochemistry and origins of natural gases in the Zhongguai area of Junggar Basin, China: Journal of Petroleum Science Engineering, v. 119, p. 17–27, doi:10.1016/j.petrol.2014.05.007.

Chen, Z., Y. Cao, X. Wang, L. Qiu, Y. Tang, and G. Yuan, 2016, Oil origin and accumulation in the Paleozoic Chepaizi–Xinguang field, Junggar Basin, China: Journal of Asian Earth Sciences, v. 115, p. 1–15, doi:10.1016/j.jseaes.2015.09.019.

Dutton, S. P., and R. G. Loucks, 2010a, Diagenetic controls on evolution of porosity and permeability in lower Tertiary Wilcox sandstones from shallow to ultradeep (200–6700m) burial, Gulf of Mexico Basin, U.S.A.: Marine and Petroleum Geology, v. 27, p. 69–81, doi:10.1016/j.marpetgeo.2009.08.008.

Dutton, S. P., and R. G. Loucks, 2010b, Reprint of: Diagenetic controls on evolution of porosity and permeability in lower Tertiary Wilcox sandstones from shallow to ultradeep (200–6700m) burial, Gulf of Mexico Basin, U.S.A.: Marine and Petroleum Geology, v. 27, p. 1775–1787, doi:10.1016/j.marpetgeo.2009.12.010.

Egeberg, P. K., and P. Aagaard, 1989, Origin and evolution of formation waters from oil fields on the Norwegian shelf: Applied Geochemistry, v. 4, p. 131–142, doi:10.1016/0883-2927(89)90044-9.

Emery, D., K. J. Myers, and R. Young, 1990, Ancient subaerial exposure and freshwater leaching in sandstones: Geology, v. 18, p. 1178–1181, doi:10.1130/0091-7613(1990)018<1178:ASEAFL>2.3.CO;2.

Falvey, D. A., and M. F. Middleton, 1981, Passive continental margins evidence for a prebreakup deep crustal metamorphic subsidence mechanism: Oceanlogica Acta, p. 103–114.

França, A. B., L. M. Araújo, J. B. Maynard, and P. E. Potter, 2003, Secondary porosity formed by deep meteoric leaching: Botucatu eolianite, southern South America: AAPG Bulletin, v. 87, no. 7, p. 1073–1082, doi:10.1306/02260301071.

Frape, S. K., P. Fritz, and R. T. McNutt, 1984, Water-rock interaction and chemistry of groundwaters from the Canadian Shield: Geochimica et Cosmochimica Acta, v. 48, p. 1617–1627, doi:10.1016/0016-7037(84)90331-4.

Fu, G., M. Dong, Z. Zhang, L. Sun, and R. Pan, 2010, Formation process and distribution of laumontite in Yanchang 3 reservoir of Fuxian exploration area in North Shanxi Province and the controls of the high quality reservoirs: Earth Science—Journal of China University of Geosciences, v. 35, p. 107–114.

Giles, M. R., 1987, Mass transfer and problems of secondary porosity creation in deeply buried hydrocarbon reservoirs: Marine and Petroleum Geology, v. 4, p. 188–204, doi:10.1016/0264-8172(87)90044-4.

Giles, M. R., and R. B. De Boer, 1990, Origin and significance of redistributional secondary porosity: Marine and Petroleum Geology, v. 7, p. 378–397, doi:10.1016/0264-8172(90)90016-A.

Grant, N. T., A. J. Middleton, and S. Archer, 2014, Porosity trends in the Skagerrak Formation, Central Graben, United Kingdom Continental Shelf: The role of compaction and pore pressure history: AAPG Bulletin, v. 98, no. 6, p. 1111–1143, doi:10.1306/10211313002.

Guo, X., K. Liu, S. He, G. Song, Y. Wang, X. Hao, and B. Wang, 2012, Petroleum generation and charge history of the northern Dongying Depression, Bohai Bay Basin, China: Insight from integrated fluid inclusion analysis and basin modelling: Marine and Petroleum Geology, v. 32, p. 21–35, doi:10.1016/j.marpetgeo.2011.12.007.

Higgs, K. E., H. Zwingmann, A. G. Reyes, and R. H. Funnell, 2007, Diagenesis, porosity evolution, and petroleum emplacement in tight gas reservoirs, Taranaki Basin, New Zealand: Journal of Sedimentary Research, v. 77, p. 1003–1025, doi:10.2110/jsr.2007.095.

Huang, S., P. Huang, Q. Wang, Y. Liu, M. Wu, and M. Zou, 2007, The significance of cementation in porosity preservation in deep-buried sandstone: Lithologic Reservoirs, v. 19, p. 7–13.

Jia, Z. Z., C. Y. Lin, L. H. Ren, and C. M. Dong, 2016, Selective dissolution of eodiagenesis cements and its impact on the quality evolution of reservoirs in the Xing'anling Group, Suderte Oil Field, Hailar Basin, China: Petroleum Science, v. 13, p. 402–417, doi:10.1007/s12182-016-0110-9.

Lai, J., G. Wang, Y. Ran, and Z. Zhou, 2015, Predictive distribution of high-quality reservoirs of tight gas sandstones by linking diagenesis to depositional facies: Evidence from Xu-2 sandstones in the Penglai area of the central Sichuan basin, China: Journal of Natural Gas Science and Engineering, v. 23, p. 97–111, doi:10.1016/j.jngse.2015.01.026.

Lai, J., G. Wang, Y. Ran, Z. Zhou, and Y. Cui, 2016, Impact of diagenesis on the reservoir quality of tight oil sandstones: The case of Upper Triassic Yanchang Formation Chang 7 oil layers in Ordos Basin, China: Journal of Petroleum Science Engineering, v. 145, p. 54–65, doi:10.1016/j.petrol.2016.03.009.

Li, P., Y. Zhou, F. Hao, J. Tian, and D. Tong, 2006, Restoration of eroded strata thickness in Cretaceous/Jurassic unconformity in hinterland of Junggar Basin (in Chinese with English abstract): Acta Petrolei Sinica, v. 27, p. 34–38.

Ma, D., D. He, D. Li, J. Tang, and Z. Liu, 2015, Kinematics of syn-tectonic unconformities and implications for the tectonic evolution of the Hala'alat Mountains at the northwestern margin of the Junggar Basin, Central Asian Orogenic Belt: Geoscience Frontiers, v. 6, p. 247–264, doi:10.1016/j.gsf.2014.07.004.

Marchand, A. M. E., R. S. Haszeldine, P. C. Smalley, C. I. Macaulay, and A. E. Fallick, 2001, Evidence for reduced quartz-cementation rates in oil-filled sandstones: Geology, v. 29, p. 915–918, doi:10.1130/0091-7613(2001)029<0915:EFRQCR>2.0.CO;2.

Marchand, A. M. E., P. C. Smalley, R. S. Haszeldine, and A. E. Fallik, 2002, Note on the importance of hydrocarbon fill for reservoir quality prediction in sandstones: AAPG Bulletin, v. 86, no. 9, p. 1561–1571.

Nguyen, B. T. T., S. J. Jones, N. R. Goulty, A. J. Middleton, N. Grant, A. Ferguson, and L. Bowen, 2013, The role of fluid pressure and diagenetic cements for porosity preservation in Triassic fluvial reservoirs of the Central Graben, North Sea: AAPG Bulletin, v. 97, no. 8, p. 1273–1302, doi:10.1306/01151311163.

Olson, J. E., S. E. Laubach, and R. H. Lander, 2009, Natural fracture characterization in tight gas sandstones: Integrating mechanics and diagenesis: AAPG Bulletin, v. 93, no. 11, p. 1535–1549, doi:10.1306/08110909100.

Pittman, E. D., and R. E. Larese, 1991, Compaction of lithic sands: Experimental results and applications: AAPG Bulletin, v. 75, no. 8, p. 1279–1299.

Qiu, N., M. Zha, and X. Wang, 2000, Simulation of geothermal evolution history in Junggar Basin: Xinjiang: Petroleum Geology, v. 21, p. 38–41.

Sun, Y., X. Liu, Y. Zhang, W. Dong, Y. Xu, G. Shi, Y. Lin, and A. Li, 2014, Analcite cementation facies and forming mechanism of high-quality secondary clastic rock reservoirs in western China: Journal of Palaeogeography, v. 16, p. 517–526.

Tang, Z., P. John, and F. J. Longstaffe, 1997, Diagenesis and reservoir potential of Permian–Triassic fluvial/lacustrine sandstones in the southern Junggar Basin, northwestern China 1: AAPG Bulletin, v. 81, no. 11, p. 1843–1865.

Taylor, T. R., M. R. Giles, L. A. Hathon, T. N. Diggs, N. R. Braunsdorf, G. V. Birbiglia, M. G. Kittridge, C. I. Macaulay, and I. S. Espejo, 2010, Sandstone diagenesis and reservoir quality prediction: Models, myths, and reality: AAPG Bulletin, v. 94, no. 8, p. 1093–1132, doi:10.1306/04211009123.

Tobin, R. C., T. McClain, R. B. Lieber, A. Ozkan, L. A. Banfield, A. M. E. Marchand, and L. E. McRae, 2010, Reservoir quality modeling of tight-gas sands in Wamsutter field: Integration of diagenesis, petroleum systems, and production data: AAPG Bulletin, v. 94, no. 8, p. 1229–1266, doi:10.1306/04211009140.

Van der Plas, L., and A. C. Tobi, 1965, A chart for judging the reliability of point counting results: American Journal of Science, v. 263, p. 87–90, doi:10.2475/ajs.263.1.87.

Wan, M., 2011, Causes of Permian dense conglomerate reservoir and favorable block prediction in Zhongguai Bulge (in Chinese): Xinjiang Oil and Gas, v. 7, p. 17–20.

Wang, Y. Z., 2010, Genetic mechanism and evolution model of secondary pore development zone of Paleogene in the North Zone in Dongying Depression (in Chinese with English abstract), Ph.D. thesis, China University of Petroleum (Huadong), Qingdao, China, 141 p.

Yuan, G., Y. Cao, Z. Jia, J. Gluyas, T. Yang, Y. Wang, and K. Xi, 2015a, Selective dissolution of feldspars in the presence of carbonates: The way to generate secondary pores in buried sandstones by organic CO_2: Marine and Petroleum Geology, v. 60, p. 105–119, doi:10.1016/j.marpetgeo.2014.11.001.

Yuan, G. H., Y. C. Cao, K. L. Xi, Y. Z. Wang, X. Y. Li, and T. Yang, 2013, Feldspar dissolution and its impact on physical properties of Paleogene clastic reservoirs in the northern slope zone of the Dongying sag (in Chinese with English abstract): Acta Petrolei Sinica, v. 34, p. 853–866.

Yuan, G. H., J. Gluyas, Y. C. Cao, N. H. Oxtoby, Z. Z. Jia, Y. Z. Wang, K. L. Xi, and X. Y. Li, 2015b, Diagensis and reservoir quality evolution of the Eocene sandstones in teh northern Dongying Sag, Bohai Bay Basin, east China.: Marine and Petroleum Geology, v. 62, p. 77–89, doi:10.1016/j.marpetgeo.2015.01.006.

Zhang, X., S. Huang, Y. Lan, K. Huang, and R. Liang, 2011, Thermaldynamic calculation of laumontite dissolution and its geologic significance: Lithologic Reservoirs, v. 23, p. 64–69.

Zhou, Z., C. Pan, S. Fan, and L. Han, 1989, Geothermal characteristics of the Junggar Basin and its significance to oil searching: Xinjiang Petroleum Geology, v. 10, p. 67–74.

Zhu, S., X. Zhu, X. Wang, and Z. Liu, 2012, Zeolite diagenesis and its control on petroleum reservoir quality of Permian in northwestern margin of Junggar Basin, China: Science China. Earth Sciences, v. 55, p. 386–396, doi:10.1007/s11430-011-4314-y.

Zhu, X. M., Y. G. Wang, D. K. Zhong, Q. Zhang, Z. H. Zhang, S. W. Zhang, and X. X. Lv, 2007, Pore types and secondary pore evolution of Paleogene reservoir in the Jiyang Sag (in Chinese with English abstract): Acta Geologica Sinica, v. 81, p. 197–204.